

**Republic of Iraq**  
**Ministry of Higher Education and Scientific Research**  
**University of Kerbala**  
**College of Engineering**  
**Department of Mechanical Engineering**



# **Cooling Enhancement for Turbine Blades Passages by Using Ribs and Thermal Barrier Coating**

**A Thesis**

**Submitted to the College of Engineering / University of Kerbala in Partial  
Fulfillment of the Requierments for the Degree of Master of Science in  
Mechanical Engineering**

by

**Eng. Shaheed Mahdy Talib Abu-Aless Al-Musawi**

**(B.Sc. University of Baghdad 2003)**

Supervised by

**Assit.Prof.Dr. Mohammed Wahhab AL-Jibory**

**Dr. Farhan Lafta Rashid**

**2019A.D.**

**1440 A.H.**

بِسْمِ اللَّهِ الرَّحْمَنِ الرَّحِيمِ

((الم {1} ذَلِكَ الْكِتَابُ لَا رَيْبَ فِيهِ هُدًى

لِّلْمُتَّقِينَ {2} الَّذِينَ يُؤْمِنُونَ بِالْغَيْبِ وَيُقِيمُونَ الصَّلَاةَ

وَمِمَّا رَزَقْنَاهُمْ يُنْفِقُونَ {3} وَالَّذِينَ يُؤْمِنُونَ بِمَا أُنزِلَ

إِلَيْكَ وَمَا أُنزِلَ مِنْ قَبْلِكَ وَبِالْآخِرَةِ هُمْ يُوقِنُونَ

{4} أُولَئِكَ عَلَى هُدًى مِّن رَّبِّهِمْ وَأُولَئِكَ

هُمُ الْمُفْلِحُونَ {5} ))

صَدَقَ اللَّهُ الْعَلِيِّ الْعَظِيمِ

سورة البقرة

## ACKNOWLEDGMENT

---

Deepest gratitude goes to Allah for his uncountable blessings. I would like to express my sincere thanks to my two supervisors Dr. Mohammed W. Al-jibory and Dr. Farhan Lafta Rashid for their invaluable guidance, support and endless help throughout the period of the research. They guided me with a friendly patience the development of this work.

Thank and gratitude to Dr. Ahmed Hashim from the college of Education for pure sciences /Department of physics/University of Babylon for his help in nanoparticle measurements field.

Many thanks go to my family for providing me all the facilities and supporting during the period of preparing this work.

Thanks and gratitude to all of my colleagues who supported me in the study and research stages, especially the brothers Mohammad Raza and Hassan Qahtan

My thanks and appreciations to all the staff-members of the Mechanical Engineering Department, University of Kerbala.

***Shaheed***  
***2019***

## **DEDICATION**

**To my dear father whom I have not seen**

(The symbol of Faith, martyrdom and heroism)

**To my dear mother**

(The symbol of affection and struggle)

**To Beloved Wife**

(The spring of love)

**To Lovely sons (Mahdi and Ahmad)**

(The spirit of life)

**To my dear uncles and cousins**

(The symbol of sacrifice)

**To my Soulmate Mostafa Saad**

(The symbol of honesty)

**To everyone I had learned from my life**

**I dedicate this modest effort...**

*Shaheed  
2019*



## **Supervisors' Approval**

We certify that this dissertation entitled (**Cooling Enhancement for Turbine Blades Passages by Using Ribs and Thermal Barrier Coating**) was prepared by engineer (**Shaheed Mahdi Talib**) and carried out completely under our supervision at the Mechanical Engineering Department / College of Engineering /University of Kerbala, in partial fulfillment of the requirement for the degree of master Science in Mechanical Engineering.

**Signature:**

**Asst. Prof.**

**Dr. Mohammed Wahhab AL-Jibory**

**Mech. Eng. Dept**

**University of kerbala**

**Date: / /2019**

**Signature:**

**Dr. Farhan Lafta Rashid**

**Mech. Eng. Dept**

**University of kerbala**

**Date: / /2019**

## Linguistic Approval

I certify that this thesis entitled “**Cooling Enhancement for Turbine Blades Passages by Using Ribs and Thermal Barrier Coating**” was prepared by **(Shaheed Mahdi Talib)** under my linguistic revisions, and its language meets the English academic writing.

Signature:

Name: Baqer A. Alhabeeb

Mechanical Engineering Department, University of Kerbala

University of Kerbala

Date: / /2019

---

## Examination Committee Approval

---

We certify that we have read this thesis entitled **(Cooling Enhancement for Turbine Blades Passages by Using Ribs and Thermal Barrier Coating)** and as an examining committee examined the student **(Shaheed Mahdi Talib)** in its content and that in our opinion it meets the standard of a thesis and is adequate for the award of the Master Degree of Sciences in Mechanical Engineering / Thermo-Fluids Mechanics.

**Signature:****Name: Assit. Prof.****Dr. Mohammed Wahhab AL-Jibory**

(Supervisor)

**Date: / / 2019****Signature:****Name: Dr. Farhan Lafta Rashid**

(Supervisor)

**Date: / / 2019****Signature:****Name: : Assit. Prof.****Dr. Ahmed Hashim Yousif**

(Member)

**Date: / / 2019****Signature:****Name: Dr .Haider Nadham Azziz**

(Member)

**Date: / / 2019****Signature:****Name: Prof.Dr.Ihsan Y.Hussain**

(Chairman)

**Date: / / 2019**

Mechanical Engineering Department Approval

**Signature:****Name: lect. Dr. Hazim Umran****Date: Alwan 2019**

Dean of the Engineering College Approval

**Signature:****Name: Assit. Prof. Dr. Laith Shakir Raseed (Dean of the College of Engineering)****Date: / / 2019**

### Abstract

The flow and heat transfer in four elliptical cross sectional channels (having the same hydraulic diameter but different in channel aspect ratio) have been investigated at conditions that simulate those in air cooled turbine blades.

A numerical and experimental investigation of the effectiveness of using internal elliptical ribs of four different configurations (elliptical boot ship, triangular rib with right angle and with the flow direction, elliptical rib of two equal legs elliptical triangular rib with right angle, and inverse the flow direction) with the effect of the channel aspect ratio ( $AR=1, 1.3, 1.6$  and  $2$ ) with and without thermal barrier coating has been conducted. The flow and heat transfer characteristics for a fully developed turbulent flow in an elliptical channel heated with constant surrounding temperature and Reynolds numbers based on channel hydraulic diameter values of (11000, 13500, and 16000) has been tested in this study.

The numerical simulation study includes solving the three dimensional governing equations (Continuity, Reynolds Averaging Navier-Stokes and Energy equations) in turbulent regime with ( $k-\epsilon$ ) model as the perfect model using the FLUENT software version (16.1). The effect of different ribs geometries with rib height to hydraulic diameter ratio ( $e/D_h=0.135$ ) and rib-rib spacing (pitch) to rib height ratio ( $p/e=10$ ) in an elliptical channel of 0.5 m long, internal cross section of ( $57 \times 29$ ,  $50 \times 31$ ,  $43 \times 33$ ,  $37 \times 37$ ) mm and 1.5 mm wall thickness were simulated. Four different configurations of ribs named as rib (1, 2, 3, and 4).

In the experimental part of this study, a rig was designed and constructed to simulate conditions in gas turbine blade. The operational conditions are: inlet coolant air temperature of 300 K and the surrounding constant hot air temperature of (673K). The considered cases were compared with a smooth elliptical channel (channel without ribs) at the same operational conditions. The channel with AR

(2) was the best channel in heat transfer, and the channel with ribs provided higher thermal performance than the smooth ones. The ribbed channels (rib1, rib 2, rib3, and rib 4) increased the Nusselt number and thermal performance factor by (5.0, 4.8, 2.4 and 1.4) and (2.31,1.87,1.09 and 0.55) times, respectively when it is compared with the smooth channel case.

Case of rib 1 fitted in channel with AR (2) showed the best result (lower pressure drop and higher heat transfer enhancement). While case of rib 4 fitted in channel of AR (2) showed the worst result. The experimental and numerical results were compared and showed a good agreement with a maximum difference of (3.8%).

The additional work involves coating the channel of the best case with composite Nano-materials (thermal painting mixed with Yttrium oxide nanoparticle ( $Y_2O_3$ ) by (5wt. %) as a thermal barrier coating. Nusselt number was enhanced for the channel with coating by (9.97%) times the case of channel without coating.

# NOMENCLATURES

## Latin Symbols

Symbol	Description	Units
$A$	Surface Area	$m^2$
$AR$	Aspect Ratio	[-]
$AI$	Inner Surface Area	
$a,b,c$	Constants	[-]
$C_p$	Heat Capacity of Air	J/kg.K
$d$	Diameter	m
$D_h$	Hydraulic Diameter	m
$e$	Rib Height	m
$F$	Force	N
$f$	Friction Factor	[-]
$g$	Acceleration due to gravity	$m/s^2$
$H$	Channel Height	m
$h$	Heat Transfer Coefficient	$W/m^2.K$
$k$	Thermal Conductivity	$W/m.K$
$L_c$	Characteristic Length	m
$L_t$	Test Section Length	m
$L_e$	entrance length	m
$L_{the}$	thermal entrance length	m
$\dot{m}$	Mass Flow Rate	kg/s
$Nu$	Nusselt Number= $h D_h / k$	[-]
$Pr$	Prantdle Number= $\mu C_p / k$	[-]
$P$	Rib Spacing(Pitch)	m
$PR$	Pitch Ratio	[-]
$P_w$	Wetted Perimeter	m
$Q$	Heat Transfer Rate	W
$q$	Heat Flux	$W/m^2$
$Re$	Reynolds Number= $\rho u D_h / \mu$	[-]
$R_{th}$	Thermal Resistance	$m^2K/W$
$r_i$	Inner radius	m
$r_o$	Outer radius	m
$T$	Temperature	K
$T.I.$	Turbulent Intensity	[-]
$u$	Flow Velocity	m/s
$W$	Width of the channel	m

## Greek Symbols

Symbol	Description	Units
$\Delta$	Difference	[-]
$\eta$	Thermal Performance Factor	[-]
$\mu$	Air Dynamic Viscosity	N s/ m <sup>2</sup>
$\rho$	Air Density	kg/m <sup>3</sup>
$\theta$	Angle of attack	degree

## Subscripts

Subscripts	Description
c	Characteristic
g	Surrounding Gas
h	Hydraulic
i	Inlet
O	Outlet
o	Without Ribs
S	Surface
Th	Thermal
W	Wall
X	Local value

## Abbreviations

Abbreviations	Description
ANSYS	Analytical System
CFD	Computational Fluid Dynamic
HTE	Heat Transfer Enhancement
LHV	Lower Heating Value
TIT	Turbulent Inlet Temperature

## TABLE OF CONTENTS

Abstract	I
Table of Contents	III
Nomenclature	IX
<b>Chapter One: INTRODUCTION</b>	
1.1 Background	1
1.2 Gas turbine cycle	1
1.3 Internal Cooling	3
1.4 Rib Turbulated Cooling	5
1.5 Thermal Barrier Coatings (TBCs) in Gas Turbines	8
1.6 Objective and Plan of the present study	10
<b>Chapter Two: LITERATURE REVIEW</b>	
2.1 Numerical Studies	11
2.2 Experimental Studies	14
2.3 Numerical and Experimental Studies	17
2.4 Coating Studies	21
2.5 Summary	26
2.6 Point of originality	27
<b>Chapter Three: THEORETICAL MODELS AND NUMERICAL SOLUTION</b>	
3.1 Introduction	30
3.2 Description of the Physical Model	31
3.3 Assumptions	34
3.4 Governing Equations of Fluid Flow	35
3.4.1 Continuity Equation	35
3.4.2 Momentum Equation	35
3.4.3 Energy Equation	36
3.4.4 Reynolds-Averaged Navier-Stokes (RANS)	36
3.4.5 The standard K- $\epsilon$ pturbulence model	37
3.5 Thermal Performance factor formulation	37
3.6 Boundary Conditions Used in CFD Calculations	39
3.6.1 boundary conditions at inlet	39
3.6.2 Boundary conditions at outlet	39
3.6.3 Boundary conditions at wall of channel	39
3.7 CFD Software Package	40
3.8 Validate ANSYS results for the smooth channel	41



3.9 Total Cell Count	41
3.10 Generation the Mesh	41
3.11 Grid Independence Test	43
3.12 Set Up and Flow Specification	47
3.13 Number of Iterations and Convergence	47
3.14 Summary	48
<b>Chapter Four: EXPERIMENTAL WORK</b>	
4.1 Introduction	49
4.2 Experimental Devices and Test Rig	48
4.2.1 Test section	51
4.2.2 Cooling air supply system	52
4.2.3 Heating system	54
4.2.4 Ribs	55
4.2.5 Measuring tools	58
4.2.5.1 Thermocouples and data logger	58
4.2.5.2 Digital manometer	60
4.2.5.3 Anemometer	60
4.3 Experimentation	61
4.3.1 Experimental rig task	61
4.3.2 Measuring procedures	61
4.4 Data Reduction	62
4.5 Thermal Barrier Coating	64
4.5.1 Method of coating the channel	65
4.5.2 Test under the optical microscope	68
4.5.3 Test of corrosion	70
4.6 Sample of Calculation	72
4.6.1 Reynolds number and entrance length:	72
4.6.2 Discharge in cold fluid side:	72
4.6.3 Calculation for ribbed channel	73
4.6.3.1 Total area of heat transfer for smooth channel	73
4.6.3.2 Heat transfer rate:	73
4.6.3.3 Heat transfer coefficient	73
4.6.3.4 Nusselt number	73
4.6.3.5 Friction factor	74
4.6.5 Thermal performance factor	74
4.6.4.2 Heat transfer rate	73

4.6.4.3 Heat transfer coefficient	73
4.6.4.4 Nusselt number	74
4.6.4.5 Friction factor	74
4.6.5 Thermal performance factor	74
<b>Chapter Five: RESULTS AND DISCUSSION</b>	
5.1 Introduction	75
5.2 Numerical Results	75
5.2.1 Temperature distribution	76
5.2.1.1 Effect of aspect ratio and rib geometry on coolant air temperature	77
5.2.1.2 Inner wall surface temperature variation	79
5.2.1.3 Effect of rib geometry and channel aspect ratio on coolant air temperature	81
5.2.2 Coolant air velocity distribution	84
5.2.3 Effect of rib geometry and aspect ratio on average Nusselt number	92
5.2.4 Effect of rib geometry on friction factor ratio	91
5.2.5 Effect of rib geometry and aspect ratio on thermal performance factor	94
5.3 Experimental Results	98
5.3.1 Effect of rib geometry on inner wall surface temperature	98
5.3.2 Effect of rib geometry on coolant air temperature	99
5.3.3 Effect of rib geometry on the average Nusselt number	100
5.3.4 Effect of rib geometry on the friction factor ratio	101
5.3.5 Effect of rib geometry on the thermal performance factor	101
5.4 Results Comparison	102
5.4.1 Comparison of coolant air temperature	102
5.4.2 Comparison of inner wall temperatures	105
5.4.3 Comparison of average Nusselt number	105
5.4.4 Comparison of friction factor ratio	106
5.4.5 The thermal enhancement performance	106

# **CHAPTER ONE**

## **INTRODUCTION**

**CHAPTER ONE**  
**INTRODUCTION**

**1.1 Background**

Gas turbines are used for aircraft propulsion and in land-based power generation and industrial applications. Modern development in turbine-cooling technology plays important role in increasing of the thermal efficiency and power output of advanced gas turbines. Various major factors affect on both thermal efficiency of a gas turbine plant and specific fuel consumption as: (i) Increase in the turbine inlet temperature or firing temperature. (ii) Reduction of cooling air usage (iii) Improving components efficiencies and (iv) Enhancement of cycle [1].

**1.2 Gas Turbine Cycle**

As shown in figure (1.1) a gas turbine works on a Brayton cycle. The efficiency of an ideal Brayton cycle depends on the compression ratio which depends on the gas’s temperature entering the turbine. If the inlet temperature of gas increases, the efficiency of the Brayton cycle increases. However, the inlet gas temperature is limited due to the physical properties of the turbine blades.

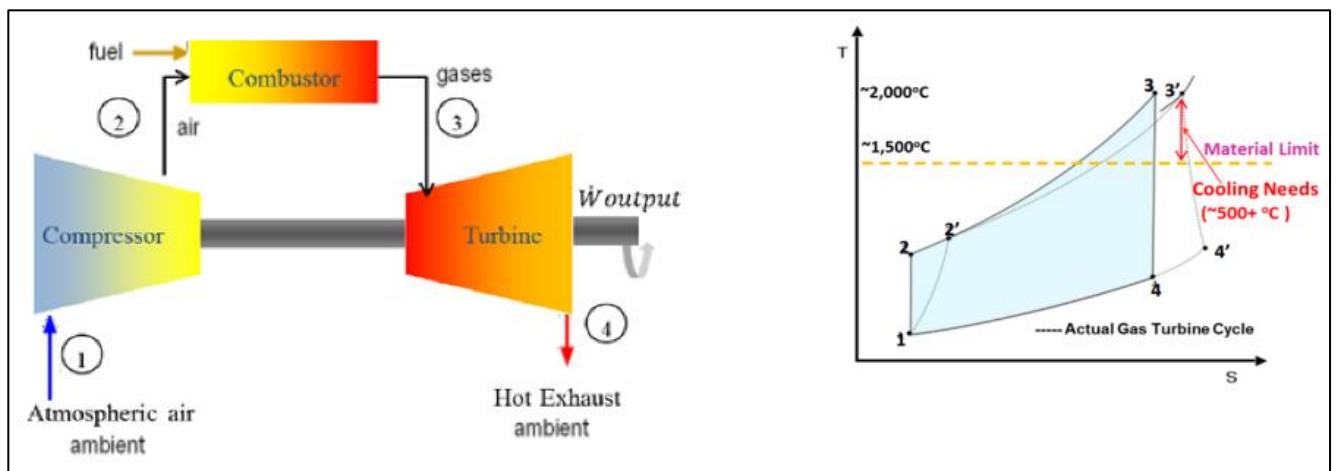


Figure (1.1): Schematic diagram of the Brayton cycle [2]

It is desirable to push the cycle efficiency of the gas turbine as high as possible. One method to achieve that is to increase the gas temperature at the turbine inlet ( $T_3$ ) as shown in figure (1.1). The increase in turbine inlet temperature is limited in practice by the capability of the metal alloys from which the turbine components are made (combustion liners, vanes, and blades). The component operating temperature must be maintained well below the material melting temperature. The turbine inlet temperature is an indication of gas turbine power output. It can be increased in three different ways:

- (i) Developing of cooling techniques.
- (ii) Using of thermal barrier coatings.
- (iii) Using high performance materials [46].

Blades of gas turbine operate under severe stress conditions induced by high gas temperatures and high rotating speeds. There are three main methods protecting the blades:

- (i) Thermal barrier coatings (TBCs)
- (ii) Internal cooling.
- (iii) External cooling.

In general, gas turbine cooling is achieved by bleeding some relatively cool air from the compressor and using it inside the gas turbine blades to remove heat from blade. The cooling air flows through internal cooling passages inside the blade. These passages are specifically designed to maximize the heat transfer. In modern gas turbine blades, this is usually done by the use of contact area enhancers and turbulence promoters, such as ribs and pin-fins in the passages. Some of this cooling air is ejected onto the

surface of the turbine blade to form an insulating film with the goal of reducing contact of the blade with the hot mainstream gas [3].

There are different methods used to cool a modern gas turbine blade such as film cooling, rib turbulators, jet impingement, shaped internal cooling passages, dimple cooling, as shown in figure (1.2). The pin-fin is used to cool trailing edge. While rib turbulators are employed to cool the internal passages, and jet impingement is employed to cool the leading edge.

Many efforts worldwide were established to press the increase in the thrust to weight ratio of gas turbine engines in the aerospace industry field. To improve the efficiency of combustion and reduce fuel consumption, gas turbine engine operating temperature can attain as high as 1350 °C. Such a high operating temperature needs the use of many advanced structural materials, extensive cooling of components, and adoption of various coatings. Thermal barrier coatings (TBCs) have successfully been used in gas turbine engines for increasing operating temperature and improving efficiency of the engine. Over the past three decades, a variety of TBCs materials and TBCs deposition techniques have been developed. Newly, nanostructured TBCs grow with the potential of commercial applications in various industries [4].

### **1.3 Internal Cooling**

Several cooling systems are used to improve heat removal from the turbine blade. These arrangements are selected according to which region of the blade is required to be cool. Figure (1.2) represents the common efficient applications of turbine internal cooling which used in modernistic turbine blades.

In a turbine blade, it is found three major internal cooling region. zone within leading edge was cooled by utilizing impingement cooling. Central region is cooled by air ducted into serpentine passages which are usually fitted with ribs. Finally, the trailing region provided with an arrangement of pin-fins.

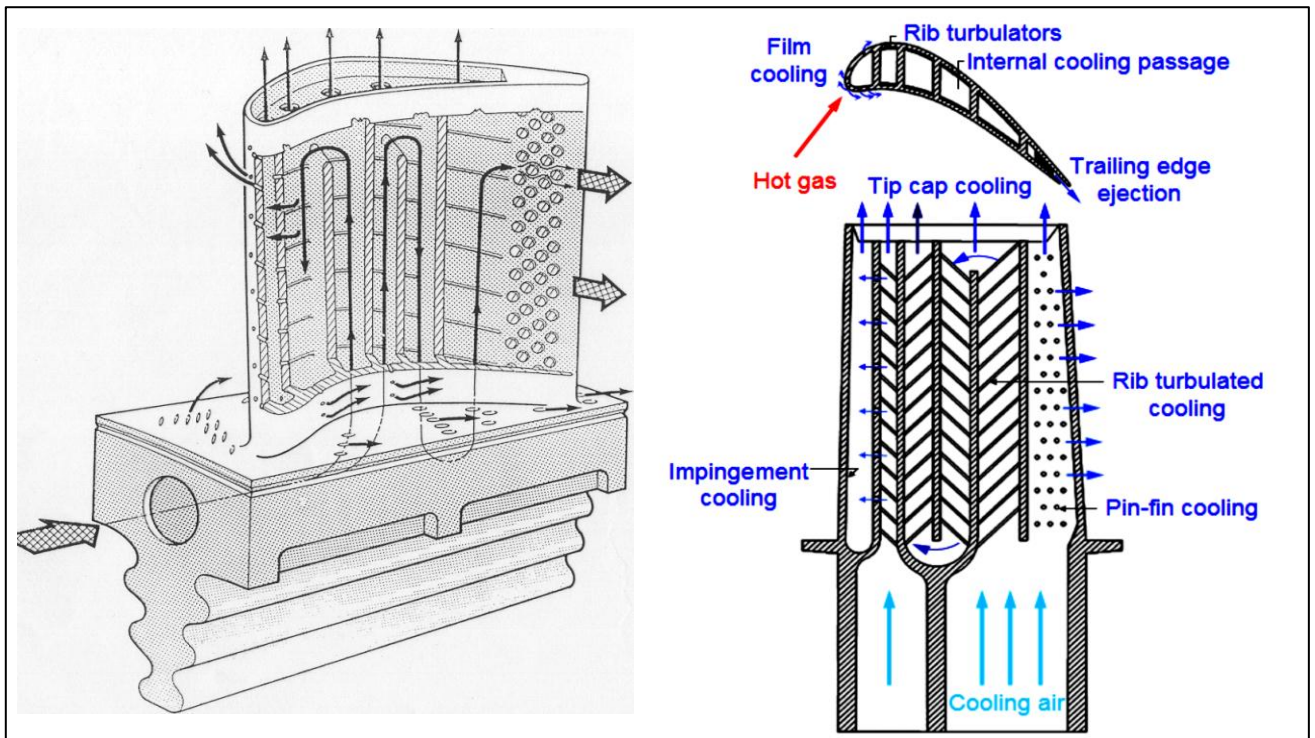


Figure (1.2): Cooling concepts of a modern gas turbine engine [5]

Passages having ribs turbulators on the interior walls are utilized near the central part of the turbine blades. Restated rib turbulators are cast into the serpentine passage to enhance the heat transfer coefficient. Rib turbulators have a vast variety of widths, heights, shapes, angle with the air flow and placement in the internal cooling channel. Each arrangement has its private benefits and limitations in terms of heat transfer coefficient improvement and produced losses.

### 1.4 Rib Turbulated Cooling

To improve the heat transfer in precedent advanced gas turbine blades, repeated rib turbulence promoters are used. The ribs are manufactured by casting it on the two opposed walls of internal cooling passages. In special cases ribs are made on one side to handle the external loads increasing at pressure and suction sides. Figure (1.3) shows a section of ribs presented in the channel.

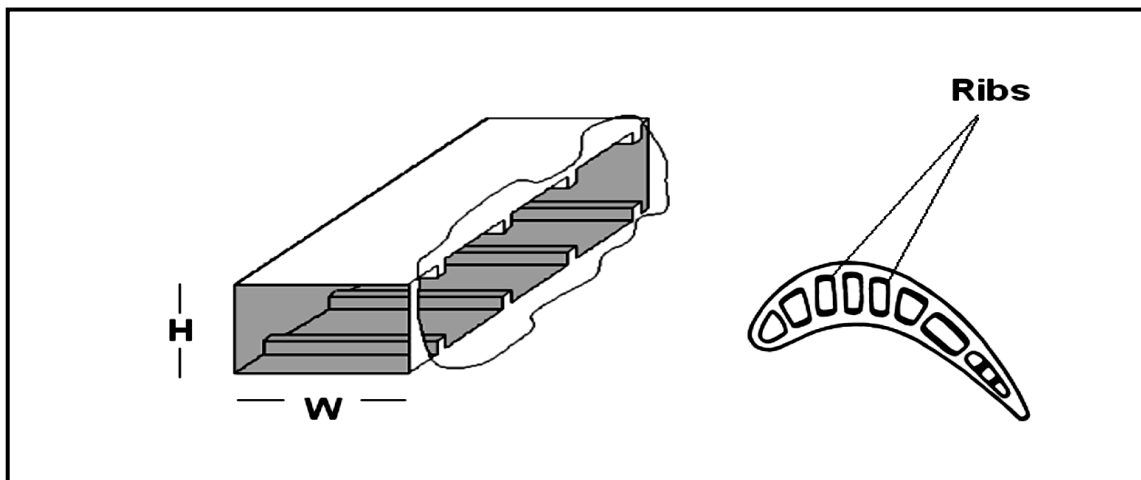


Figure (1.3): A ribbed channel [6]

Chandra et al. [7], Han [8] and Han et al. [9] have shown that there are several geometrical parameters that change the heat transfer coefficient. The parameters include blockage ratio, reciprocal ribs positioning, passage aspect ratio, rib shape, angle of attack, and rib pitch to height ratio.

Due to the presence of the ribs, the flow is separated into two streams: one on top of the rib and the other between the ribs. Figure (1.4) shows the flow separation and reattachment due to the presence of ribs. The boundary layer is disturbed as well as the turbulence of the flow rises due to separation and reattachment. The mixing process cool down wall temperature by absorbing heat. These two phenomena improve of heat transfer rate.

Thermal energy is transfer from the outer surfaces of the turbine blades to the interior regions by conduction, then, it is extracted by internal cooling.



The internal cooling passages are frequently displayed as short rectangular or square channels with different aspect ratios.

The aim of presenting the ribs at regular spaces is to improve the heat transfer rates. Ribs are manmade protrusions that are sited in a controlled technique along the walls. Separation in the flow caused by ribs causes increasing in the friction loss. The improvement of the heat transfer has a drawback in the rising pressure drop which sometimes be several times larger when it is compared with the smooth passage case[10].

The thermal performance of the fitting rib in the channel depends on the pressure drop and the heat transfer. These two factors are related to the rib height ( $e$ ). Although ribs may be fixed at a varying orientation, most researches concentrate on the ribs placed orthogonally (at 90 degrees) to the mainstream flow. The rib width and the space between the two following ribs, the pitch ( $p$ ), has great importance [10].

The heat transfer performance in the ribbed channel also depends on the rib shape, Reynolds number, cool air and the channel aspect ratio. When the cool air moves over the ribs, the flow separates and attaches as exposed in the figure (1.4).

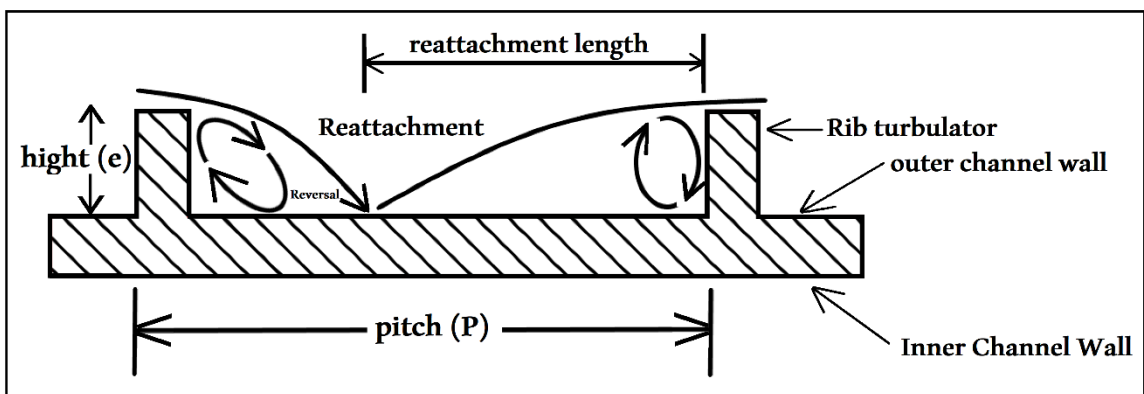


Figure (1.4): Rib position on the wall and turbulent flow with separation and reattachment flow

The heat transfer coefficient of the channel fitted with ribs increases due to the reattached and separated boundary layer, and produces the secondary flow which adds improvement to the heat transfer from the wall to the coolant, also causes turbulent mixing in the passages leading raise the flow velocity [10].

The repeated-rib surface can be classified as a roughness geometry which may cause a problem in boundary layer separation and re-attachment. As seen in the figure (1.5) the large spacing of the rib makes the flow detaching and developing a recirculation zone downstream of the rib. Moreover, the flow reattaches 6-8 rib heights downstream from the separation point. The experimental measurements in the studies [11 and 12] show the maximum heat transfer occurs effect of the channel aspect ratio and at  $p/e=10$ .

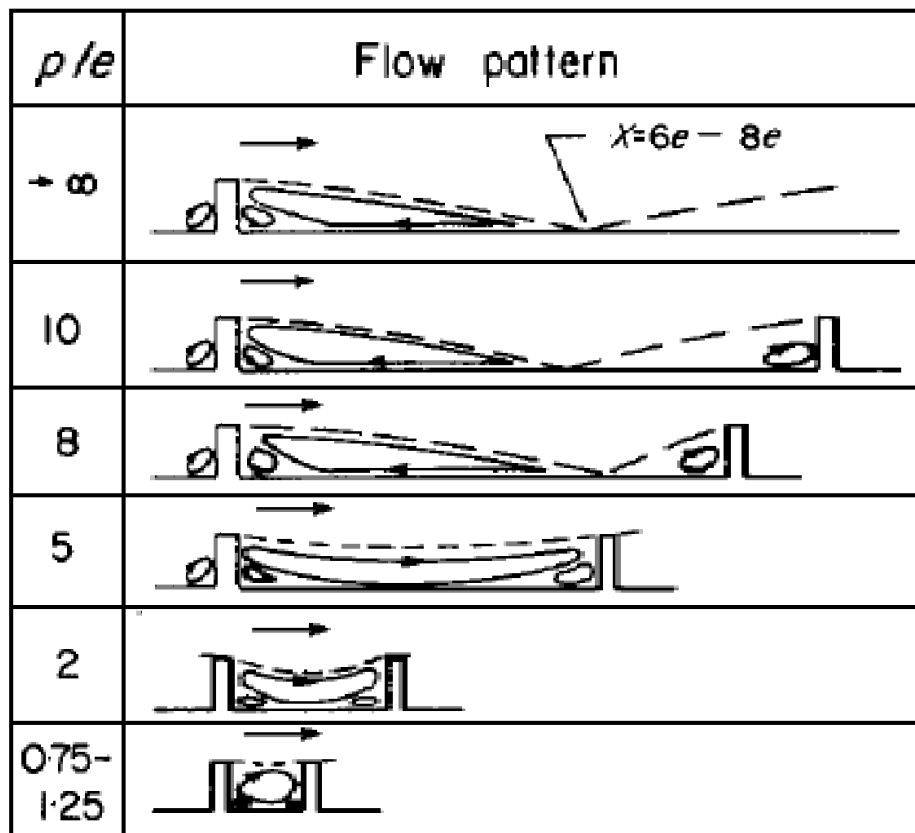


Figure (1.5): Flow pattern as a function of  $x$  [13]

### 1.5 Thermal Barrier Coatings (TBCs) in Gas Turbines

Blades usually coated with thermal barrier utilized for protecting the components of the super alloy from the stream hot gas in the gas turbine used in marine propulsion, power generation, and aircraft propulsion, and as shown in figure (1.6) a usual engine of gas turbine and the TBCs coated turbine blade. The persistent is necessary for increasing efficiency of a gas turbine in which the inlet temperature of the turbine becomes higher than desired. For instance, a temperature in commercial aircraft and land-based power generation gas turbine engines and rocket hot sections and fighting aircraft turbines reach 1500 °C and 1600 °C, respectively [14]. Clearly, a melting point of nickel-based super-alloys is about 1300 °C. To raise the turbine inlet temperature, three important developments should be aproched:

- Technology of airfoil cooling.
- High-performance materials.
- Thermal barrier coating [15].

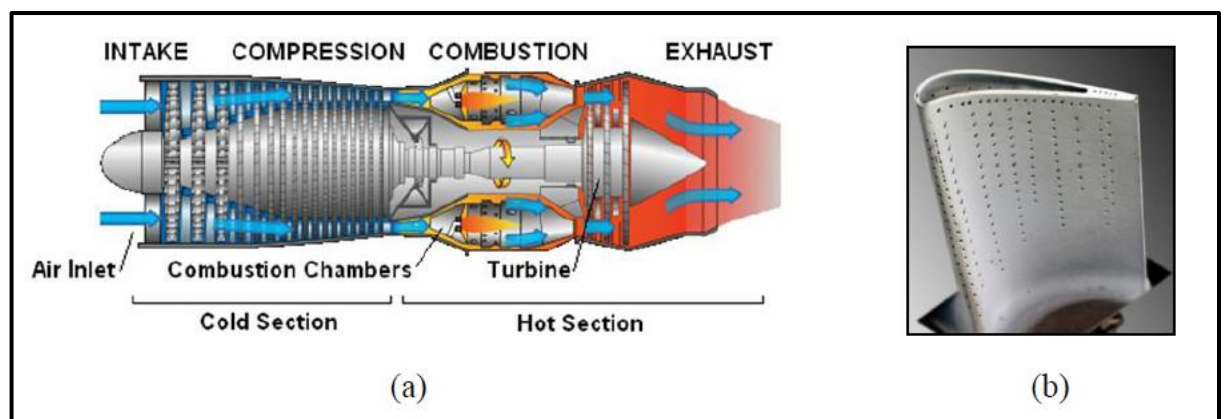


Figure (16.): (a) Gas turbine engine [16]; (b) TBCS coated turbine blade [4]

Although composites of ceramic matrix are promising turbine materials, they are still below their immature stage, and in the foreseeable future, no materials can compensate nickel-base super alloys as the turbine materials. With the well-developed air cooling design, the internal parts air cooling combined with the external film cooling can decrease the metal temperature up to (200-300) °C [14]. However, it reduces the engine efficiency by fuel consumed to pump and compress the cooling air through cooling passages and increase the complication and engines manufacture cost by fabricating internal passages within the airfoils and holes or slots for cooling gas ejected out to the external surface of the turbine vanes or blades [17]. The metal surface temperature can be reduced by using TBCs more to (100-200) °C., and preserve the super alloy components from hot gases erosion and corrosion. That results increase in the efficiency, energy, and durability of gas turbine engines [18]. Therefore, thorough studies have been focused to improve the TBCs characteristics.

As a result of the difficult operating conditions of the TBCs, each of the next phenomena happen and effect with each other : oxidation, diffusion, phase transformation, radiation, sintering, creep deformation, fracture, thermal expansion, thermal conduction, and fatigue [19]. During the last ten years, intensive researches have been focused on TBCs failure mechanisms. Also, they focused on improvement of thermal insulation ability, stability at larger temperatures with creating novel microstructures new materials, and development of coating production technologies, for the conventional (YSZ) worked below 1200 °C for a long period [20,21]. With continued development, the thermal radiation and the working temperature of TBCs were performed an increasingly important performance of the whole heat transfer as a result of its power dependent on temperature. Several studies concentrated on thermal radiation characteristics of standard (YSZ TBCs)

and enhancement the reflectance of the coating by designing multilayer-structured TBCs and control of fabrication parameters [22]. Few other researches focus on radiation properties of new TBCS materials.

### 1.6 Objective and Plan of the present study

1. The major objective of this study is to enhance the cooling system using in gas turbine blades.
2. This will be accomplished by simulation of the cooling passages as a channel that allows experimental work. Hence, numerical and experimental investigation of flow and heat transfer in a channel fitted with different configuration of ribs is done as in table (2.1).
3. The chosen flow conditions simulate those taking place at the gas turbine blade. Four elliptical channels with different aspect ratio (AR=1,1.3,1.6, and 2), and different configuration of ribs are chosen and compared with the smooth channel case.
4. All cases include numerical and experimental investigation of flow and thermal performance of ribs exposed to constant surface temperature (673 k), with air as the working fluid at different Reynolds number ( $Re = 11000, 13500$  and  $16000$ ).
5. Then coated the channel of the best case with composite nanomaterials ( $Y_2O_3$  and thermal painting) and compared the results with the same cases without coating. Analysis and discussion of results are done for final conclusions and recommendations.

# **CHAPTER TWO**

## **LITERATURE REVIEW**

## CHAPTER TWO

### LITERATURE REVIEW

#### Introduction

The numerical and experimental literatures served in this chapter are interested in the effects of different shapes of rib turbulators fitted with four aspect ratio channel with different Reynolds number for improvement of heat transfer. Also, it has reviewed the effect of rib configuration on heat transfer and flow characteristics.

#### 2.1 Numerical Studies

**Veysel Ozceyhan (2008)** [23] performed numerical research to examine the heat transfer augmentation in the tube fitted with a ring having triangular cross sectional ribs. Three various rib thicknesses were taken for a numerical analysis. The air as a working fluid and applied uniform heat flux on the outer surface of the wall of a tube. Reynolds number ( $Re$ ) of this search was changes from 8000 to 36000. ANSYS-FLUENT 6.1 was utilized such as numerical calculations with standard ( $k-\epsilon$ ) turbulence model used successfully to administer these models. The results shows that the greatest overall heat transfer enhancement ratio of (1.34) was achieved for  $(e/D) = 0.75$ .

**Yongsiri et al. (2014)** [24] performed numerical investigation to enhanced heat transfer on turbulent flow through a rectangular channel which roughened by inclined discrete ribs. Numerical results of turbulent flow and heat transfer in a channel fitted with inclined detached ribs were displayed in the research.  $Re$  was varying from 4000 to 24000. The pressure

loss, heat transfer, and thermal performance for using ribs with various angle of attack ( $\theta$ ) for  $0^\circ$ ,  $15^\circ$ ,  $30^\circ$ ,  $45^\circ$ ,  $60^\circ$ ,  $75^\circ$ ,  $105^\circ$ ,  $120^\circ$ ,  $135^\circ$ ,  $150^\circ$  and  $165^\circ$ , were investigated and compared with rib of angle( $\theta$ ) =  $90^\circ$ . The result shows that the influence of angle of attack is trivial when Re is low. In contrast, when Re is high, the ribs with  $\theta=60^\circ$  and  $120^\circ$  would be more effective in thermal performance and heat transfer.

**Altaie et al. (2015)** [25] performed a numerical study of heat transfer enhancement in a circular tube with rectangular open rings. The analyses used forced convection with turbulent flow of cooling air with a velocity of (10 m/s) in a tube of steel with 0.5 m long and 30 mm in diameter with 15 mm thickness. The outside surface of the tube has a constant temperature of 1400, 1200 and 1000 K. Combination k- $\epsilon$  model was used in simulating turbulence by program ANSYS-FLUENT 14.5. Tube was fitted with open ring having a rectangular cross-section and (p/e) was 10. It was found that fitting ribs inside tube increase heat transfer as compared with smooth tube also increase in the thermal performance.

**Aditi et al. (2016)** [26] conducted a numerical investigation for the influence of rib height on friction factor and heat transfer in a square channel roughened with inclined ribs having a gap. The model was validated depending on a previous experimental study using forced convection heat transfer and friction factor characteristics of a ribbed surface with different rib height of separate inclined ribs. Inclined ribs with a gap were fixed on the bottom and top wall of the square channel. Re ranged from 5,000 to 40,000, relative roughness pitch (p/e) was 10. The influence of height to hydraulic diameter ratio of five ribs on heat transfer with regard to Nusselt number (Nu) and friction factor. The result shows that varying ( $e/D_h$ ) affect on friction factor, and Nu. The best heat transfer and thermal performance reached (2.18) in the study.



**Sourabh Kumar (2016)** [27] Studied the influence of secondary flow as a result of the existence of ribs in heat transfer. This was accomplished by casting two types: continuous repeated and broken v-shape in the square passage in the core of the blade. Two different combinations of 600 V and broken 60° V ribs in the passage were studied. The research obtained data of average Nu into the ribbed channel for (Re=56000). Large-Eddy simulation was accomplished on the continuous and broken V arrangements to analyze the flow model inside the channel. The results pointed out that ribs were essentially responsible to vortex generation and improvement in hat transfer.

**Deepak Kumar Patel (2016)** [28] performed a numerical investigation for the three dimensional simulations to study fluid flow characteristics and heat transfer of a rectangular channel employing ANSYS-CFX. Characteristics of heat transfer was investigated for Re varying from ( $8 \times 10^3$  to  $18 \times 10^3$ ). A model geometry was created in CATIA V5 R20; then, it was meshed, analyzed and post processed utilizing ANSYS CFX software. Heat transfer characteristics and fluid flow of various rib shapes were simulated, and the results obtained using k- $\omega$  model. The rectangular channel had AR, channel length,  $D_h$  and (p/e) was 5, 550 mm, 66 mm, 10, respectively as shown in the figure (2.1). Three models of the rectangular channel were modeled with a bottom section of the channel provided by the aluminum plate. The plate was roughened with three various rib configurations. Other surface of the aluminum plate was kept with steady heat flux (1000) W/m<sup>2</sup>. The reasonable variation was observed in the heat transfer simulation data of various ribs shape. The researcher noticed that there was a notable variation in friction factor, heat transfer rate, friction factor ratio, Nu ratio and the thermal performance factor. Also, the study found that that the change on rib configuration fixed in the rectangular channel could improve the heat transfer rate.

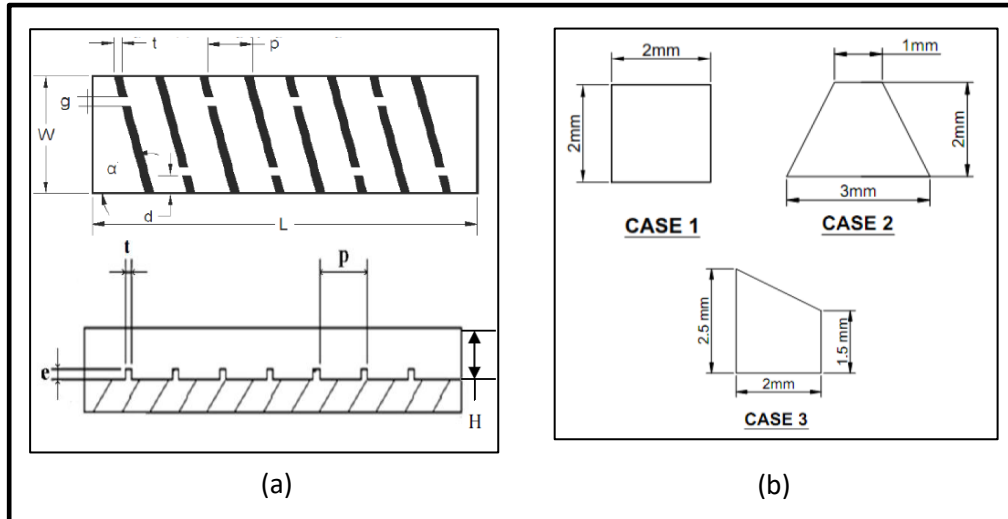


figure (2.1) (a) Physical geometry of rectangular duct (b) shape of the ribs

**Arkan Altaie and Mohammad J. Kadham (2016)** [29] performed a numerical study of heat transfer characteristics of horizontal square channel 500 mm in length using internal square-circle ribs of 7.5x7.5mm cross section ribs spacing =75 mm, with air as the working fluid.  $Re$  was set to  $34.267 \times 10^3$ . The steel channel (ASM4120) was subjected to different constant surrounding hot air temperatures (673, 773 and 873 K). temperature was increased by ( $\Delta T=9, 13$  and  $15$  K) for using ribs at constant surrounding air temperature of (673, 773 and 873 K), respectively. Increasing the surrounding air temperature increasing the coolant air temperature at the channel center line. However, it had no effect on the coolant air velocity. Using ribs increases fluctuation in coolant air velocity, so that temperature of coolant air is increased, and so heat transfer rate will be enhancing.

All mentioned studies were carried out using workbench program Fluent14.5 by using  $K-\epsilon$  model.

## 2.2 Experimental Studies

**HAN et al. (1988)** [30] studied the compounding effect of using different angle of attack of rib and channel aspect ratio on heat transfer coefficient distribution in a rectangular channel. Where the ribs fixed on the upper and lower side of the channel, air flowed with  $Re=10000$  to  $60000$ , angle of attack of the rib varying from  $30^\circ$  to  $90^\circ$ , and the aspect ratio was ranging from 1 to 4. The results showed that the effect of varying angle of attack was slightly in the channel with aspect ratio (2). Thermal performance was changing from 1.05 to 1.85 depending on the angle of attack and channel aspect ratio. Semi-empirical friction heat transfer and heat transfer correlations were obtained for an account for rib spacing, rib angle, channel aspect ratio,  $Re$ , and rib height. The results could be utilized in the designing channel of the blade of the gas turbine.

**Amro et al. (2007)** [31] performed an experimental investigation of the heat transfers in a triangular channel having rounded edge which roughened with ribs as a model that simulates the passage in the blade of gas turbine. The method of a transient liquid crystal was used to measure the heat transfer. Experimental results are reported for a number of new 3D rib configurations for Reynolds numbers between 50 000 and 200 000. The results showed that the ribs of  $60^\circ$  were better than the ribs of  $45^\circ$  in heat transfer. Also, ribs of  $60^\circ$  provided high friction factors. The enhancements of overall heat transfer depend on the rib and its angle.

**Sachin Baraskar et al. (2012)** [32] presented an experiment research of friction factor properties and heat transfer of fixing ribs on one wall of the rectangular channel. The channel was designed with the aspect ratio of 8, ribs with and without gap and with ribs spacing to height ( $p/e$ ) =10. Heat transfer and friction properties of this ribbed channel were compared to the smooth channel with similar condition. The influence of rib was studied for

a range of  $Re$  from 5000 to 14000. The maximum enhancement in Nusselt number and friction factor is observed to be 2.57 and 2.85 time of that of the smooth duct.

**Umesh Potdar et al. (2012)** [33] presented an experimental work in the stationary square channel with v-shaped and 45° inclined arc of circle rib turbulators to find the thermal and hydraulic performance. Ribs were fitted on opposite walls. The heat transfer coefficient and frictional factor were calculated. Stationary channel with aspect ratio one ( $W/H=1$ ) was considered in the analysis. The thermal and hydraulic performance were measured by calculating the  $Nu$  and frictional factor. Square ribs ( $w/e = 1$ ) were considered as the baseline configuration. Rib geometries involved three ribs: height-to-channel hydraulic diameter ratios (blockage ratios) ( $e/D_h$ ) of 0.083, 0.125 and 0.167, as well as rib spacing (pitch to height ratio) of 10. The heat transfer performance for the channel was calculated with  $Re$  ranging from  $45 \times 10^3$  to  $75 \times 10^3$ . The results obtained for the channel with different ribs configuration proved that the increase in rib width increases the thermal performance of the channels. The optimal cooling configuration was obtained by combined effect of rib width, rib spacing and flow parameters.

**Shailesh et al. (2013)** [34] performed an experimental investigation for ribs with/out gaps,  $(p/e) = 10$ ,  $(e/D_h) = 0.06$ , two attack angles ( $60^\circ$  and  $90^\circ$ ) and with  $Re = 5 \times 10^3$  to  $40 \times 10^3$ . The thermal heat transfer performance of continuous and discontinuous ribs with  $(d/w) = 0.2$  and  $g/e = 1$  was investigated under the same conditions. The results of friction factor ratio and heat transfer were obtained from the ribbed channel and compared with the channel without ribs. The result shows that the performance of inclined ribs was better than the transverse ribs with and without gaps. The best case of thermo-hydraulic performance was found in the case of inclined ribs with gaps at  $Re = 5000$ , and it was about (2.03).

**Heeyoon Chung (2014)** [35] performed an experimental investigation of the influence of channel aspect ratio and an intersecting rib on performance in rectangular channels with two angled ribs and three channel aspect ratio from 1 to 4. In the study using three types channels having the same hydraulic diameter ( $D_h=40\text{mm}$ ) but different in channel aspect ratio ( $AR=1,2, \text{ and } 4$ ) . The  $Re$  ranged from 10000 to 20000 in a rib-roughened channel with angled ribs. The result shows that intersecting rib raised the thermal efficiency for every case. Despite the channel aspect ratios and  $Re$ , the effect of the intersecting rib was strongest for  $AR = 2.0$ .

**Srivastava and alt. (2018)** [36] performed an experimental study for the influence of angle of attack on the forced convection heat transfer and friction factor of the ribbed channel. The square channel ( $AR=1$ ) was ribbed on its bottom and the top wall with the square-shaped rib as v-rib and having a gap on its length. The attack rib angle ( $\theta$ ) was increased from  $30^\circ$  to  $75^\circ$ , the ratio of width( $W$ ) to the height of the channel ( $W/H$ ) was 1, relative roughness pitch ( $p/e$ ) was 10. The flow rate of air corresponded of  $Re$  was ranged from  $5 \times 10^3$  to  $40 \times 10^3$ . The pressure drop and heat transfers of different configurations were manifested in the form of friction factor and  $Nu$ . The result showed that the changed the angle of attack has an effect on friction factor and  $Nu$ . The highest increase of friction factor ( $f$ ) and  $Nu$  were 8.1 and 4.7 times that of the smooth channel, respectively. As the results, the highest performance of 2.6 times that of smooth channel, was given for broken v-shaped ribs with angle of attack flow as  $60^\circ$  .

**Sebastian Ruck (2018)** [37] performed an experimental investigation for heat transfer measurements to examine the thermal-hydraulics in the square, round-edged ribbed channel ( $p/e = 10$ ), the ribs fixed on one wall at  $Re$  ranged from 50000 to 250000. Three shapes of ribs were investigated: transverse ribs, transverse ribs with square cross sections and upstream

directed  $60^\circ$  v-shaped ribs with round-edged rib front and rear surfaces. The thermal performance, Friction factors, roughness functions, and ratios of Nu, were manifested. The upstream directed v-shaped ribs having the highest thermal performance and best heat transfer.

### 2.3 Numerical and Experimental Studies

**Mohammad et al. (2002)** [38] presented numerical predictions of a three dimensional flow and heat transfer for a two-pass rectangular channel with  $45^\circ$  rib turbulators and channel aspect ratio of 2:1. The rib height to hydraulic diameter ratio ( $e/D_h$ ) was 0.094, and the rib spacing to height ratio ( $P/e$ ) was 10. Two channel orientations were studied:  $\theta = 90^\circ$  and  $135^\circ$  corresponding to the mid portion and the trailing edge regions of a turbine blade, respectively. The researchers investigated the effect of the channel aspect ratio and the channel orientation on the nature of the flow and heat transfer enhancement. A multi block Reynolds-averaged Navier-Stokes (RANS) model was employed in conjunction with a near wall second moment turbulence closure. The convective transport equations for momentum, energy, and turbulence quantities were solved in curvilinear, body-fitted coordinates using the finite-analytic method. The numerical results compared reasonably well with experimental data for both stationary and orientation rectangular channels with rib turbulators at Re of 10,000.

**Mi-Ae Moon (2014)** [39] presented an experimental and numerical investigation to estimate performances for heat transfer of different rib shapes. The friction loss and heat transfer performance for ribbed rectangular channels with an assortment of rib configurations were analyzed by employing equations of 3D Reynolds averaged Navier Stokes. The study used numerical simulations for sixteen different shapes: isosceles triangular, inverse right angle triangular, fan shaped, right angle triangular, house

shaped, square, reverse pentagonal, reverse cut trapezoidal, pentagonal, cut trapezoidal, reverse right angle trapezoidal, reverse boot shaped, right angle trapezoidal, boot shaped, semicircular ribs, and isosceles trapezoidal as shown in the figure (2.2). The proportion of width, height, and pitch of the rib to the hydraulic diameter of channel were established to, 0.047, 0.047 and, 10 respectively. The speciale Sarkar gatski pressure–strain model with the Reynolds-stress model were utilized to analyze the turbulence. Under the same conditions, the results were validated by computations of the area-averaged Nu by comparison to the experimental data. The influence of the ratio of rib pitch to the width and Re on the performances of different ribs were additionally studied for Re=5000 to 50000 and pitch to the width from 5 to 10. The result showed that the best performance heat transfer with a pressure drop was the boot shaped rib.

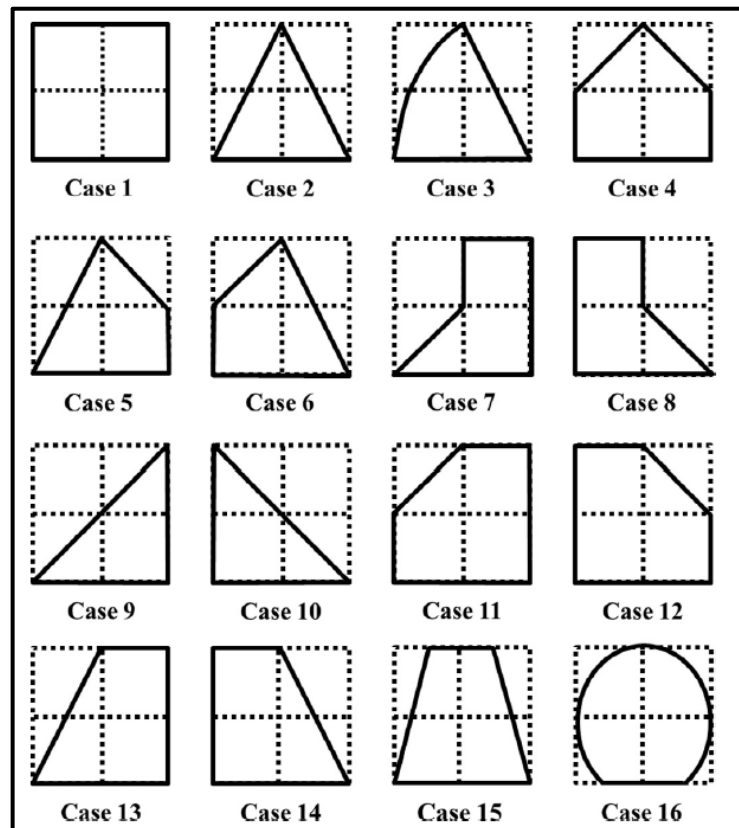


Figure (2.2) Various cross-sectional rib shapes.

**Hasan Jorunt (2014)** [40] presented an experimental and numerical investigation of the heat transfer properties of a circular 500 mm long pipe using internal ribs in six cases: rings of different heights, open ring, spiral square ribs, spiral slot, ring of same heights and square ribs (namely: 1,2,3,4,5, and 6). The seventh case was a pipe without ribs for pitch =100 mm. Coolant air enters the test section at 300 K with constant surface temperatures (573, 873, and 1173 K) and  $Re=31170$ . The heat transfer coefficient enhancement for internal ribs was higher than that for plain pipe for the same conditions. The results showed that using rings with different heights removed more heat than the other cases compared with smooth tube. These results were all compared with case 7 (smooth tube).

**Rashid (2015)** [41] presented an experimental and numerical investigation for the heat transfer of a circular 500 mm long tube using internal ribs in eight cases. these cases include helical ribs with square cross section, helical ribs with rectangular cross section, rings, helical ribs with triangular cross section, rings (letter G shape), rings with middle arm, open rings (letter C shape) and rings with triple arms. These cases were called case: 1, 2, 3, 4, 5, 6, 7 and 8 for pitch =85 mm. Coolant air enters the test section at 300 K. The test section was kept with constant surface temperatures: 673, 773, 873 and 973 K, and different  $Re$  of  $24.253 \times 10^3$ ,  $26.119 \times 10^3$  and  $27.984 \times 10^3$ . The heat transfer coefficient enhancement for internal ribs was higher than that for smooth tube for the same conditions. The results showed that using rings with different heights removed more heat than the other cases compared with smooth tube. The obtained numerical.

**Peter Forsyth (2017)** [42] presented an experimental and numerical research of improvement and combination of heat transfer and aerodynamic flows in a model internal cooling channel fitted with ribs for giving view to the secondary flows development. Static instrumentation was installed at the



end of a long smooth passage and used to measure local flow features in a series of experiments where ribs were incrementally added upstream. This improves test turnaround time and allows higher-resolution heat transfer coefficient distributions to be captured, using a hybrid transient liquid crystal technique. The composite distribution of heat transfer coefficient of the passage is stated. Prominently, the behavior is governed by the development of the secondary flow in the passage throughout. Examination data of the aerodynamic and heat transfer were together compared to numerical simulations developed employing a commercial computational fluid dynamics solver. It was possible to examine the veracity of the underlying assumptions of the experimental strategy via conducting numbers of simulations. The results capture the developing size and strength of the vertical structures in secondary flow. The local flow field was shown to be strongly coupled to increase of the heat transfer coefficient. However, the numerical simulations failure to catch few enhancements on the smooth and ribbed surfaces. In general, by comparing the numerical and experimental data, there is a good consensus in heat transfer coefficient prophecy.

**Al-Jibory (2018)** [43] presented an experimental and numerical study for the effect of using circular rib in rectangular channel on flow and heat transfer. The researcher used ribs to enhance the cooling of gas turbine blade. The boundary conditions set of cool air at 300 k, hot surrounding air at 400 °C, Re of the air at 7901. The dimensions of the channel were (30x60 mm) cross section, length of 500 mm and the circular ribs with  $p/e=10$ . ANSYS FLUENNT 14.1 was used to for simulation and analyses. The results were obtained for thermal performance factor, temperature distribution of the coolant air at centerline of the channel, temperature of inner wall surface of the channel, velocity, and temperature distribution contours. The better result was found for the ribs with fins.

## 2.4 Coating studies

**Al Taie (1990)** [44] presented an experimental work on thermal barrier coatings (TBC) on gas turbine blade at turbine inlet temperatures (973, 1073 and 1173) K. The study used six TBC systems. It found that C-YPSZ was the best insulator. However, blades coated with zirconia suffered loss near the edges, and the two alumina based systems were lost more than a blade. It was demonstrated that thickness of 0.3 mm of C-YPSZ increased the surface temperature by 250 K and decreased metal temperature by 270 K for the turbine entry temperature of 1673 K. Metal temperature reduction was 310 K for a coating thickness of 0.5 mm.

**Arai and Suidzu (2012)** [45] devised a cooling system for the applications gas turbine which had an important advantage by decreasing the quantity of coolant air and rising cooling efficiency. The porous ceramic coating was improved with a spraying plasma process. Thermal conductivity and adhesion strength were measured. The composite of polyester and (8 wt.%) yttrium-stabilized-zirconia was used as the coating material. It was shown that the porous ceramic coating has superior permeability for cooling gas. The strong adherence of porous coating was low at only 20% associated with the thermal barrier coating used in current gas turbine blades. A simulation test of hot gas flow around the gas turbine blade proved the remarkable decrease of the coating surface temperature by the mechanism of transpiration cooling.

**Orhan Aydin, (2002)** [46] used a simplified gas turbine blade model was used for investigating the effectiveness for a new TBC material. The model consists of two concentric cylinders with the high-temperature gas flow in the circular space and with low-temperature fluid in the inner cylinder which outside surface was coated by thermal barrier coating material. The new coating material was silica-based. The study found that

that a gas turbine blade coated with this thermal barrier coating material, causing in improve heat transfer, which in turn enhance power output.

## 2.5 Summary

From the literature reviews, there are many numerical and experimental studies deal with enhanced heat transfer with increasing pressure drop and friction factor for laminar and turbulent flow inside circular, square and rectangular duct with and without using ribs at different shape. As in table (2.1) a three dimensional steady state interior flow is considered in this work.

The present study deals with a numerical and experimental tests in order to study the effect of using four different rib configurations fitted in the different elliptical channel with four different aspect ratios (AR=1,1.3,1.6, and 2) including:

1. Elliptical cross sectional channel fitted with boot ship shape rib. (rib1)
2. Elliptical cross sectional channel fitted with elliptical triangular rib with right angle and with the flow direction. (rib 2)
3. Elliptical cross sectional channel fitted with elliptical triangular rib with right angle and inverse the flow direction. (rib 3)
4. Elliptical cross sectional channel fitted with elliptical rib of two equal legs. (rib 4)

The four types of ribs are illustrated in table (2.2) which contain isometric view, front view, side cross section of rib.

In the numerical simulation, Average Navier-Stokes and Energy Equations were used in the known package Fluent version (16.1) in the turbulent regime with appropriate turbulent model (k- $\epsilon$ ).

In the experimental part of this study, the conducted in four channels with 0.5 m long elliptical channel with the same hydraulic diameter (37 mm)

but the difference in aspect ratio. The experiments were done to investigate the flow and heat transfer characteristic, in the smooth, ribbed and ribbed with and without coating.

## 2.6 Point of originality

The following point of originality are claimed for the present work;

1. Different types of rib geometry were taken (elliptical ribs), different from that mentioned in open literature.
2. The use of different shape cross section channels (elliptical channels).
3. The use of new composite nanomaterials (thermal painting and  $Y_2O_3$  nanoparticles) is also new.

Table (2.1) summarizes the previous research discussed in this chapter and include Researches name, the channel aspect ratio, rib configuration, the rang of Re, the resulted found by researchers

Table (2.1): Summary of numerical and experimental studies.

Numerical Studies						
No.	Researches	Year	channel shape	Rib shape	Reynolds Number	Results
1	Veysel Ozceyhan	2008	Circular channel	ring having triangular cross sectional ribs	8000-36000	improvement heat in transfer ratio was 1.34 after fitted ribs
2	K. Yongsiri	2014	rectangular channel	inclined discrete ribs	4000-24000	The results showed that the effect of using angle of attack ribs in improving heat transfer increased with increasing Reynold number
3	Arkan Altaie et al.	2015	circular	open ring having a rectangular cross-section	35000	results found that fitting ribs inside tube would be increase heat transfer as compared with smooth tube and increase the thermal performance

4	Priyank Lohiya	2015	square	inclined ribs with a gap	5,000 - 40,000	The results showed that varying $(e/D_h)$ effect on friction factor and on Nusselt number. the best heat transfer and thermal performance reach 2.18
5	Surah Kumar	2016	square	Two type : v-shape continuous ,and V-shaped and broken	56000	Improvement in heat transfer after using the two type of rib
6	Deepak	2016	rectangular	Three various rib configuration	8000-18000	Result was found that that the change on rib configuration fixed in the channel effect on improve the heat transfer rate
7	Arkan Altaie and Mohammad J. Kadham	2016	square	circle ribs	34267	Result found that using circular rib in square channel improve thermal performance

### Experimental study

No.	Researches	Year	Channel shape	Rib shape	Reynolds Number	Results
8	J.C.HAN	1987	rectangular	different angle of attacks	10000-60000	Using rib in channel enhance thermal performance from 1.05 to 1.85
9	M. Amro	2007	triangular	different rib configuration	50000-200000	Results found that The enhancements of overall heat transfer depend on the rib and also structure rib angle
10	Sachin Baraskar	2012	rectangular channel	square rib	5000-14000	The best enhancement in friction factor and the Nusselt number was perceived to be 2.85 and 2.57 times of that of the smooth channel, respectively

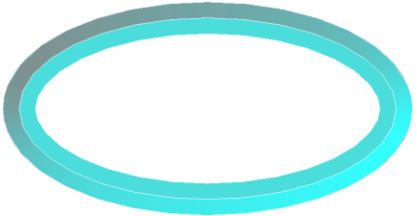
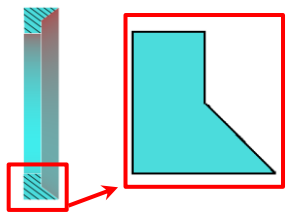

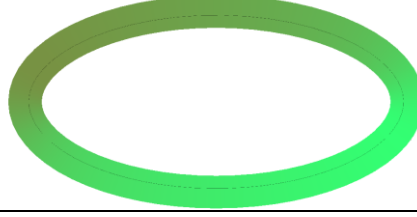
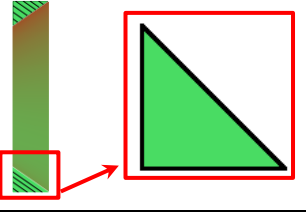
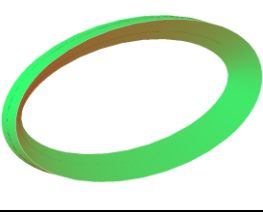
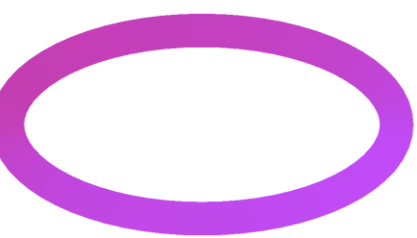
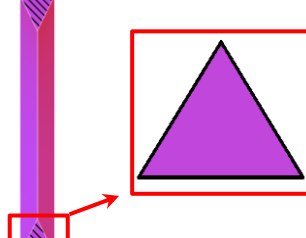

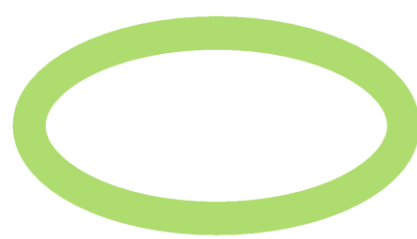
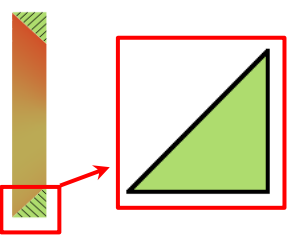

11	Umesh Potdar	2012	square	V-shaped	45000-75000	The results proved that the increase in rib width increases the thermal performance of the channels
12	Shailesh	2013	rectangular	Inclined ribs Rib with and without gap	5000-40000	results were found that the performance of inclined ribs is best than the transverse ribs with and without gaps. The best case of thermos hydraulic performance was found to be the case of inclined ribs with gaps
13	Heeyoon Chung	2014	rectangular channel with different aspect ratio	Inclined ribs	10000 - 20000	Result found that using rib enhance heat transfer performance especially at AR=2
14	K. Yongsiri	2018	square	square v-rib	5000-40000	using rib enhance performance factor to be 2.6
15	Sebastian Ruck	2018	square, round-edged ribbed channel	Three variously shaped ribs	50000 - 250000	result found that V-shaped ribs were the highest thermal performance and best heat transfer
<b>Experimental and numerical studies</b>						
No.	Researches	Year	Channel shape	Rib shape	Reynolds Number	Results
16	Mohammad et al.	2002	rectangular channel	inclined rib	10,000	using rib enhance heat transfer

17	Mi-Ae Moon	2014	rectangular channel	16 different rib configuration	5000- 50000	the result shows that the best performance heat transfer with a pressure drop was the boot shaped rib
18	Hasan Jorum	2014	circular	6 different rib configuration		The results showed that using rings with different heights removed more heat than the other cases compared with smooth tube
19	F. L. Rashid	2015	circular	8 different shape configuration	24253- 27984	The results showed that using rings with different heights removed more heat than the other cases compared with smooth tube
20	Hasan Qahtan	2018	rectangular	circular rib with and without fin	7901	Using rib in channel the better result was found for the ribs with fins
<b>Coating work</b>						
	<b>Researches</b>	<b>Year</b>	<b>Working</b>			<b>Results</b>
21	<b>Arkan Al Taie</b>	1990	used six TBC systems to insulate the turbine blade			found that C-YPSZ was the best insulator.
22	<b>Orhan Aydin</b>	2002	investigate the electiveness of a new thermal barrier coating material to enhancement blade turbine cooling			improve the heat transfer
23	<b>Arai and Suidzu</b>	2012	used porous ceramic coating to insulate the turbine blade			decrease of the coating surface temperature

No.	Researches	Year	Channel shape	Rib shape	Reynolds Number	Results
24	The present work	2018	Four elliptical channel with different aspect ratio from 1 to 2 With and without coating	Four elliptical different rib configurations	11000-16000	1. Cooling was enhanced by different rib geometries, enhancement thermal performance factor( $\eta$ ) was achieved by 211.1 % and 232.1 % without/with coating by composite Nanomaterials.



Table (2.2) four type of elliptical rib of the present work

No. of rib	Front view	Side cross section	Isometric view
Rib 1			
Rib 2			
Rib 3			
Rib 4			

# **CHAPTER THREE**

## **THEORETICAL MODELS AND NUMERICAL SOLUTION**

---

---

**CHAPTER THREE****THEORETICAL MODELS AND NUMERICAL SOLUTION****3.1 Introduction**

Computational Fluid Dynamics (CFD) has been matured in a few aspects and been widely used in industrial applications. There are different algorithms proposed and developed by researchers. Numerical simulation allows the analysis of complicated phenomena without resorting to expensive prototypes. Thus, numerical methods have to be adopted to solve the conservation of energy, momentum, and mass governing differential equations in the Cartesian coordinate system ( $x, y, z$ ). Therefore, a complete numerical analysis is used in the present work to simulate the flow and heat transfer over a channel ribbed with different configurations coated with a thermal barrier to predict the heat transfer characteristics. The computations are achieved by using ANSYS FLUENT 16.1 software.

The next parts of this chapter give a short description of the mathematical and physical governing equations included in various ways of the heat transfer and the fluid flow. The analyses interact the coolant air passing through four cylindrical tubes with elliptical cross-section fitted with different rib shapes. To study the influence on the turbulence model which includes a solution of pair transport equations, the favored model is ( $k - \epsilon$ ). Thus, the numerical techniques will solve those equations in Cartesian coordinate systems.

ANSYS FLUENT version (16.1) software was used in the present work to create a grid of a system geometry and simulate heat transfer outlet from the channels of the sixteen ( $4 \times 4$ ) geometry models. After that a comparison with the effect of coating these pipes with nanocomposite material was conducted.

In this study, the heat transferred from the hot air surrounded the test section tube ( $T_h$ ) to the coolant air ( $T_c$ ) across the tube wall material. Figure (3.1) shows a cross-section of the simulated case which declares the temperature nodes and the in both presenting of thermal coating barrier or without coating. Heat transfers by convection from  $T_h$  to  $T_s$ , by conduction from  $T_s$  to  $T_w$  and by convection from  $T_w$  to  $T_c$ .

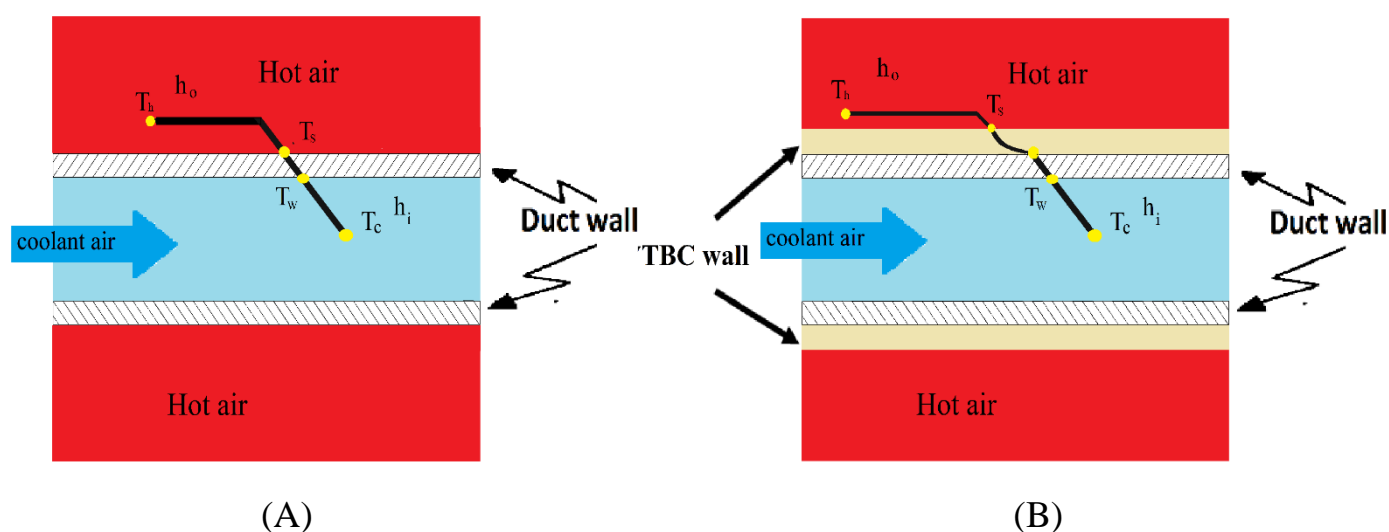


Figure (3.1): Simulated case, (A): Without TBC, (B) With TBC

### 3.2 Physical Model Description

A scheme of the geometrical model of channel used in the study is shown in figure (3.2). It consists of a rectangular box dimensioned (700, 500 and 500) mm of length, width and height, respectively. Also, it includes a constant temperature of hot air, elliptical channels with 500 mm length and 1.5 mm wall thickness and with dissimilar four cross-sections having the same hydraulic diameter with different aspect ratio of major to minor diameter ( $a/b$ ) ( $60 \times 32, 53 \times 34, 46 \times 36$ , and  $40 \times 40$ ) mm. The system geometry was drawn by using AutoCAD 2017. The used channels are provided with different shapes and configurations of ribs as shown in the table (3.1). They were set in the fully developed region and heated under constant hot air temperature. The geometry was created in several steps:

By using AutoCAD 2017 drawing elliptical channels which filling with fluid, with the dimensions as shown in the table (3.1) and in figure (3.4) and drawing the ribs:

1. With the specified dimensions then moved to be fitted internally in the elliptical channel.
2. Export the final model as (ACIS )formula file which that can be imported by ANSYS program.
3. Import the final model volume to FLUENT by (import external geometry and then by generate) to complete other procedures: meshing, setup, solution and results as in figure (3.3).

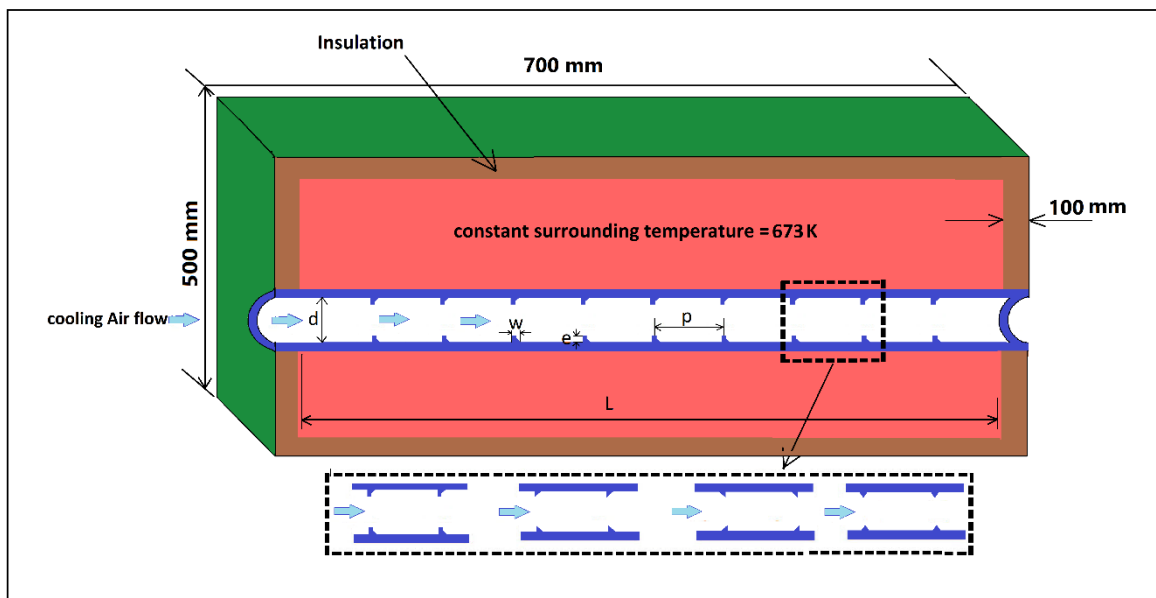


Figure (3.2): System geometry

**Table (3.1): Ribs models**

Case NO.	Dimensions In mm			Ribs Models
	P	e	w	
1	50	5	5	
2	50	5	5	
3	50	5	10	
4	50	5	5	

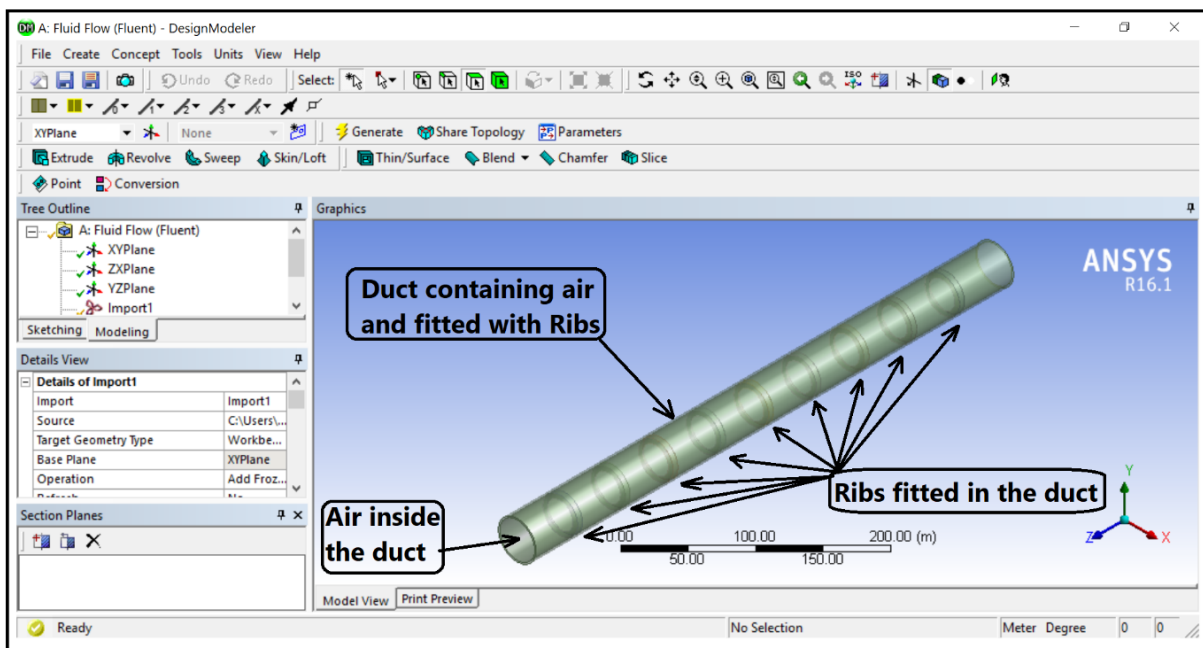


Figure (3.3): The channel fitted with ribs after imported and generation the shape

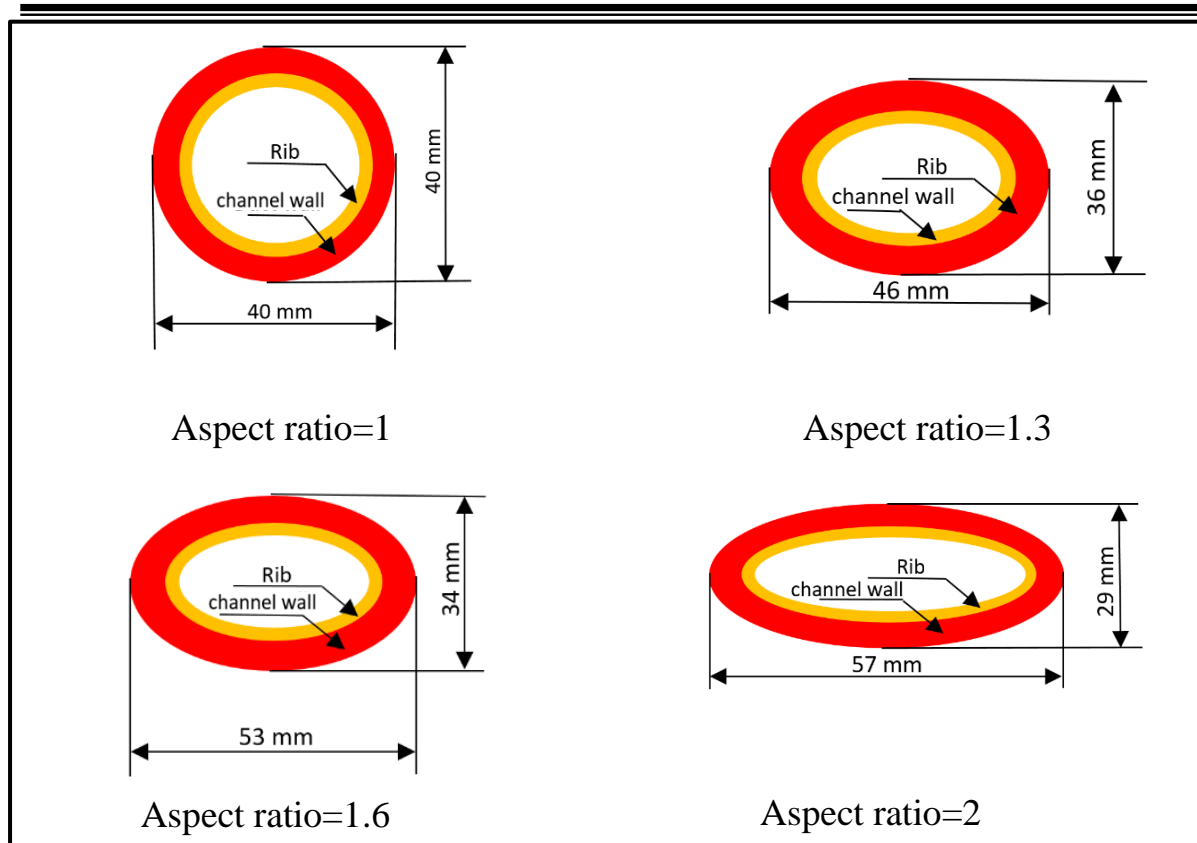


Figure (3.4): Side view of the ribs fitted in an elliptical channel with different aspect ratio

### 3.3 Assumptions

In this study, stainless-steel was considered for the channel material. Air was used as the coolant fluid. The heat transfer and the flow properties are assumed to be as follows:

1. Body forces and viscous dissipation are ignored.
2. incompressible and turbulent flow.
3. Fully developed flow.
4. Newtonian fluid.
5. Steady state.
6. Three-dimensional flow.
7. The radiation effects are neglected.
8. Constant fluid (air) properties.

---

### 3.4 Governing Equations of Fluid Flow

the fluid motion and heat transfer are governed by continuity, momentum, and energy equations. These equations were independently constructed by Navier and Stokes and are called the Navier-Stokes equations. These can be formulated in either a conservative form or in non-conservative form. For a nearly incompressible fluid, the density is constant, and consequently, many textbooks give the Navier-Stokes equations on a density normalized formulation. The Governing equations of continuity, momentum, and energy are solved for turbulent flow [47, 48].

#### 3.4.1 Continuity Equation

The continuity equation describes the mass conservation:

$$\left( \frac{\partial(\rho u)}{\partial x} + \frac{\partial(\rho v)}{\partial y} + \frac{\partial(\rho w)}{\partial z} \right) = 0 \quad \dots(3.1)$$

Where,  $\rho$  is air density, ( $u$ ,  $v$ , and  $w$ ) are the velocity components of the fluid at any position inside the flow field for space  $x$ ,  $y$ , and  $z$ , respectively [49].

#### 3.4.2 Momentum Equations

From Newton's Second Law of Motion, the momentum equations have been derived involving the balance of the forces sum acting on the fluid element. These forces are equal the product between the acceleration and mass of a fluid element. By employing Newton's Second Law on 3-dimensional fluid elements and balancing the forces in all three directions, the following equations were obtained [50]:



---

X – Component

$$\rho \left( \frac{\partial u}{\partial t} + u \frac{\partial u}{\partial x} + v \frac{\partial u}{\partial y} + w \frac{\partial u}{\partial z} \right) = \rho f_x - \frac{\partial p}{\partial x} + \mu \left( \frac{\partial^2 u}{\partial x^2} + \frac{\partial^2 u}{\partial y^2} + \frac{\partial^2 u}{\partial z^2} \right) \quad \dots (3.2)$$

Y- Component

$$\rho \left( \frac{\partial v}{\partial t} + u \frac{\partial v}{\partial x} + v \frac{\partial v}{\partial y} + w \frac{\partial v}{\partial z} \right) = \rho f_y - \frac{\partial p}{\partial y} + \mu \left( \frac{\partial^2 v}{\partial x^2} + \frac{\partial^2 v}{\partial y^2} + \frac{\partial^2 v}{\partial z^2} \right) \quad \dots (3.3)$$

Z- Component

$$\rho \left( \frac{\partial w}{\partial t} + u \frac{\partial w}{\partial x} + v \frac{\partial w}{\partial y} + w \frac{\partial w}{\partial z} \right) = \rho f_z - \frac{\partial p}{\partial z} + \mu \left( \frac{\partial^2 w}{\partial x^2} + \frac{\partial^2 w}{\partial y^2} + \frac{\partial^2 w}{\partial z^2} \right) \quad \dots(3.4)$$

The above Equations show the conservation of momentum in a fluid flow and also known as equations of Navier-Stokes [47, 51 and 52].

### 3.4.3 Energy Equations

The first law of thermodynamics exhibits the exchange of energy for a system which is the result of applied work and heat transfer through that region. In its most complete formulation, the energy equations are given as [47] and [52]:

$$\left( \frac{\partial(\rho u_i T)}{\partial x_j} = \frac{\partial}{\partial x_i} \left[ (\Gamma + \Gamma_t) \frac{\partial(T)}{\partial x_j} \right] \right) \quad \dots (3.6)$$

Where,

$$\Gamma = \text{molecular thermal diffusivity} = \frac{\mu}{Pr}$$

$$\Gamma_t = \text{turbulent thermal diffusivity} = \frac{\mu_t}{Pr_t}$$

### 3.4.4 Reynolds-Averaged Navier-Stokes (RANS)

Numerical analysis of turbulent channel flow has been largely limited to Reynolds Averaged Navier-Stokes (RANS) simulations. This is because of the low computational requirements of such calculations relative to Direct Numerical Simulation (DNS) and Large Eddy Simulation (LES). The form of the Cartesian tensor of the RANS equations gives by [47,48]:

$$\frac{\partial u}{\partial x_j} (\rho u_i u_j) = - \frac{\partial P}{\partial x_i} + \frac{\partial}{\partial x_i} \left[ \mu \left( \frac{\partial u_i}{\partial x_j} + \frac{\partial u_j}{\partial x_i} - \frac{2}{3} \delta_{ij} \frac{\partial u_i}{\partial x_i} \right) \right] + \frac{\partial}{\partial x_j} (\overline{\rho u'_i u'_j}) \quad \dots (3.7)$$

Through time-averaging the instant Navier-Stokes equation, supplementary terms appeared that reflect the influence of turbulence. Those are the (Reynolds stresses,  $-\overline{\rho u'_i u'_j}$ ), which should be modeled.

### 3.4.5 The standard k–ε turbulence model

This two-equation model is the most generally used turbulence model for engineering simulations. The (k-ε) model was based on the Boussinesque approximation of the Reynolds turbulent stresses. The turbulent eddy diffusivity is expressed in terms of turbulence parameters k and ε. Two additional scalar transport equations, one for the turbulent kinetic energy k and the other for the turbulence dissipation ε, are solved to model the turbulence effects. The eddy viscosity of this model is obtained as:

$$\mu_t = \rho C_\mu \frac{k^2}{\varepsilon} \quad \dots(3.8)$$

$$\nabla \cdot (\rho k \bar{V} - \frac{\mu_t}{\sigma_k} \nabla k) = P - \rho \varepsilon \quad \dots(3.9)$$

$$\nabla \cdot (\rho \varepsilon \bar{V} - \frac{\mu_t}{\sigma_\varepsilon} \nabla \varepsilon) = C_1 P \frac{\varepsilon}{k} - C_2 \rho \frac{\varepsilon^2}{k} \quad \dots(3.10)$$

where  $P$  is the usual Reynolds stress turbulence production term given as:

$$P = \mu_t \left[ 2 \left[ \left( \frac{\partial u}{\partial x} \right)^2 + \left( \frac{\partial v}{\partial y} \right)^2 + \left( \frac{\partial w}{\partial z} \right)^2 \right] + \left( \frac{\partial u}{\partial y} + \frac{\partial v}{\partial x} \right)^2 + \left( \frac{\partial u}{\partial z} + \frac{\partial w}{\partial x} \right)^2 + \left( \frac{\partial w}{\partial y} + \frac{\partial v}{\partial z} \right)^2 \right] \quad \dots (3.11)$$

### 3.5 Thermal Performance factor formulation

The hydraulic diameter can be written as [53,54]:  $D_h = \frac{4A}{P_w}$  ... (3.12)

Reynolds number express as:  $Re = \frac{u \times D_h}{\nu}$  ... (3.13)

---

The mass flow rate is defined in the equation:

$$\dot{m} = \rho \times u \times A_C \quad \dots(3.14)$$

The heat that is transposed from the out wall surface to the inner wall surface through the channel walls. The transferred heat is carried away through the air flowing inner the channel while the outer surface of the channel losses only a small amount of the heat produced by natural convection. Energy balance is used to the air flowing through the channel. The next assumptions are made for applying the energy balance principle:

1. Only heat transfer happens at the inner surface of the channel.
2. The fluid (air) have not done shaft work.
3. Constant mass flow rate.
4. Constant out wall surface temperature.

The rate of heat transfer can be defined as the amount of heat transferred per unit time. The energy balance equation is displayed as follows:

$$Q = \dot{m}c_p(T_o - T_i) \quad \dots (3.15)$$

The equation of heat transported (Q) to air caused by forced convection can be written as [50]:

$$Q = hA(T_w - T_c) \quad \dots (3.16)$$

Nusselt number can be written as  $Nu = \frac{h D_h}{k} \quad \dots(3.17)$

The friction factor can be determined using:

$$f = \frac{2 \rho \Delta P D_h A_C^2}{L \dot{m}^2} \quad \dots (3.18)$$

Thermal enhancement factor ( $\eta$ ) can be defined as the ratio of heat transfer coefficient with ribs to the heat transfer coefficient without ribs [ 55, 56]:

$$\eta = \frac{h}{h_o} = \frac{Nu}{Nu_o} = \frac{Nu/Nu_o}{(f/f_o)^{1/3}} \quad \dots (3.18)$$

### **3.6 Boundary Conditions Used in CFD Calculations**

In order for solving the governing equations and for simulating heat transfer and the flow through the elliptical channels fitted with different rib geometries, boundary conditions need to be imposed on the boundaries of the numerical domain. As shown in figure (3.5), the following boundary conditions are specified:

#### **3.6.1 Boundary conditions at inlet**

In the inlet channel, the temperature inlet of coolant air is 300 K. The air enters the computational domain is specified to have a uniform velocity. The velocity at the inlet was calculated based on the Reynolds number referred to the channel hydraulic diameter with values of ( $Re=11000, 13500$ , and  $16000$ ). The velocity at the inlet was calculated based on the Reynolds number referred to the channel hydraulic diameter and entrance flow conditions.

#### **3.6.2 Boundary conditions at the outlet**

ANSYS FLUENT 16.1 package was used to determine the outlet boundary conditions involving pressure, the temperature for coolant air at channel centreline, inner wall surface channel temperature, and coolant air velocity at channel centreline.

#### **3.6.3 Boundary conditions at the wall of the channel**

The channel wall was set with boundary conditions of a constant ambient hot air temperature of 673 K for the smooth and all ribbed channel.

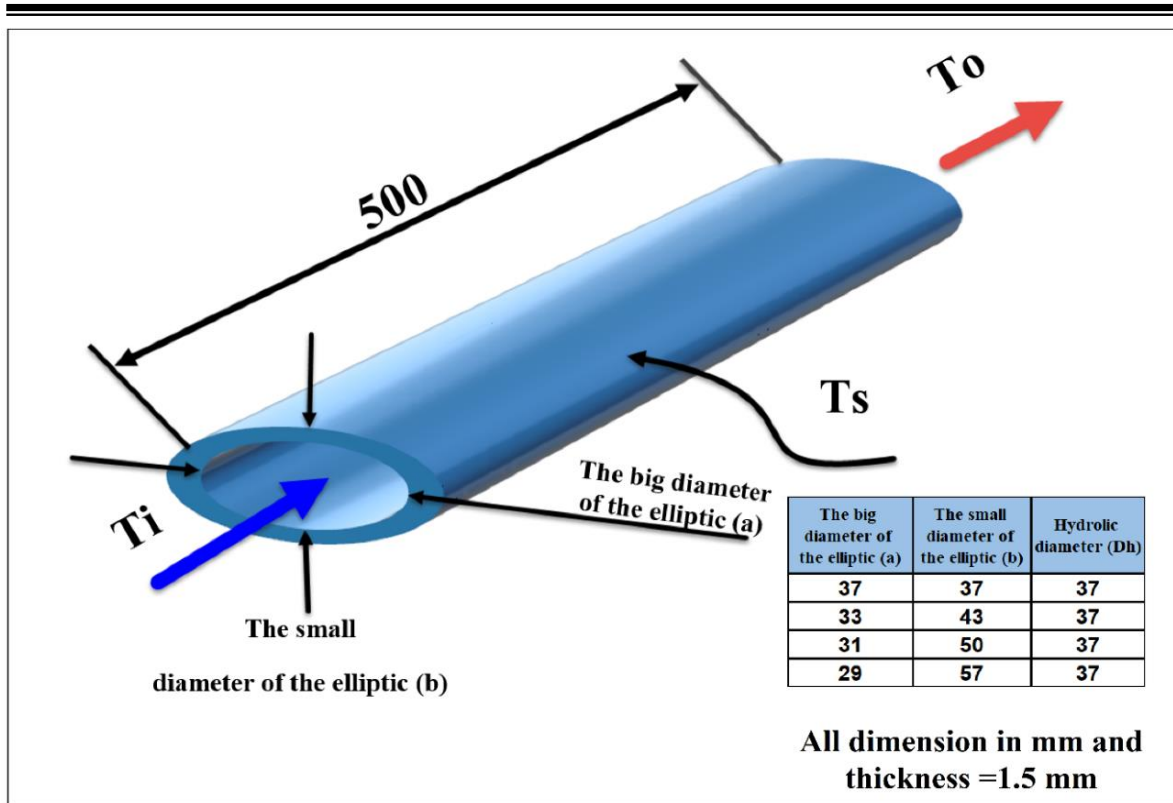


Figure (3.5): Boundary conditions for the present work

### 3.7 CFD Software Package

The flow conditions were simulated using FLUENT version 16.1.

In ANSYS, the same basic procedures are:

1. During preprocessing.
2. The problem geometry is defined.
3. The volume occupied by the fluid is divided into discrete cells (the mesh). The mesh may be uniform or non-uniform.
4. Defining the boundary conditions, involving specify the fluid behavior and properties at the problem boundaries. For transient problems, the initial conditions must be defined.
5. Starting the simulation, and the equations are solved iteratively as a steady state or transient then a postprocessor is used for the analysis and visualization of the resulting solution.

---

### 3.8 Validate ANSYS Results for The Smooth Channel

The average Nusselt number values obtained from the ANSYS results were compared with the values obtained from Ben Lu's[58] work as shown in figure (3.6) It was observed that the variance in the results obtained from ANSYS lies within  $\pm 5.5\%$  of the experimental result of Ben Lu's which demonstrates the reliability of the results obtained from ANSYS. After confirming the reliability of ANSYS results, it was decided to study thermal performance for the effect of fitted ribs in elliptical channels.

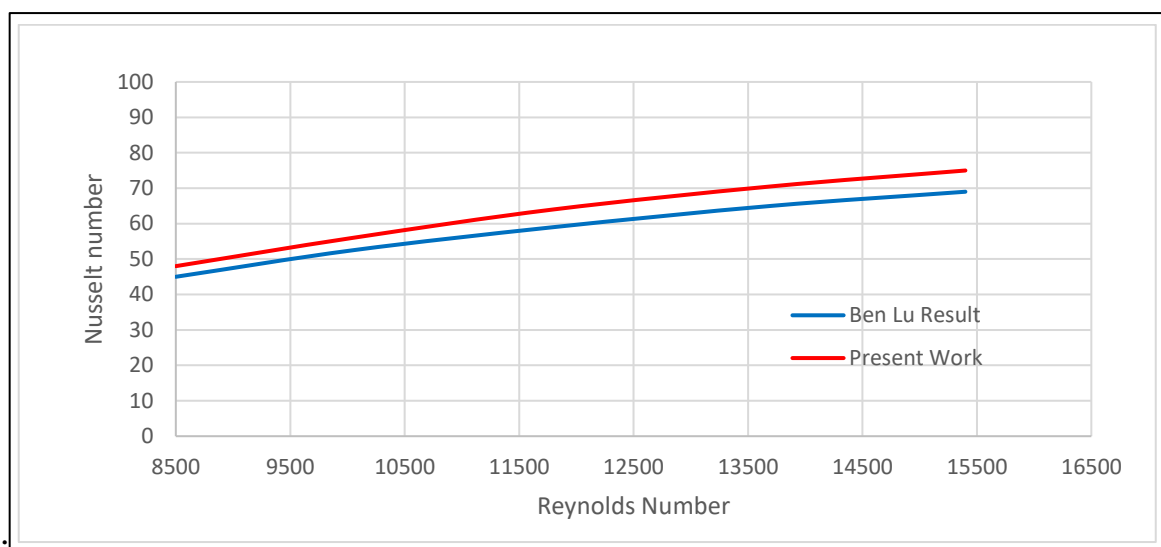


Figure (3.6): Validation of the ANSYS results for the smooth channel

### 3.9 Total Cell Count

The final point in a good mesh is the total number of cells generated. It is vital to have enough number of cells for a good resolution but memory requirements increase as the number of cells increases. For the present cases, an average of (1) million cells is used.

### 3.10 Generation the Mesh

Initially, before solving the governing equations, a volume grid inside the flow domain is generated, and the all surfaces boundaries need to be presented. This is executed by a meshing process. The generated mesh is in general affected by the positions of the critical domains of the flow and the domain geometry. It is required a huge amount of nodes in mesh at those positions for describing the

---

accuracy of variation. The mesh is built from node points which form the elements or sometimes called (cell volumes). 3-dimensional cells(elements) so include: 8-noded hexahedrons, 6-noded prisms, 5-noded pyramids and 4-noded tetrahedrons. From these mesh elements, three kinds of mesh structures can be created:

1. An unstructured and irregular grid, at which the node points are located with the computational domain without having regular topology.
2. A regular structured grid, at which the node points are regularly organized throughout a cuboid, which can be stretched to fit a particular geometry.
3. Multi-block structured grid, at which the computational domain is partitioned into various blocks, which can be structurally meshed.

Generating the mesh needs fine elements in the areas near the surface channel. Thus, the mesh has to be controlled and manipulated manually to maintain a smooth mesh transition and keep compatible mesh for a 3D model with a smallest computational rate. This is achieved by employing the size function.

It should change the setup of the mesh with the role of the part within heat transfer. The bottom wall and ribs finely meshed but the side wall was held coarser. This was achieved by taking into account that there is no radical change in cell sizes in the two regions. For capturing normal gradient of temperature and boundary layer effects, it was used Polyhedral elements with prism layers and a surface wrapper mesh types. The total number of elements is about one million cells. The figure (3.7) shows the transition of the mesh between two regions and the mesh around the rib area.

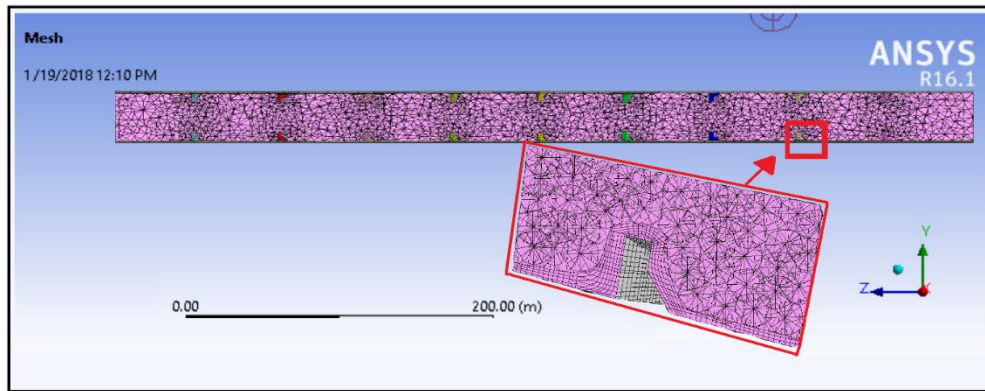


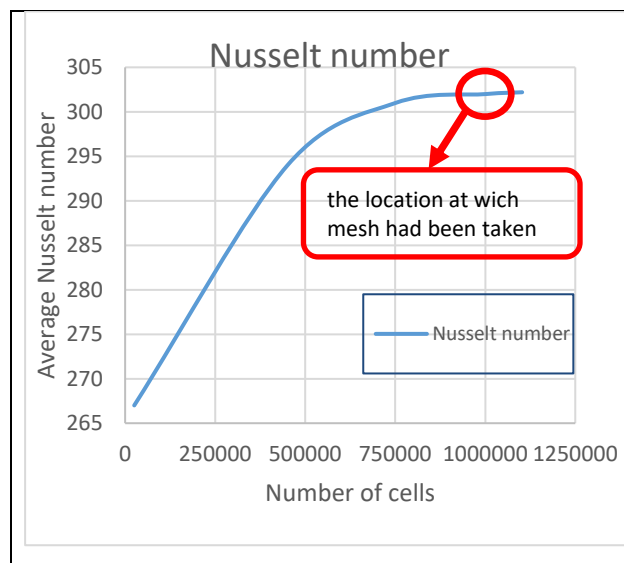
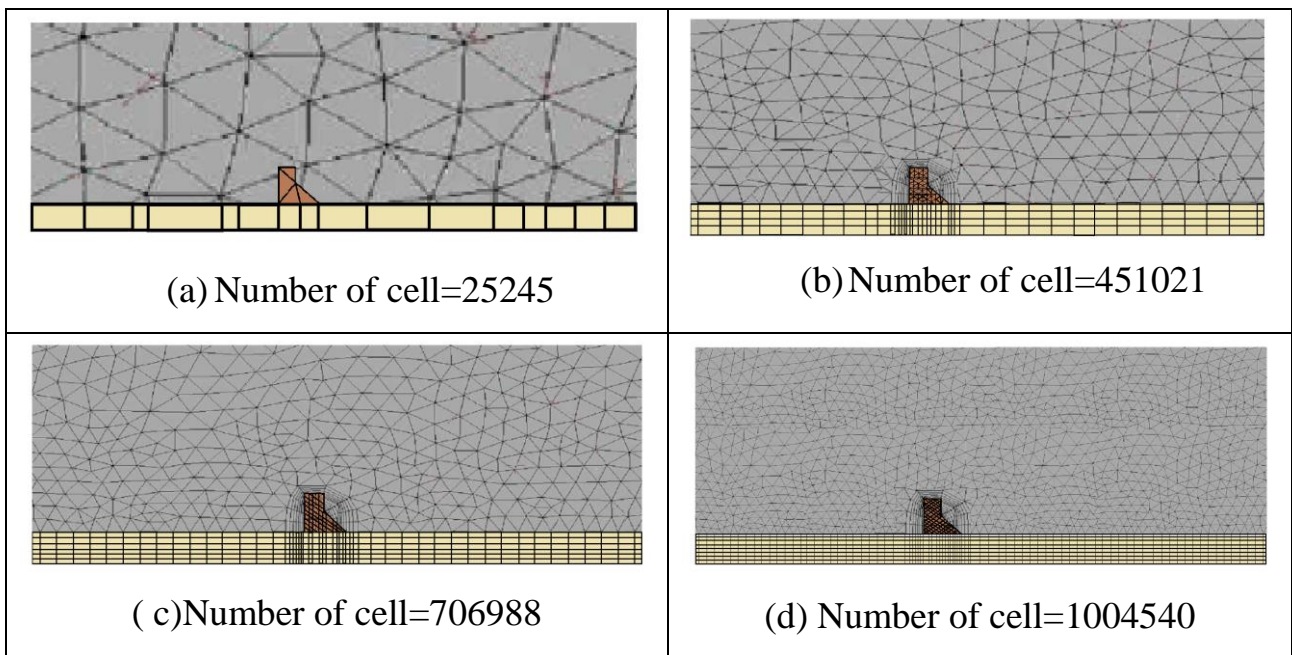
Figure (3.7): The mesh transition of the two regions and also the mesh on and around the rib

### 3. 11 Grid Independence Test

A grid-dependency study is carried out to evaluate mesh suitability for the turbulent flow through the elliptical channel fitted with ribs. A grid independence test is performed across grids with various numbers of cells, 25245, 451021, 751025, 1004540, and 1102544 that are used in 5 steps and tabulated in the table (3.2). From figure (3.8.a, b), it was found that when the number of cells increased from 1004540 to 1102544, the number of nuclei changes marginally. Therefore, there is no benefit of increasing the number of cells above this number. That is why 1002014 cells for this work computation was adopted. Figure (3.9) shows the mesh generation for case of 706988 cells and mesh generation for the case of 1004540 cells. the table (3.3) shows the mesh generation for all cases. In this study, 16 different meshes were generated for the 16 cases (four different channel fitted with four different ribs configuration) and a number of cells of the mesh for getting the required accuracy results.

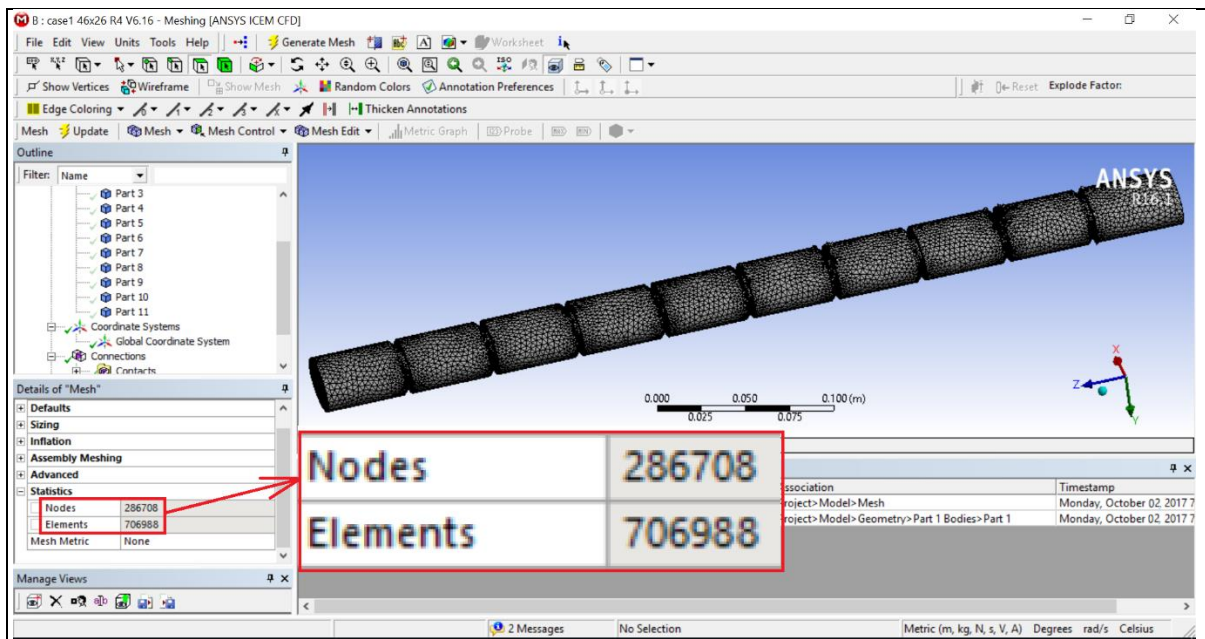


Table (3.2): The mesh images with different numbers of cells

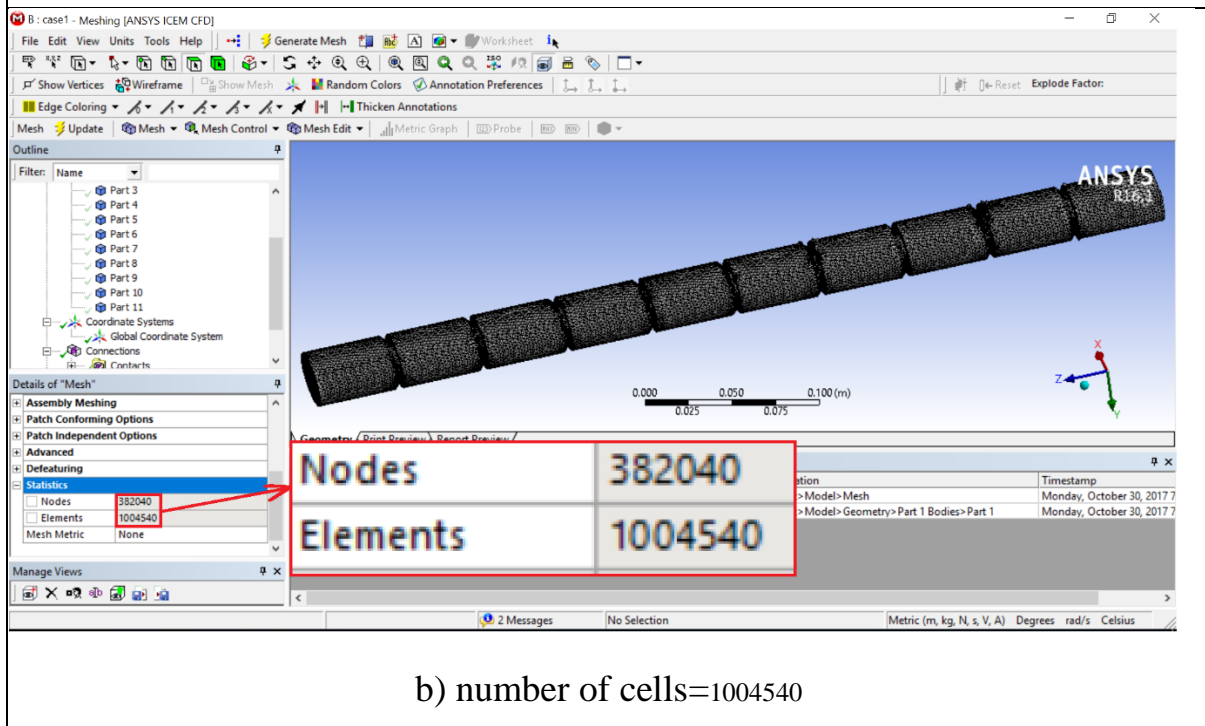


Number of cells	Nusselt number	Different in Nusselt number	The percentage of the value difference
25245	267		
451021	294	27	9.1%
706988	301	7	2.3%
1004540	302	8	2.6%
1102544	302.3	0.3	0.09%

Figure (3.8): The relation between cell no. and Nu no. accuracy



a) number of cells=706988



b) number of cells=1004540

Figure (3.9): Mesh generation for case of 706988 cells and mesh generation for case of 1004540 cells



Table (3.3): Mesh Generation for the different aspect ratio with all Cases of rib

AR	Rib No.	Side Section of Mesh	Front Mesh
AR=1	Rib1		
	Rib2		
	Rib3		
	Rib4		
AR=1.3	Rib1		
	Rib2		
	Rib3		
	Rib4		
AR=1.6	Rib1		
	Rib2		
	Rib3		
	Rib4		
AR=2	Rib1		
	Rib2		
	Rib3		
	Rib4		



### 3.12 Set Up and Flow Specification

The generated mesh was then exported to FLUENT where the different flow and physical properties were specified. The appropriate turbulent model was selected and the energy option was switched on. Their thermo-physical properties are mentioned in table 3.4.

Table (3.4): Displays the thermal physical properties that have been taken

Properties	unit	Working fluid (air)	material of the channel stainless steel
Density ( $\rho$ )	kg/m <sup>3</sup>	1.1767 2719	7900
Viscosity	kg/m-s	$1.8582 \times 10^{-5}$	
Specific heat (constant pressure)	J/kg-K	1006.6 871	477
Prandtl number		0.714	
Thermal conductivity	W/m-K	0.0262 202	14.9

### 3.13 Number of Iterations and Convergence

A solution is converged when all conservation differential equations (continuity equation, X-velocity, Y-velocity, Z-velocity, energy equation and, k, epsilon) are subject to a specified tolerance at all points. Therefore, the monitoring the convergence of the solution is great importance.

The convergence system employed to simulations is that the scaled residuals for (x, y, z) velocities, energy, and k epsilon have lowered by four orders of magnitude and their residuals are no large changing with more iterations. In the present work, it requires 1500 iterations to reach the convergence. This is the maximum number of iterations done before the solver terminates. In the present case, 1500 iterations are requested. If the residuals are still not below the proper values, then additional 1500 iterations are requested. If the residuals are still not below the proper values, then additional iterations are requested. The output iterations are shown in figure (3.11).

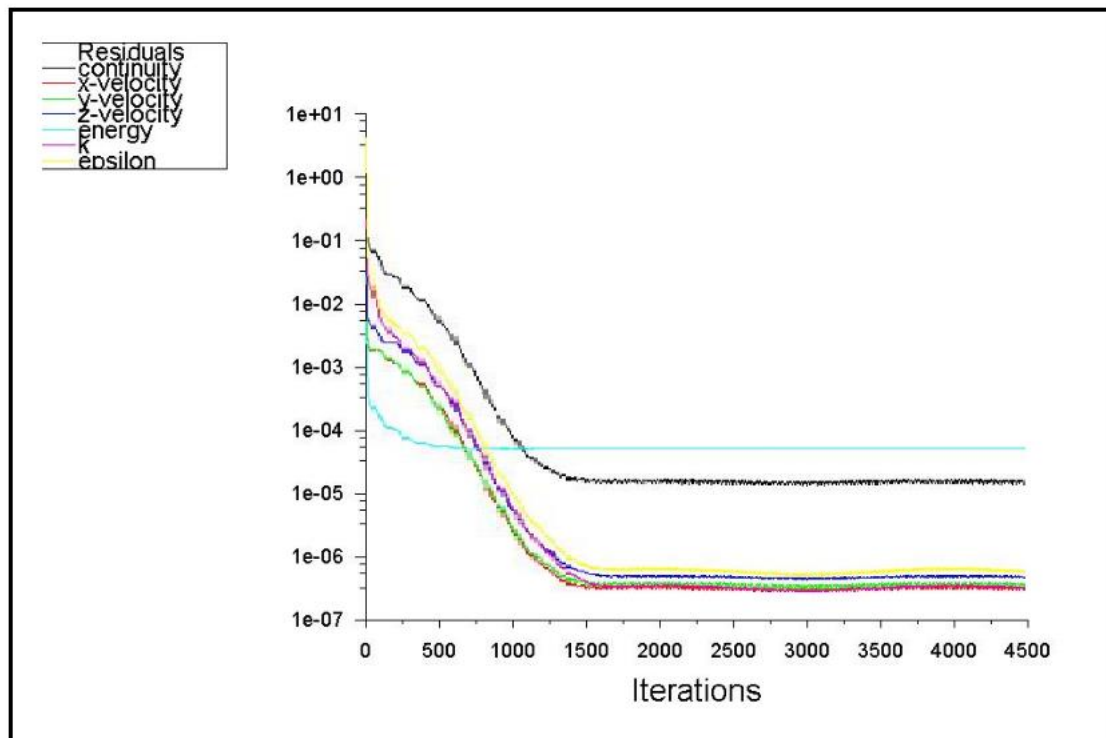


Figure (3.11): Convergence to solve discrete conservation equations for case 1

### 3.14 Summary

In the current study, the geometry of all cases was drawn using AutoCAD 2017 and then exported to FLUENT code. The governing equations are solving by finite volume scheme depend on the FLUENT coded version 16.1. The unstructured hexahedral mesh is employed for gridding the geometry, and so for the refined region close to the wall, by using a high-density mesh. The mesh then smoothed utilizing smoothing algorithms obtainable in FLUENT and then selecting boundary conditions. The flow was solved for a chosen number of iterations until taking convergence.

# **CHAPTER FOUR**

## **EXPERIMENTAL WORK**

---

## CHAPTER FOUR

### EXPERIMENTAL WORK

#### 4.1 Introduction

Beginning from the channel without rib, the experimental examination has been built. The major aim of the experimental rig was to test the smooth channel to getting a reference data a comparative purpose. The test section was manufactured in a stimulating way and combining two different types of gas turbine blade cooling methods, internal channel cooling and surface coating. This was achieved by using four elliptical channels fitted with four different configurations of ribs. The procedure of the experimental investigation of sixteen different cases is presented in this chapter. It includes calculation approach, semi-infinite solid analysis of the configuration in channel effectiveness and heat transfer coefficient based on the experimental data.

Table (3.1) in the previous chapter showed all rib models or cases used in this work. In each case, ribs are fitted in the test section with contact to the inner surface of the channel to have pitch ( $P$ ) to rib height ( $e$ ) of 10 within the range according to [11 and 12], and the rib angle of attack to the coolant air flow stream is  $90^\circ$ . The objective of the experimental investigation in the present work is to study the effect of using elliptical channel with different aspect ratio and with different rib geometries in four elliptical cross-section channels. All the channels have the same hydraulic diameter (37 mm) but different in aspect ratio on the flow and heat transfer characteristics (velocity and temperature distribution, average Nusselt number, thermal enhancement factor and average friction factor) at a range of Reynolds number (11000, 13500 and 16000). This chapter includes descriptions of all experimental details, including the test models, experimental apparatus, and experimental setup.

## 4.2 Experimental Devices and Test Rig

Figure (4.1) shows the schematic diagram of the test rig consisting of:

- 1-Test sections (four elliptical channels).
- 2-Cooling air supply system.
- 3-Heating system.
- 4-Ribs.
- 5-Measuring tools.

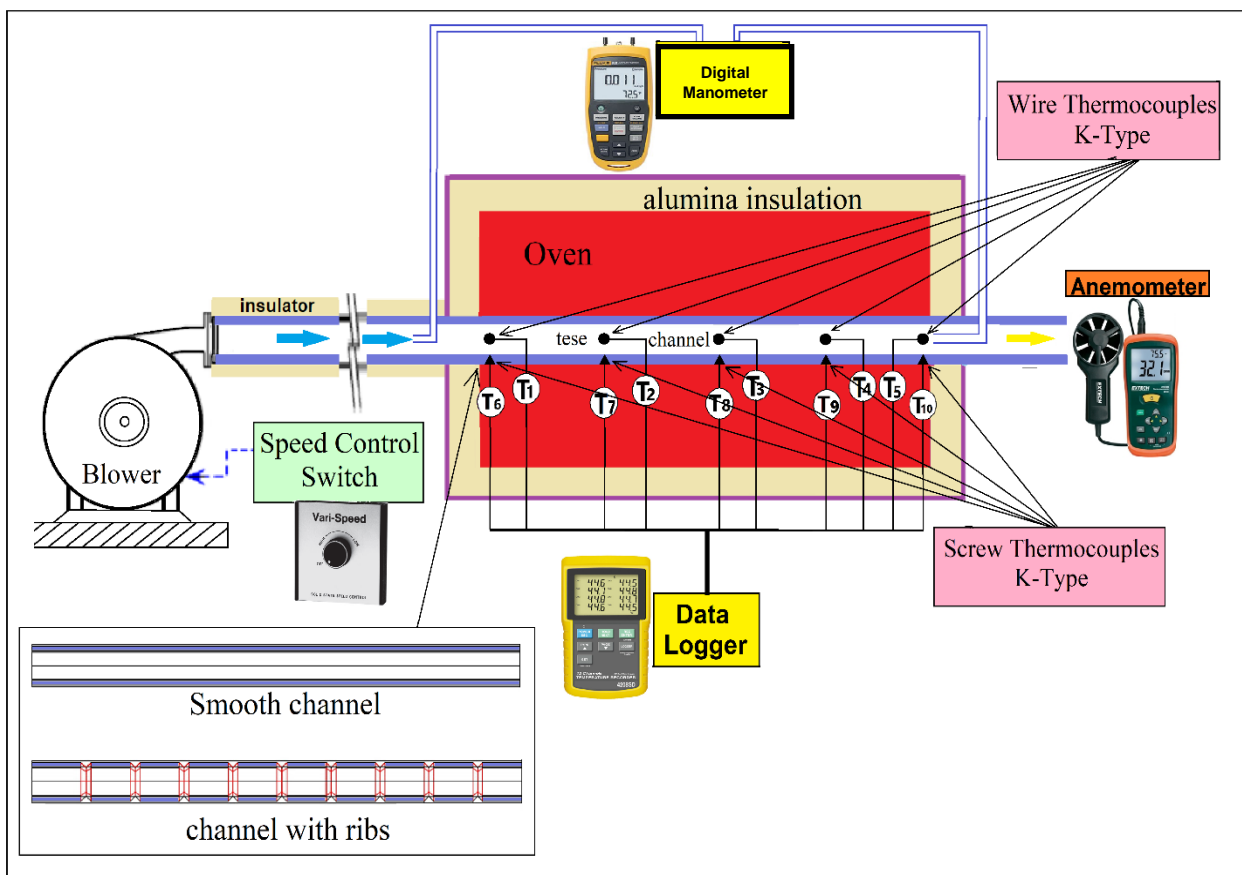


Figure (4.1): Schematic diagram of the experimental setup

The experimental rig was built in the Fluid Mechanics Laboratory at Engineering College of the University of Kerbala as the photograph of the rig shown in figure (4.2).



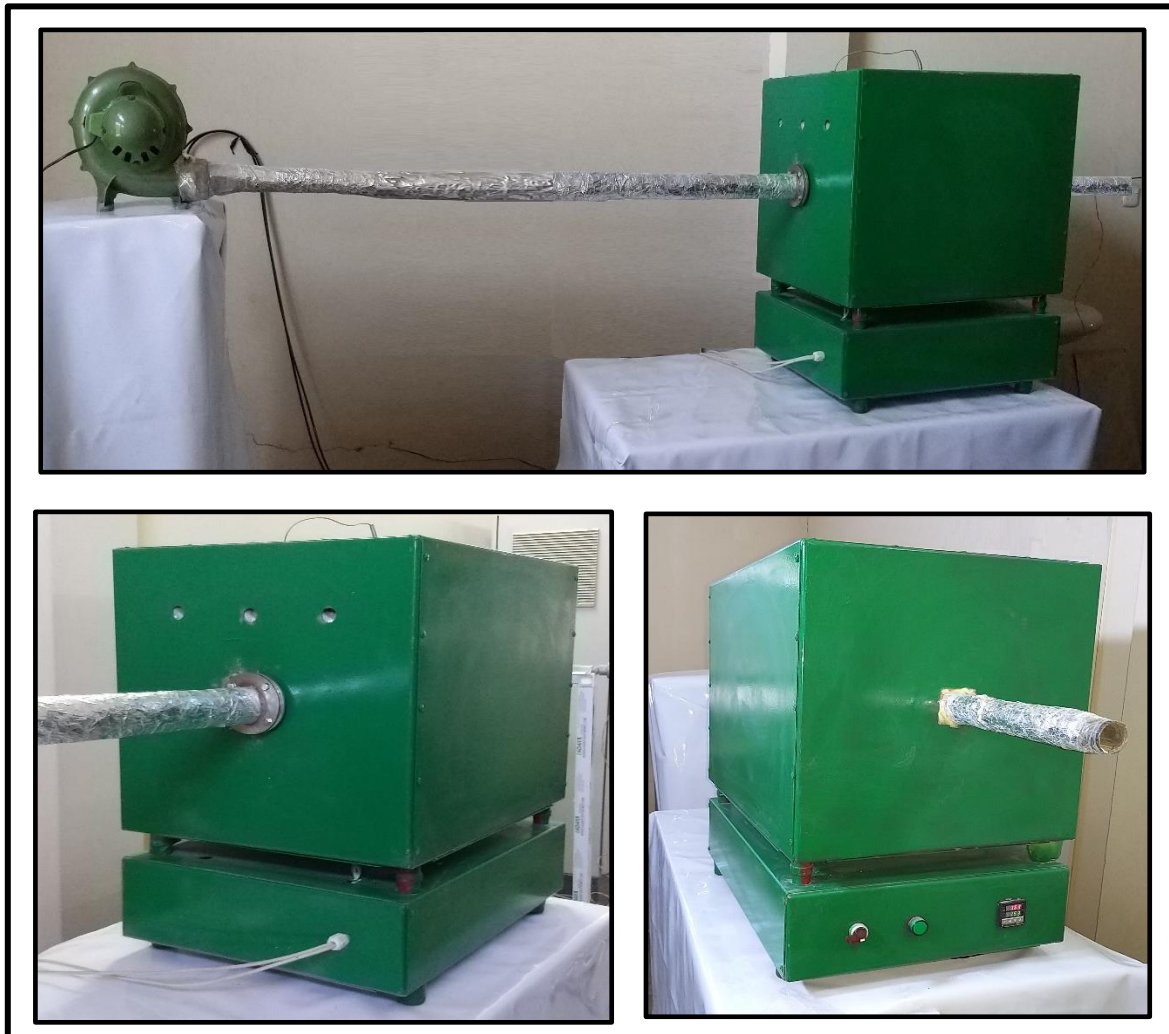


Figure (4.2): Photographic views of experimental rig

#### 4.2.1 Test section

The test section consists of a stainless steel box dimensioned ( $700 \times 500 \times 500$ ) mm, length, width and height, respectively. The box was internally insulated with alumina and provided with a heater of 4.4 kW to produce a constant hot air temperature of 673 K. It surrounds the stainless steel elliptical channel with a length of 500 mm and inner hydraulic diameter of 37 mm as shown in figure (4.3). The cooling air passes through the channel, and ribs are fitted into the channel test section at the same pitch (spacing) of 50 mm. The physical proprieties of channel and ribs material can be seen in the table (4.1).

Table (4.1): physical properties of the channel and the ribs

Metal	Thermal Conductivity (K) W/m.K	Specific heat ( $C_p$ ) W/m <sup>2</sup> .K	Density ( $\rho$ ) Kg/m <sup>3</sup>
standstill steel (ASM4120)	37.7	444	7822

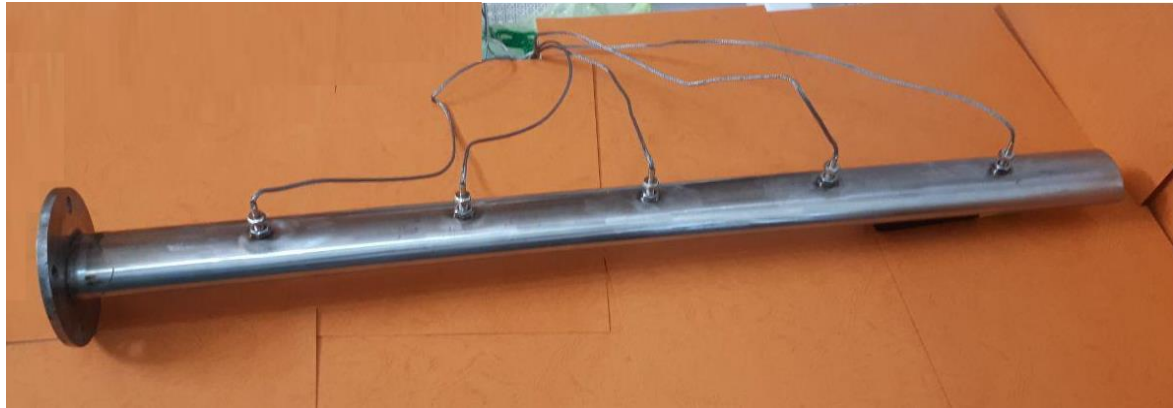


Figure (4.3): elliptical channel

#### 4.2.2 Cooling air supply system

The device that produces the channel with a cooling air consists of the following parts:

1. Centrifugal blower
2. Converging nozzle
3. Entrance channel
4. Flange
5. Insulation cover

##### 1. Centrifugal blower

A centrifugal blower was used in the experimental rig to supply the coolant air. It was driven by A.C. Motor of 220 volt 325 W at 3000-4000 RPM. The airspeed is controlled by an electric switch to control the blower, and the airflow velocity (flow rate) can be measured in the test section by digital airspeed flow meter.

##### 2. The converging nozzle

The converging nozzle (300 mm) long to connect the blower with entrance channel. The beginning of the channel is circular and its exit has an elliptical cross-section of the entrance channel.

### 3. Entrance channel

Entrance channel is manufactured with an elliptical cross-section as same as the dimension of the cross-section area of the channel test section with a length of (2m). The importance to ensure that the coolant air was having thermal and hydraulic fully development entrance length the hydraulic entrance length is ( $L_e = 0.818$ ) m according to correlation (4.1)] [51].

$$L_e = 4.4D_h Re^{1/6} \quad \dots (4.1)$$

Other authors give much longer entrance length  $L_e = 1.48$ m according to recommends as in [59].

$$L_e = 40 \times D_h \quad \dots (4.2)$$

And the thermal fully development entrance length can be calculated according to equation (4.3) to be  $L_e = 0.37$  m as in [60].

$$L_{th}e \approx 10D_h \quad \dots(4.3)$$

Where : $L_{th}e$  = thermal entrance length

And  $L_e$  = Entranc length

Thus, in this experiment, the entrance length was taken equal to 2 m which is suitable to ensure the fully thermal and hydraulic entrance length.

### 4. The Flanges

The Flanges were used to connect the entrance channel with the test sections. Also, a thermal rubber is put between the connecting flange to ensure there is no heat or air leakage.

### 5. Insulation cover

A 1 cm thick thermal wool is used to cover the converging nozzle, entrance channel and flange to prevent the heat loss by convection from the wall.

### 4.2.3 Heating system

Figure (4.4) shows the heating system consisting of a rectangular box oven with a length of 700 mm, 500 mm width and the height of 500 mm. Oven walls were insulated with alumina as a good insulator to avoid the losses of heat energy to the surrounding. As shown in the figure (4.4 a) heat was produced by heaters around the channel to assuring constant surrounding hot air temperature of 673K. The total power of the heaters is 4400 W. The temperature is restrained by a control thermostat electric (CTE) as shown a figure (4.4 c). It was designed and built to maintain a constant hot air temperature on the outer surface of the channel test section. The circuit was designed for a load voltage of 0 - 220 V, with a maximum current of 20 A. A controller thermocouple was used to maintain a constant temperature on the outer surface of the main channel test section.

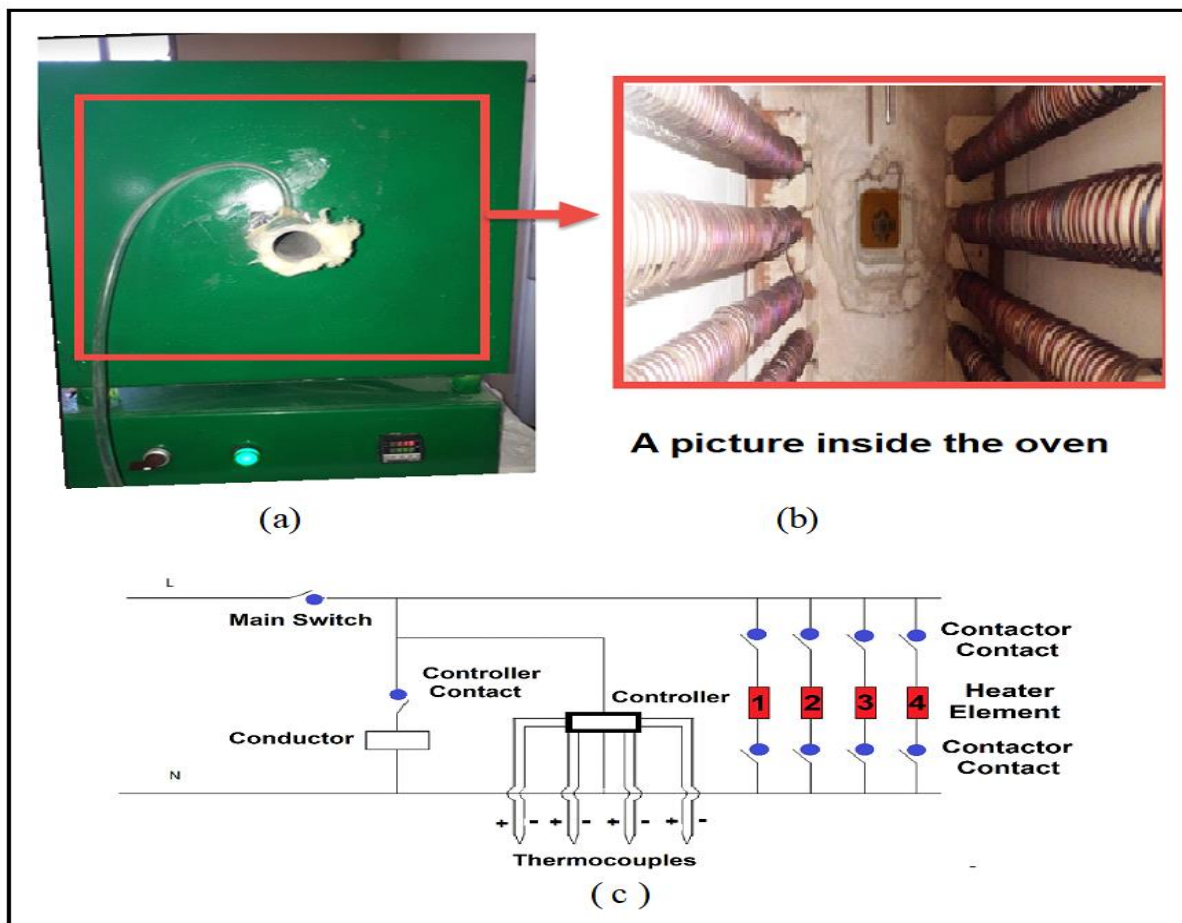


Figure (4.4): Heating system: a) Front view of the oven b) Inside section view of the oven c) thermostat electric circuit

#### 4.2.4 Ribs

Elliptical stainless steel ribs (physical properties listed in the table (4.1)) with different geometries were manufactured in the Mechanical Industries factory in Tehran by CNC machine as shown in figure (4.5) fitted in the channel by the following procedures:

1. Drilling holes in the upper wall along the channel with 50 mm apparatus then use it to fix the ribs in place.
2. For facilitating shifting the rib inside the channel and because of the channel and their ribs were manufactured with high precision using the CNC machine. The tolerance is very low between the external diameter of the ribs and the inner diameter of the channel. Therefore, liquid nitrogen was used for the purpose of cooling the ribs and thus to reduce its dimensions temporarily.
3. After cooling the rib, pushing the first rib by a Teflon rod fitting until it reached to the final location. The rib was then screwed in position.
4. Re-doing step 2 to fit all other ribs. At attack angle of  $90^\circ$  to the coolant airstream, as shown in figure (4.7) and (4.8) ribs were being placed.



Figure (4.5): Photographic of ribs machining processes



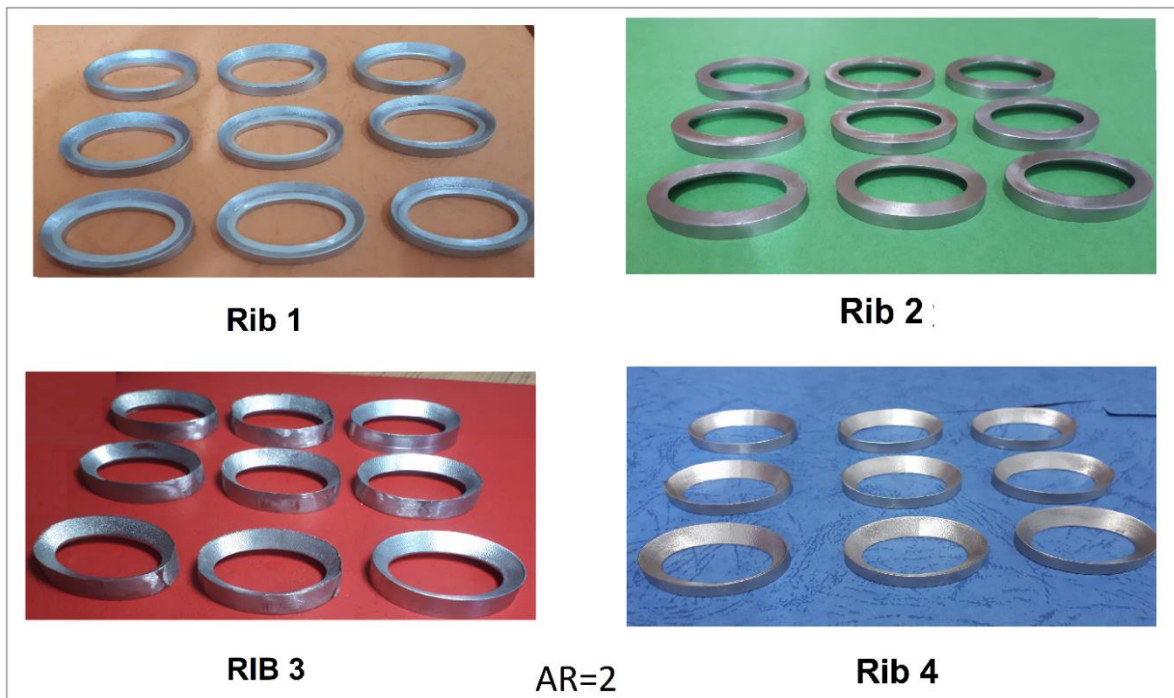
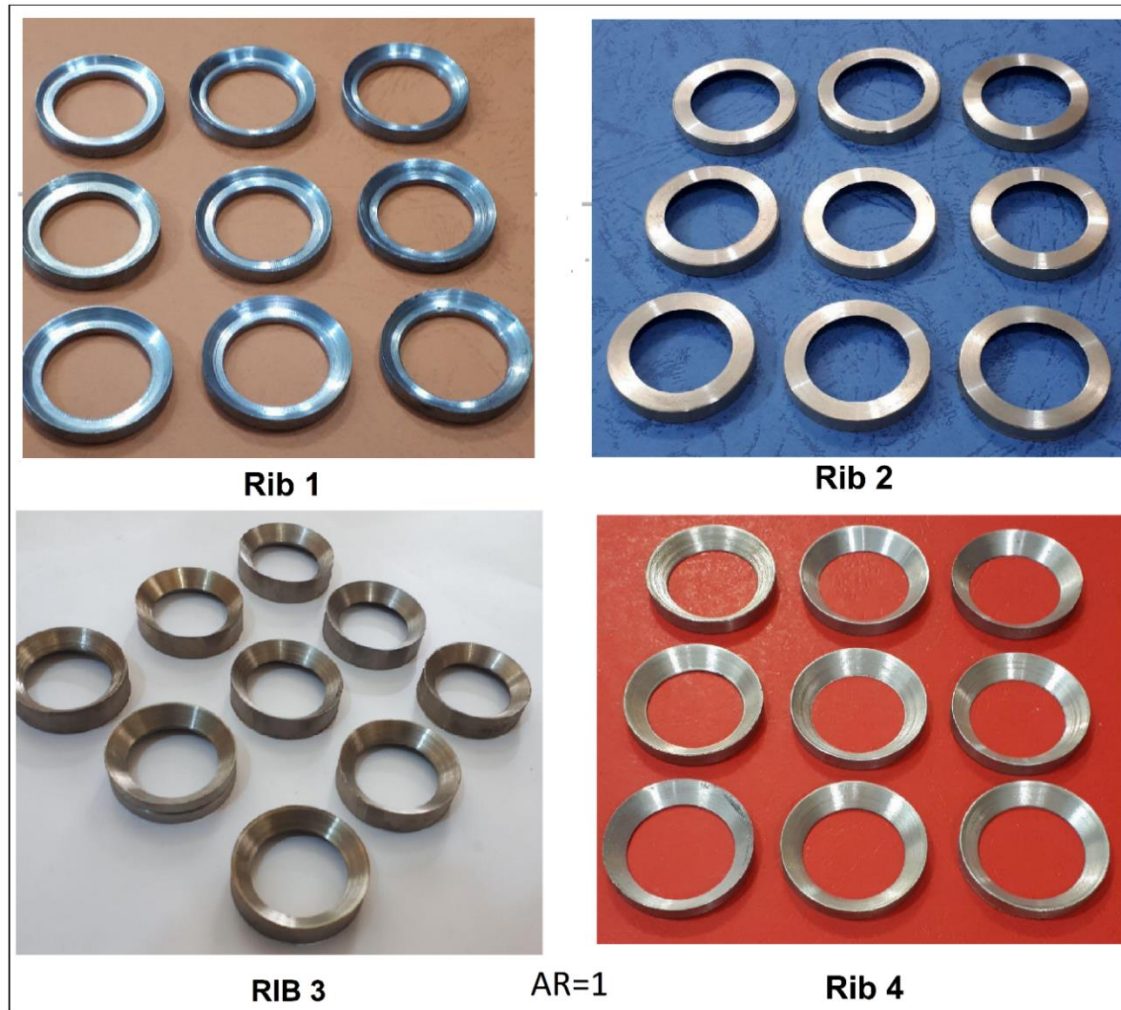


Figure (4.6) displays Photographic view of the ribs with aspect ratio 1 and 2



Figure (4.7): Photographic view displays the location of ribs inside the channel

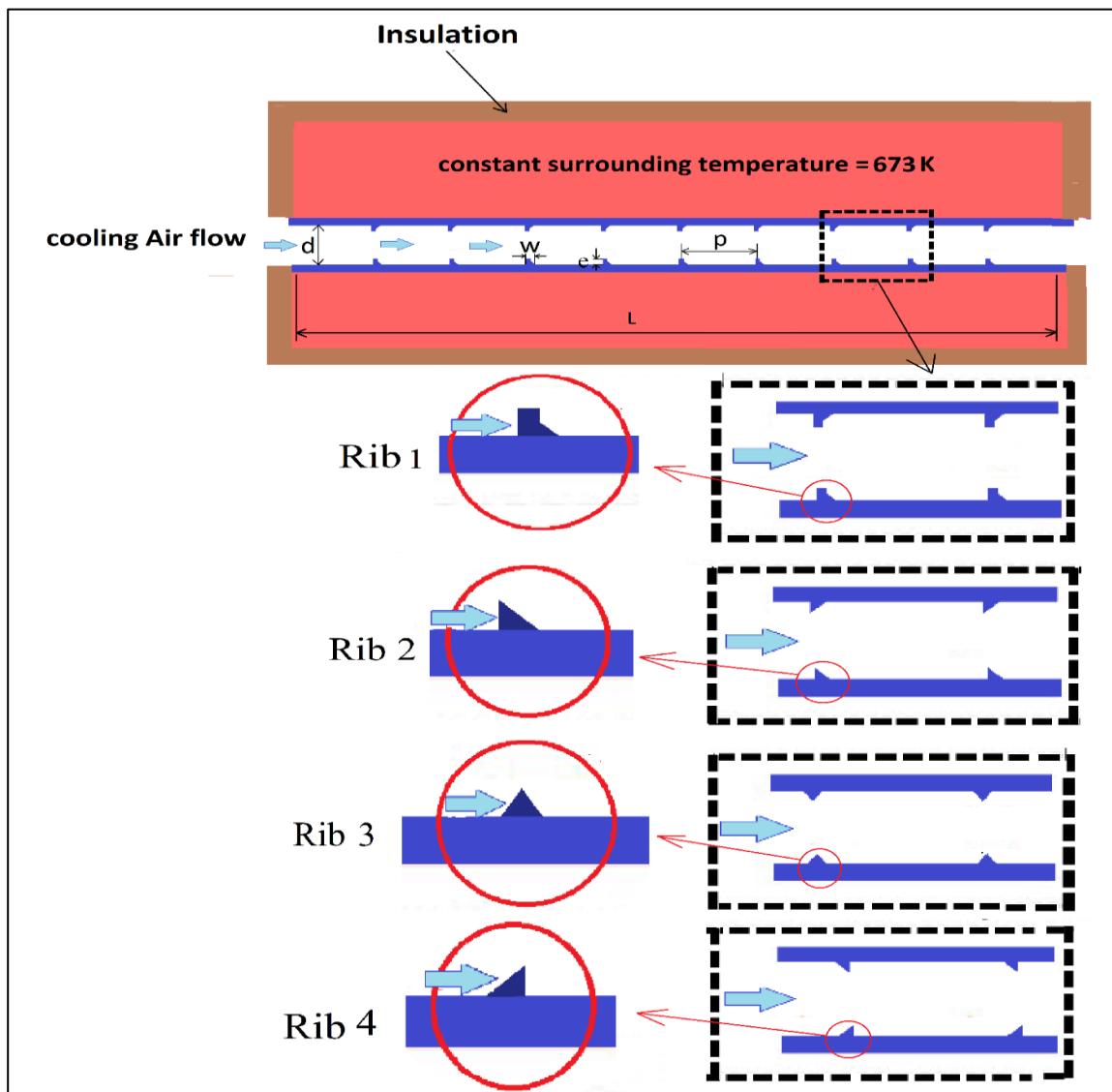


Figure (4.8): Location of ribs inside the channel

## 4.2.5 Measuring Tools

The measuring tools that used in this works were: -

### 4.2.5.1 Thermocouples and data logger

Thermocouple type-k with two methods of supporting were used to measure temperatures:

The screw type-k thermocouples were employed for measuring the internal surface temperature of the channel wall. The channel's wall is punched from the outside surface. The hole does not penetrate to the inner surface but touches it. The thermocouple is fixed in this hole by screwing it to measure the internal surface temperature of the channel wall as shown in the figure (4.9). Each thermocouple fixed on the wall is installed every 125 mm, and then connect it to the digital thermocouple reader thermometer with a specific key,

Five wire k-type thermocouples were employed for measuring the air cooling temperature at the centerline. its have been welded with tig-welding These thermocouples are fixed in the centerline of cooling air streamline.

To read the temperatures, all ten thermocouples were connected to the data logger (temperature recorder). Temperature recorder (model, BTM- 4208SD, 12 channels, read from: -100 to 1300 °C, accuracy 0.1 % ± 0.1 °C) was used to record temperature measurements. The temperature recorder and thermocouple are shown in Figure (4.10). The calibration of the ten thermocouples and data logger was performed in the Ministry of Science and Technology, Iraq, as shown in appendix (C).



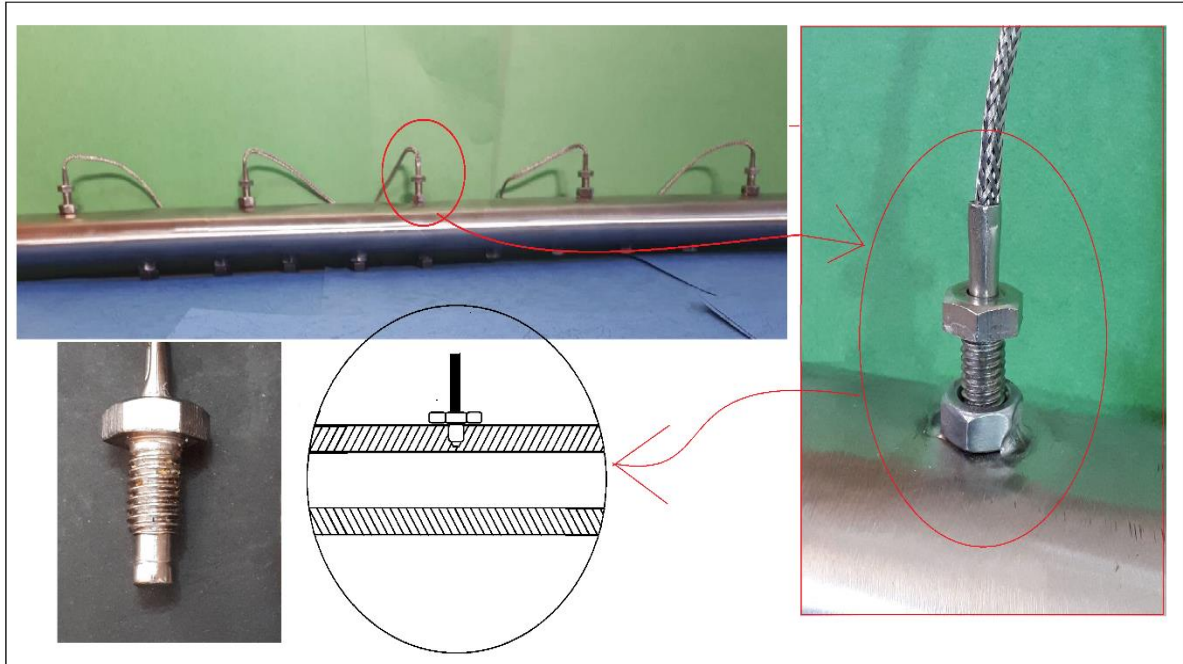


Figure (4.9): Layout of thermocouples on the test section tube



Figure( 4.10) : Reading out of thermocouples by temperature recorder

### 4.2.5.2 Digital Manometer

A manometer is a pressure measuring instrument or a pressure gauge. It is often limited to measure pressure in range of the atmospheric pressure. There are two types of manometers: analog manometers and digital manometers. The digital type with specifications listed in the table (4.2) was used in the present study. The flexible hose was connected to the manometer and joined to pressure tap (at the beginning and end of the channel). The difference in pressure gets the pressure drop, which records through the device screen as shown in the figure (4.11-a).

Table 4.2 Specification of manometer

Model	Fluke 922
Units Displayed	Pa
Accuracy	$\pm 1\% + 1$ Pascals
Resolution	1 Pascals
Pressure range	$\pm 4000$ Pascals

### 4.2.5.3 Anemometer

A digital anemometer shown in figure (4.11-b) was used to measure the velocity of air outing from the channel. Also, a hot wire anemometer shown in figure (4.11-c) was used to measure the velocity at the centerline of the channel.

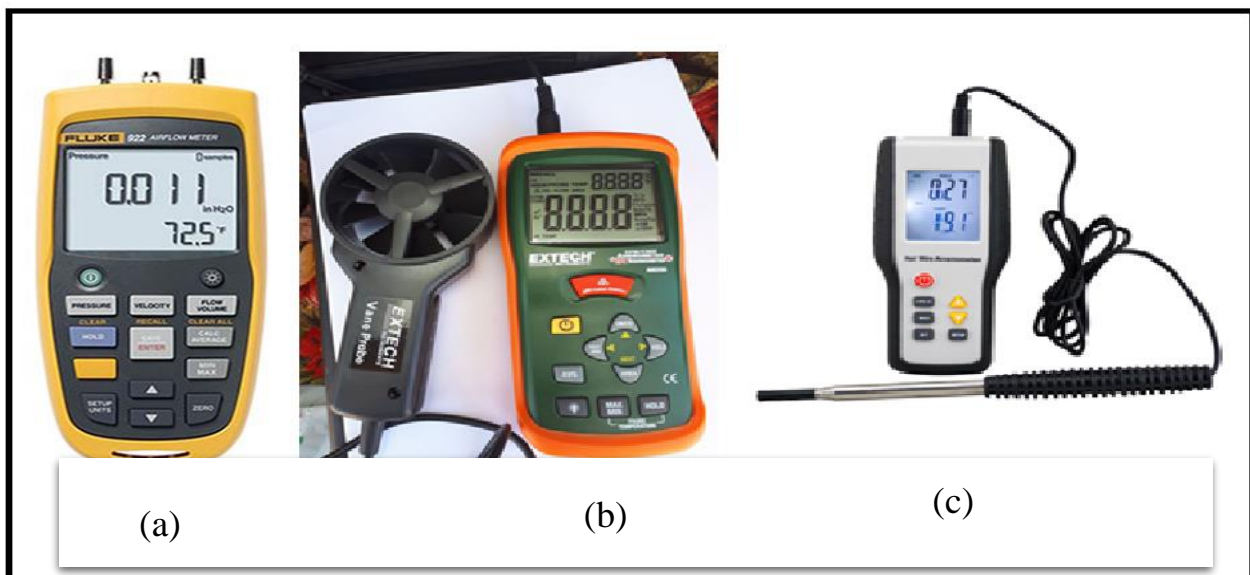


Figure (4.11): Photograph measurement tools: a) Digital manometer b) Anemometer c) Hot wire anemometer

### 4.3 Experimentation

In this work, the experimentation includes:

#### 4.3.1 Experimental rig task

Multi tests were done to verify the testing agreement before starting the reading as follows:

- 1- Calibration the measurement tools (thermocouples, digital manometer, hot-wire flow meter, anemometer) as detailed in the appendix (C).
- 2- Check the pressure tapping, thermocouples along the upper and lower surfaces, and adjust the flatness of the test rig.
- 3- Checking the steady-state (constant surface temperature and flow rate measurements).

#### 4.3.2 Measuring procedures

The experiment is performed as described in the following steps:

1. Switch on the blower and regulate its speed by the control switch until the desired flow rate at a required Reynold number of 11000 is obtained. And the airspeed is measured by the anemometer.
2. Turn on the heaters which were installed in the oven by the power switch and set up the temperature control panels at a temperature of 673 K. That keeps the temperature constant inside the oven in which the temperature of the external surface temperature of the channel remains constant. Thus, the conditions on the surface of the channel wall simulate the passages in the gas turbine blade.
3. Keep on the blower and the heaters working for a sufficient period of time until the readings are stabilized. The period took about 40 minutes and after that the temperature and pressure readings were recorded.
4. Regulate the blower gate to obtain the required flow rate ( $Re=11000$ ).

5. After obtaining the steady state record thermocouples readings (T1, T2, T3, T4 and, T5) which represent the inner wall surface temperature of the smooth channel (without ribs), record thermocouples reading (T6, T7, T8, T9 and T10) which represent air cooling temperature at the channel centerline.
6. Record the pressure reading from the digital manometer.
7. The above steps were done for the elliptical smooth channel with aspect ratio from 1 to 2.
8. The previous steps are repeated after fitted ribs 1.
9. Repeat the above steps for cases of ribs 2,3, and 4. For AR=1 and AR=2.
10. Repeat the above steps for another flow rate of (Re=13500 and 16000).
11. Repeat all the above steps using a thermal barrier coating around the channel test section for the best case, which was found from the result the case of rib 1 fitted in the channel with AR=2.

#### 4.4 Data Reduction

All experimental data were measured and recorded by hand. The reduced data of experimental test was done to obtain the average air temperature at centerline, average wall inner surface temperature at centerline, Reynold number, and mass flow rate. After that, these data were utilized for determining the friction factor, heat transfer coefficient, and Nusselt number. The average temperature of inner wall surface  $T_w$  was determined by computing the average of the temperatures recorded at different positions at the inner wall surface and was provided as the net heat transfer rate from the wall as follows:

$$T_w = \frac{T_1 + T_2 + T_3 + T_4 + T_5}{5} \quad \dots (4.4)$$

The mean air temperature.  $T_{mean}$  is the arithmetic mean of the measured values of air temperature at the entry and exit to the test section,

$$T_{\text{mean}} = \frac{T_o + T_i}{2} \quad \dots(4.5)$$

The mass flow rate can be calculated as follows:

$$\dot{m} = \rho u A_c \quad \dots(4.5)$$

$$\left( A = \frac{\pi \times a \times b}{4} \right) \quad \dots(4.6)$$

Where,  $\rho$  = air density,  $u$  = air flow velocity and  $A_c$  = channel cross sectional area,  $a$  = major diameter of elliptic,  $b$  = minor diameter of elliptic.

As [61] Pressure drop ( $\Delta P$ ) measured across test section length is utilized for finding the friction factor using the following equation:

$$f = \frac{2 \rho \Delta P D_h A_c^2}{L \dot{m}^2} \quad \dots(4.7)$$

$$h = \frac{Q}{AI (T_w - T_{\text{mean}})} \quad \dots(4.8)$$

Where  $Q$  is the heat transfer and

$$Q = \dot{m} C_p (T_o - T_i) \quad \dots(4.9)$$

$$NU = \frac{h D_h}{k} \quad \dots(4.10)$$

from the relation presented in equation (4.8), (4.9), and (4.10). The heat transfer coefficient and the Nusselt number have been calculated

The Reynolds number is calculated as follows

$$Re = \frac{u \times D_h}{\nu} \quad \dots (4.11)$$

Where,  $D_h$  = channel hydraulic diameter,  $u$  = air flow velocity and  $\mu$  = kinematic viscosity.

$$D_h = \frac{A_c}{\text{perimeter}} \quad \dots(4.12)$$

Where as in [62] perimeter of elliptic

$$\text{Perimeter of elliptic} = \pi \times \sqrt{\frac{a^2 + b^2}{2}} \quad \dots(4.13)$$

Where,  $\rho$  = air density,  $u$  = air flow velocity and  $A_c$  = channel cross section area.

#### 4.5 Thermal Barrier Coating

The heat transfer rate (cooling efficiency) can be enhanced using thermal barrier coating. In the present work, Yttrium oxide nanoparticle powder ( $Y_2O_3$ ) was mixed with a thermal polymer by (5 wt. %). The physical properties of the Yttrium oxide nanoparticles powder are listed in the table (4.3).

Table (4.3): Physical properties of Yttrium oxide nanoparticle powder [63]

Compound Formula	Molecular Weight	Appearance	Melting Point	Boiling Point	Density
	225.81	White powder	2440 °C (4420 °F)	4300 °C 7772 °F	5.0 g/cm <sup>3</sup>
$Y_2O_3$	Specific Heat	Thermal Conductivity	Thermal Expansion	Exact Mass	Monoisotopic Mass
	440 J/kg-K	0.3 W/m-K	8.0 μm/m-K	225.8099 g/Mol	225.796 DA

The channel test section was coated with double layers: first (pure thermal painting) in touch with the outer surface, and the second (Yttrium oxide nanoparticle powder with the thermal painting by (5 wt. %) covering the first layer, as shown in figures (4.12 and 4.13).

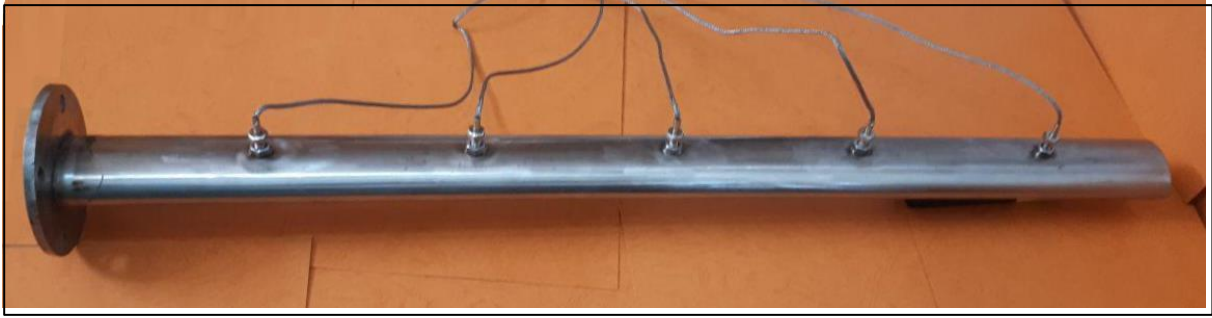


Figure (4.12): Channel test section without barrier coating



Figure (4.13): Channel test section with barrier coating

#### 4.5.1 Method of coating the channel

1-As shown in the figure (4.14) sensitive balance (Make-Sartorius, model-224-1S, resolution-0.1mg) was used to weight ( $Y_2O_3$ ) nanoparticles and it is applied in an acrylic vacuum glove box (Make-MTI corporation). The mass in grams of ( $Y_2O_3$ ) nanoparticles was required for nano-thermal coating preparation with mass concentrations is calculated to be (Wt. %=5%) using equation mass fraction:

$$wt\% = \frac{\text{mass of nanoparticle}}{\text{total mass}} \quad \dots(4.14)$$

The percentage of 5% was adopted because it achieved the required thermal insulation because the lower percentages did not achieve good thermal insulation and the most of them did not improve the insulation rate.



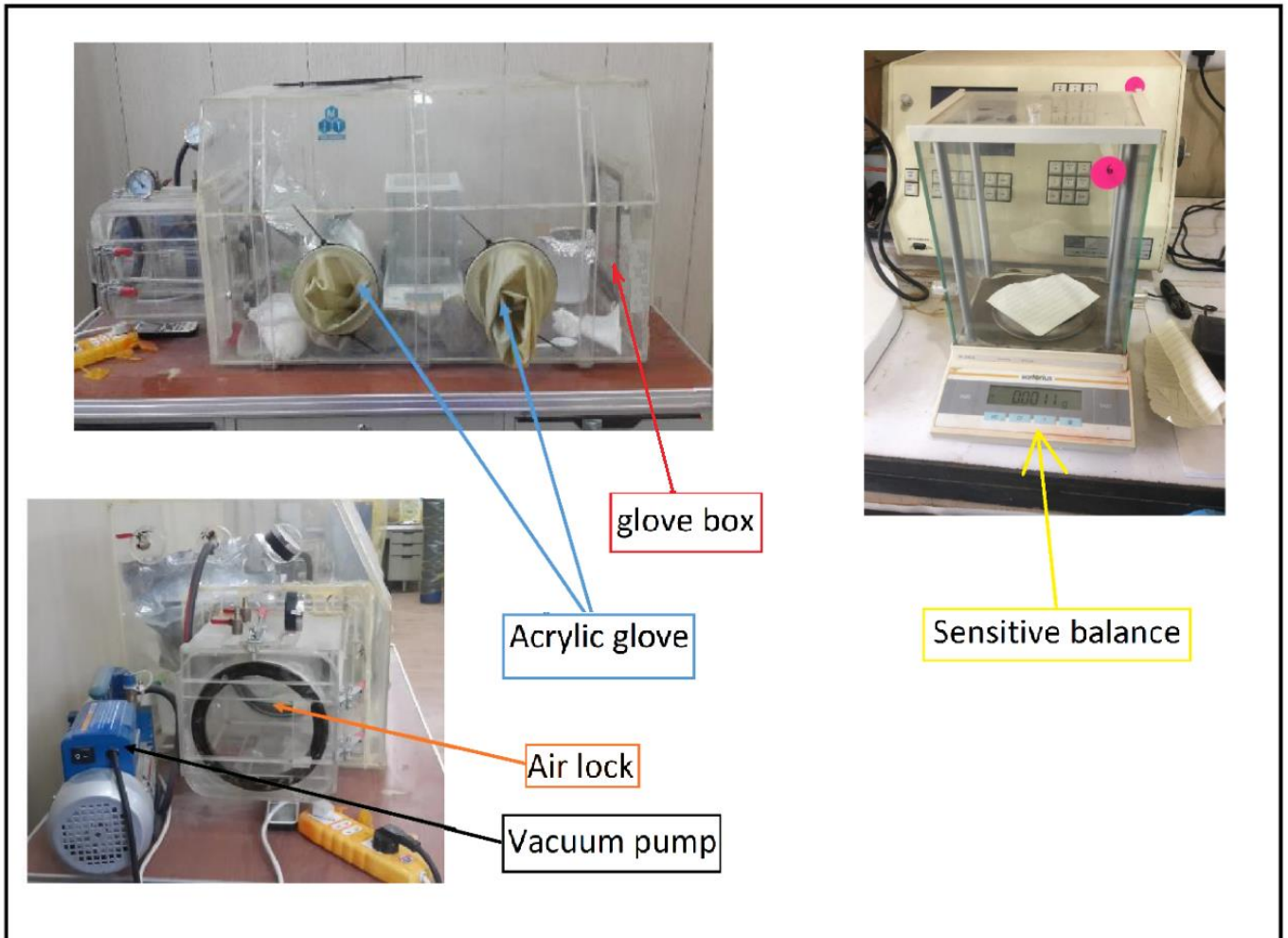


Figure (4.14): Sensitive balance and acrylic vacuum glove box.

2- For mixing the nanoparticle material with thermal painting initially, the powder was added to the painting and stirred by a magnetic stirrer for 45 min at medium speeds. The benzene is added as a dilute mixture to facilitate mixing and coating as shown in figure (4.15a).

3-Ultrasonic vibration mixer (Make- MTI corporation, model-SJIA, power-1200W, frequency- $20 \pm 3$  kHz) was used for mixing dry ( $Y_2O_3$ ). Nanoparticles with thermal painting then mixed by Ultrasonic vibration mix for 2.5 hours to break the agglomerated particles and obtained on a homogeneous mixture of the ( $Y_2O_3$ ) nanoparticles and thermal painting as shown in Figure (4.15 b).



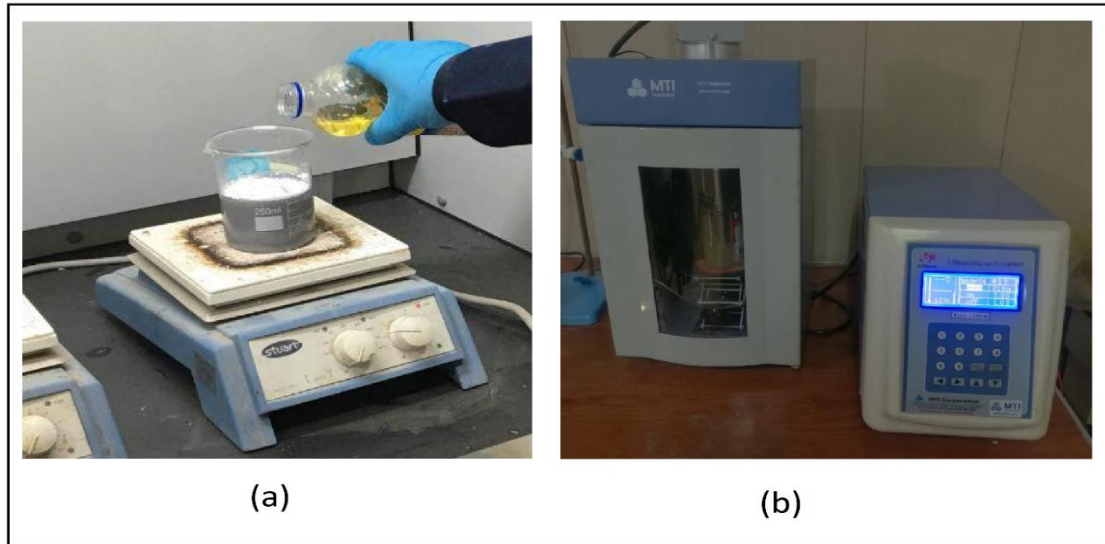


Figure (4.15): magnetic stirrer and ultrasonic vibration devices used for processes mixing of Nano thermal coating: a) Magnetic stirrer b) Ultrasonic vibration mix

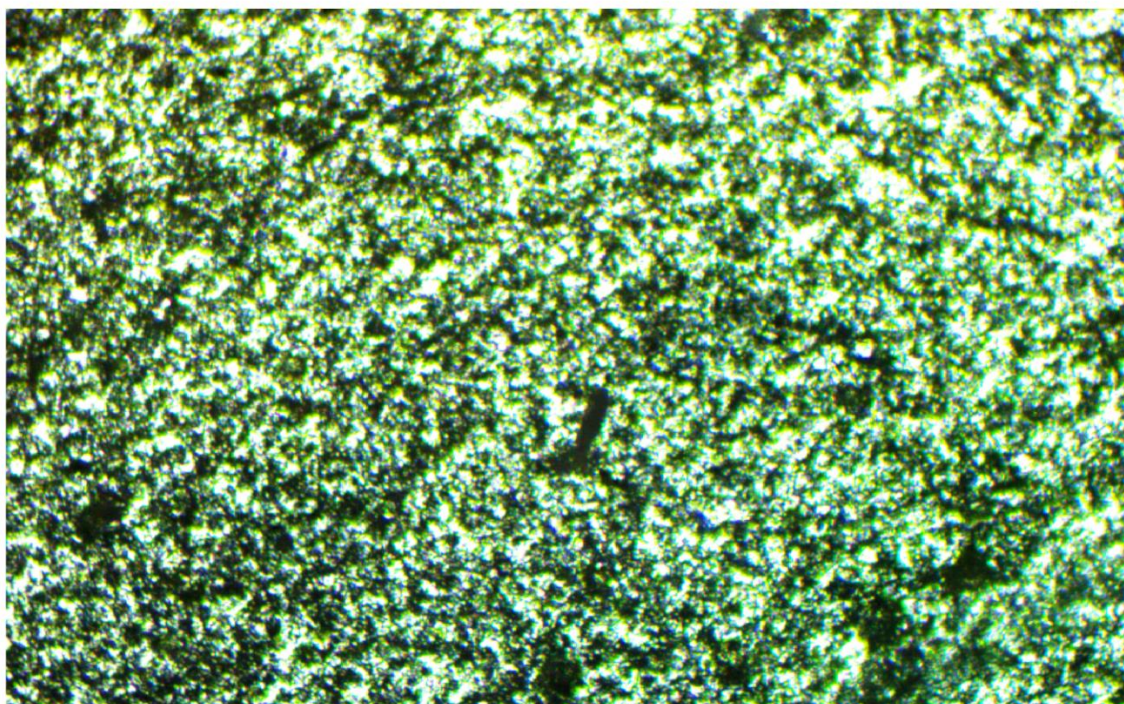
4- Immediately after the preparation process of the mixture is initiated, paint the outer surface of the channel using a paint gun connected to the compressor.

#### 4.5.2 Test under the optical microscope

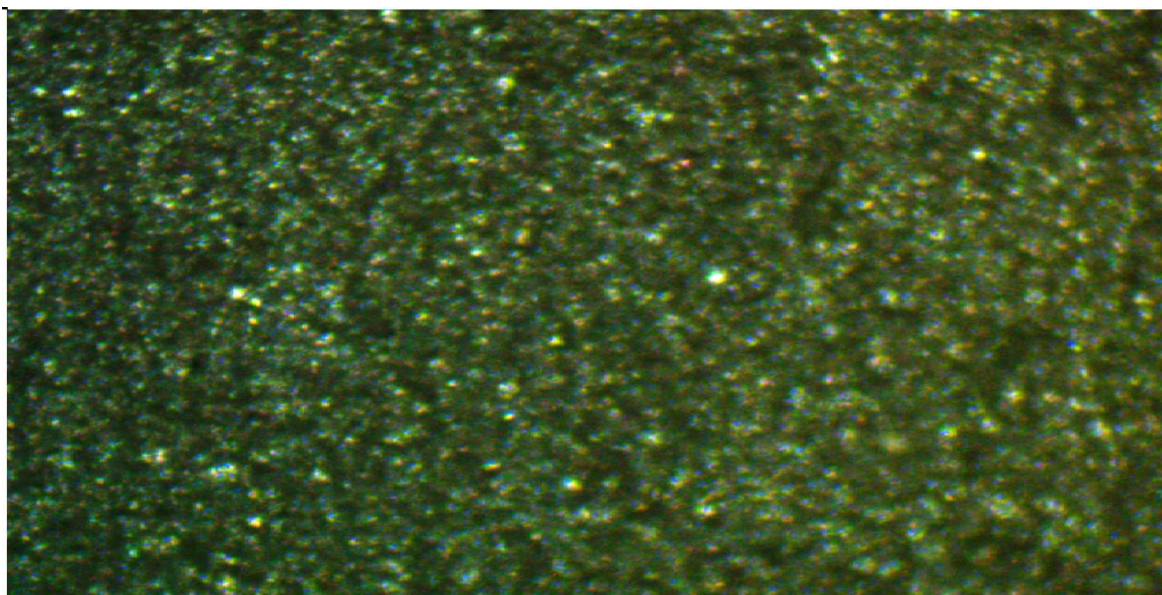
Figure (4.16) shows the photograph of the optical microscope device. Figure (4.17) depicts the photograph of the optical microscope device for channel test section surface with thermal painting only. Figure (4.18) reveals the channel test section surface with thermal painting mixed with ( $Y_2O_3$ ) nanoparticles. The photographs were taken to recognize the difference in the types of painting.



Figure (4.16): Optical microscope device



**Figure (4.17): Channel test section surface with thermal painting only**



**Figure (4.18): Channel test section surface with thermal painting mixed with  $Y_2O_3$  nanoparticles**

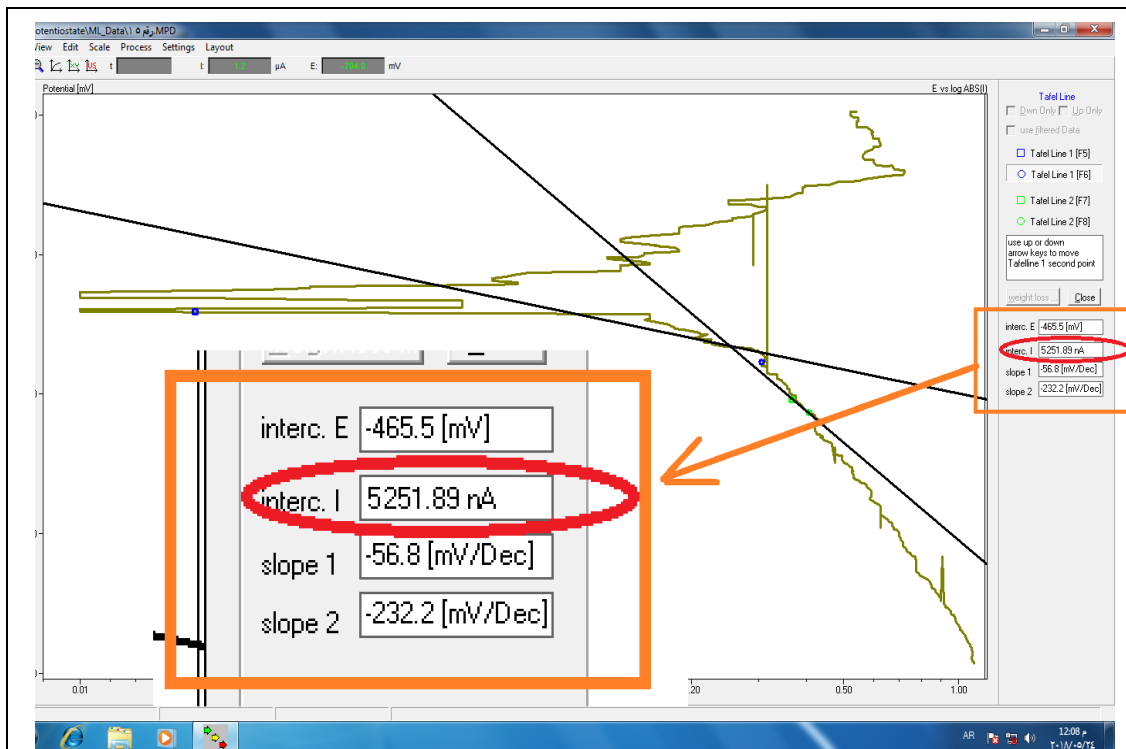


### 4.5.3 Test of corrosion

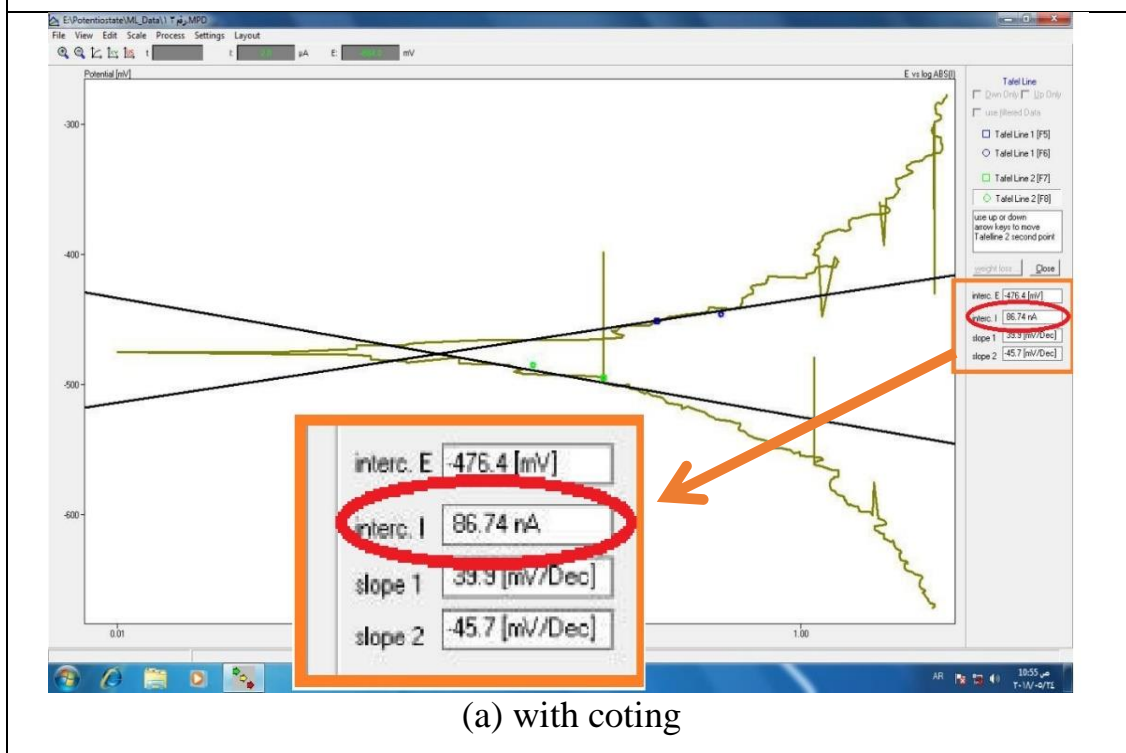
As shown in the figure (4.19) the corrosion test was conducted in the corrosion testing laboratories of the Faculty of Materials Engineering/University of Babylon to determine the resistance of the material used for the coating to corrode. The examination of a metal piece corrosion with/out coating thermal painting, first without the presence of thermal painting mixed with a nanomaterial and the second test is for a piece of metal coated with thermal painting mixed with a nanomaterial. It was found from the results, as shown in figure (4.20), that the corrosion rate decreased when using the coating with the Nano thermal painting which led to reducing the corrosion rate to 98.32 % compared to the test where the coating is absence so it is suitable for coating the blade of gas turbine because it enhances the corrosion resistance.



Figure (4.19): photographic view of the device used to measure corrosion



(a) without coating



(a) with coating

Figure (4.20): picture of the results of the examination of corrosion

## 4.6 Sample of Calculation

To find the case of rib 1 fitted in elliptical channel with channel aspect ratio of 2

### 4.6.1 Reynold number and entrance length:

$$\text{Re} = \frac{u \times D_h}{\nu} = \frac{6.8341 \times 0.037}{1.5804 \times 10^{-5}} = 16000$$

### 4.6.2 Discharge in cold fluid side:

$$A_C(\text{area of elliptic}) = (a \times b \times \frac{\pi}{4}) = \frac{0.057 \times 0.029 \times \pi}{4} = 1.297 \times 10^{-3} \text{ m}^2$$

$$\dot{m} = \rho \times u \times A_C = 1.1776 \times 6.8341 \times 1.297 \times 10^{-3}$$

$$\dot{m} = 10.438 \times 10^{-3} \frac{\text{kg}}{\text{s}}$$

### 4.6.3 Calculation for ribbed channel

To illustrate how the calculations were performed in this research, the case of the rib1fitted in elliptical channel with channel aspect ratio of 2 was taken as an example of the calculations.

#### 4.6.3.1 Total area of heat transfer for smooth channel

Area of channel = Perimeter of channel  $\times$  length of channel

$$\text{Perimeter of elliptic} = \pi \times \sqrt{\frac{a^2 + b^2}{2}}$$

$$\text{Area of smooth duct} = \pi \times \sqrt{\frac{a^2 + b^2}{2}} \times \text{length of duct}$$

$$\text{AT} = \pi \times \sqrt{\frac{0.057^2 + 0.029^2}{2}} \times 0.5 = 0.07103 \text{ m}$$

**4.6.3.2 Heat transfer rate:**

$$Q = \dot{m} C_p (T_o - T_i) = 10.438 \times 10^{-3} \times 1007 \times (335 - 300)$$

$$Q = 367.9 \frac{J}{s}$$

**4.6.3.3 Heat transfer coefficient**

$$Q = \dot{m} C_p (T_o - T_i) = h A T (T_w - T_{\text{mean}})$$

$$T_w = \frac{T_1 + T_2 + T_3 + T_4 + T_5}{5} = \frac{301 + 470 + 503 + 530 + 542}{5} = 469.2 \text{ K}$$

$$T_{\text{mean}} = \frac{T_o + T_i}{2} = \frac{300 + 335}{2} = 317.5 \text{ K}$$

$$\text{Perimeter} = \pi \times \sqrt{\frac{a^2 + b^2}{2}}$$

$$AT = \text{Perimeter of duct} \times \text{length of duct}$$

$$AT = \pi \times \sqrt{\frac{a^2 + b^2}{2}} \times \text{length of duct}$$

$$AT = \pi \times \sqrt{\frac{0.057^2 + 0.029^2}{2}} \times 0.5 = 0.07103 \text{ m}$$

$$367.9 = h \times 0.07103 (469.2 - 317.5)$$

$$h = 34.14 \frac{w}{m^2k}$$

**4.6.3.4 Nusselt Number:**

$$NU = \frac{h D_h}{k} = \frac{34.14 \times 0.037}{0.025658} = 49.231$$

### 4.6.3.5 Friction factor

The pressure drop across the test section measured by the  $\Delta P$  manometer.

$$\Delta P = 33 \text{ (Pa)}.$$

By using equation (4.6)

$$f = \frac{2 \rho \Delta P D_h A_C^2}{L m^2}$$

$$f = \frac{2 \times 1.176 \times 33 \times 0.037 \times (1.297 \times 10^{-3})^2}{0.5 \times (10.438 \times 10^{-3})^2} = 0.0886$$

### 4.6.4 Calculation for ribbed channel

#### 4.6.4.1 Total area of heat transfer

$$AT = A_{duct} + A_{ribs} - A_{contact}$$

$$AT = A_{duct} + (\text{Number of rib} \times \text{area of one rib}) \\ - (\text{Number of contact area} \times A_{contact})$$

$$AT = 0.07103 + (9 \times 0.001728) - (9 \times 0.00071) = 0.080192 \text{ m}$$

#### 4.6.4.2 Heat transfer rate:

$$Q = \dot{m} C_p (T_o - T_i) = 10.438 \times 10^{-3} \times 1007 \times (416 - 301)$$

$$Q = 1208.77 \text{ W}$$

#### 4.6.4.3 Heat transfer coefficient

$$Q = \dot{m} C_p (T_o - T_i) = h AT (T_w - T_{mean})$$

$$T_w = \frac{T_1 + T_2 + T_3 + T_4 + T_5}{5} = \frac{301 + 441 + 474 + 501 + 513}{5} = 446 \text{ K}$$

$$T_{mean} = \frac{T_o + T_i}{2} = \frac{301 + 416}{2} = 358.5 \text{ K}$$

$$1208.77 = h \times 0.080192 \times (446 - 358.5)$$

$$h = 172.26 \frac{W}{m^2k}$$

#### 4.6.4.4 Nusselt number:

$$NU = \frac{h D_h}{k} = \frac{172.26 \times 0.037}{0.025658} = 248.41$$

#### 4.6.4.5 Friction factor

The pressure drop across the test section measured by the  $\Delta P$  manometer.

$$\Delta P = 440 \text{ (Pa)}.$$

By using equation (4.6) [61].

$$f = \frac{2 \rho \Delta P D_h A_c^2}{L \dot{m}^2}$$

$$f = \frac{2 \times 1.176 \times 440 \times 0.037 \times (1.297 \times 10^{-3})^2}{0.5 \times (10.438 \times 10^{-3})^2} = 1.182376$$

#### 4.6.5 Thermal performance factor

By using equation (4.6) [60].

$$\eta = \frac{\left( \frac{Nu_{rib}}{Nu_{smooth}} \right)}{\left( \frac{f_{rib}}{f_{smooth}} \right)^{\frac{1}{3}}}$$

$$\eta = \frac{\left( \frac{248.41}{49.231} \right)}{\left( \frac{1.182376}{0.0886} \right)^{\frac{1}{3}}} = 2.127$$



# **CHAPTER FIVE**

## **RESULTS AND DISCUSSION**

---

---

## CHAPTER FIVE

### RESULTS AND DISCUSSION

#### 5.1 Introduction

The numerical and experimental results of the flow and heat transfer characteristics in four channels with elliptical cross sections having the same hydraulic diameter, with different in aspect ratio, the different shapes of ribs, with and without thermal barrier coating are presented in this chapter. The numerical results were compared with the experimental results and were in good agreement.

The effect of the shape of rib configuration, aspect ratio, Reynolds number, relative roughness pitch and coating the outer surface of the channel with nanocomposite material, were presented and discussed in this chapter. All results obtained were compared with a smooth channel (reference case). The length of the channel was considered as one unit.

#### 5.2 Numerical Results

The numerical results of the present work of four elliptical channels fitted with ribs with different aspect ratio are presented in this section.

Figure (5.1) presents the value of the Nusselt number for the four elliptical channels varying with the Reynold number in the case of a smooth channel (without ribs). It is clear from the figure that the value of the Nusselt number in each channel is at its highest value when Re equals to 16000 and an aspect ratio is 2. That was resulted due to the increase of the channel aspect ratio, which minimizes the distance between the wall surface of the channel and the centerline of coolant air. In this case, and that will increase the conductivity and heat transfer between the air and the channel surface and thus increase the Nusselt number with increase channel aspect ratio.

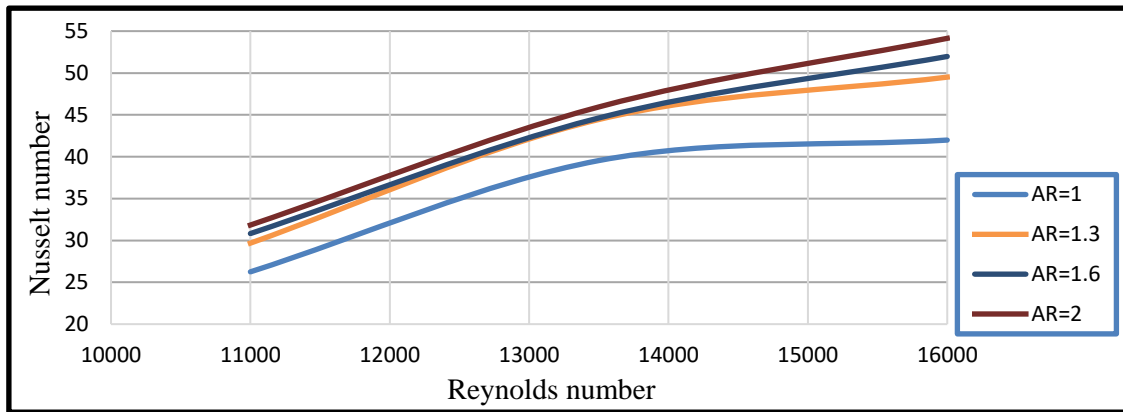


Figure (5.1): Numerical average Nusselt number variation with Reynolds number for different channel aspect ratio for smooth channels

### 5.2.1 Temperature distribution

Figures (5.2) and (5.3) show the temperature distribution contours through the elliptical channels for coolant air of ( $Re=16000$ ), inlet air temperature (300 K) and surrounding hot air temperature (673 K) with different rib configurations. The ribs were fitted in the channel and caused a clear disturbance if it is compared with the smooth channel. These ribs created wakes which developed to vortices. This led to increasing the heat transfer from the channel wall to the coolant air stream, i.e. increased the coolant air temperature. Different temperature contours were seen depending on the shape of rib geometries and the cross-section of the channel.

Figure (5.2) depicts the air temperature distribution contour through the smooth channel, with different aspect ratio. It shows that the coolant air temperature at channel centerline increases only slightly throughout the channel, and increased with increasing aspect ratio of the channel.

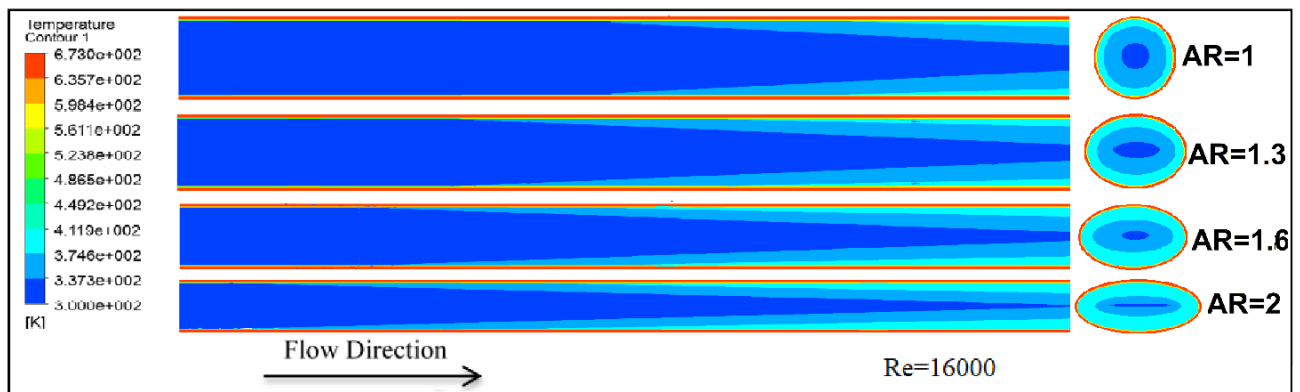


Figure (5.2): Coolant air temperature distribution contours for four smooth channels with different aspect ratio (AR)

---

---

### 5.2.1.1 Effect of aspect ratio and rib geometry on coolant air temperature

Figure (5.3.a, b, c, and d) represents the temperature distribution contours for different rib configuration fitted in elliptical passages with different aspect ratio. Figure (5.3.a) shows the air temperature distribution contour through the circular channel of aspect ratio= 1, fitted with different circular ribs. It reveals that the coolant air temperature was affected in the channel centerline and raised in the second half of the channel. That happens due to the effect of circulation generated by the ribs, which clearly enhances the heat transfer between the hot channel walls and the coolant air stream. It also shows that fitting rib1 in the passage has the greatest influence on improving the heat transfer from the channel walls to the coolant air. However, a clear temperature rise is noticed by using rib 4, which is worst. Figure (5.3.b) shows contours of temperature distribution for the elliptical ribs named (rib 1, rib 2, rib 3, and rib 4) which are fitted in other channels of the aspect ratio of (1.3). It reveals that using rib 1 is the best and rib 4 is the worst case in heat transfer. The same behavior can be seen in (5.3. c, and d) which represent channel with AR (1.6) and AR (2). Figures (5.3.a, b, c, and d) also show the influence of the varying aspect ratio on coolant air temperature. Increasing the aspect ratio of the channel causes increase in coolant air temperature because of the increasing of the aspect ratio in which the space between the channel wall is reduced and the heat transfer was enhanced. It is clear that the case of the AR (2) is the preferred case in which the coolant air temperature rises. Moreover, it is the best case in heat transfer enhancement. Thus, the best case in improving heat transfer is the case of rib1 fitted in the elliptical channel with AR (2) which gave more temperature rise compared with the other cases.

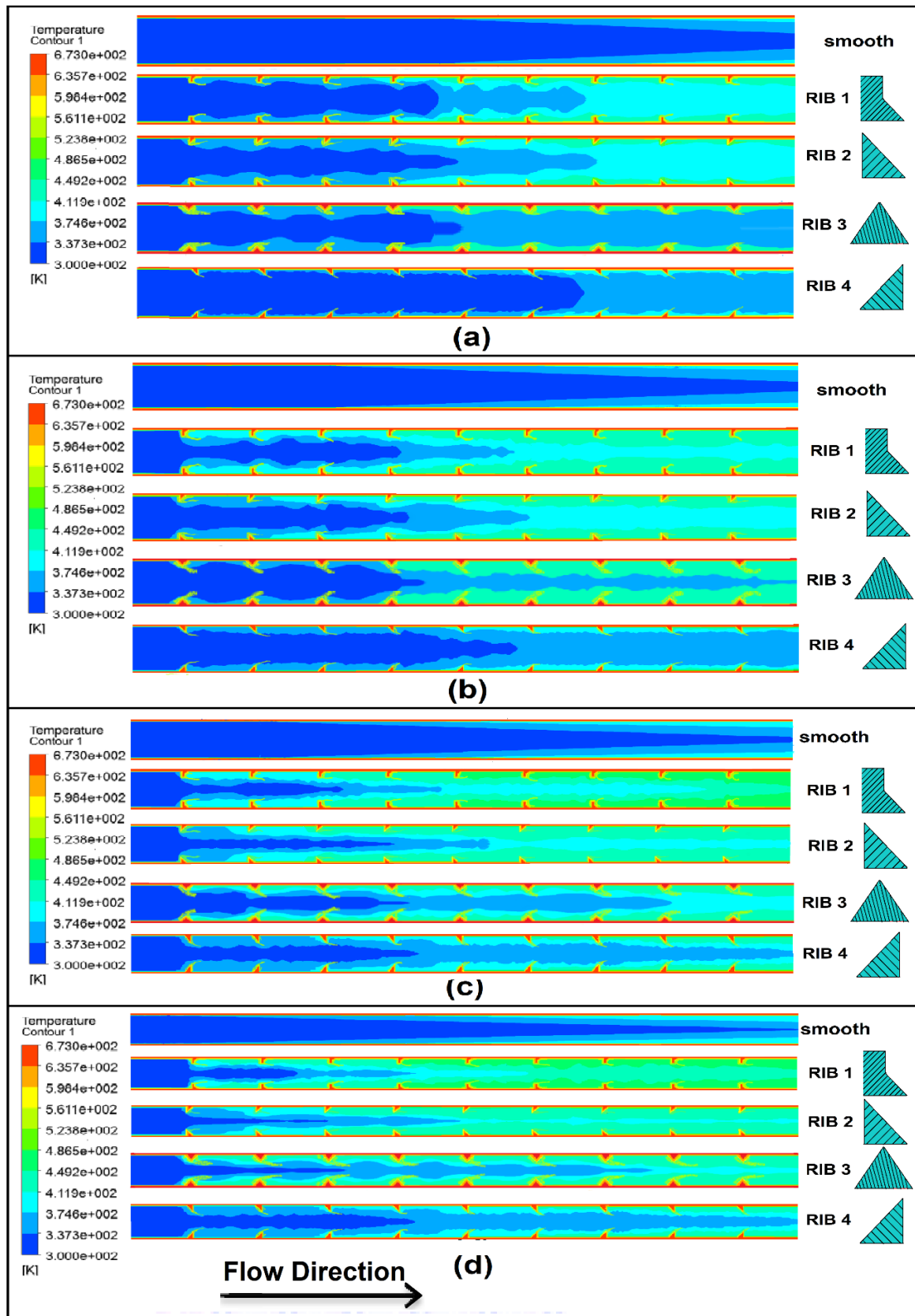


Figure (5.3.a, b, c, and d): Temperature distribution contours for ribs fitted in elliptical passage with  $Re=16000$  and different Aspect ratio: a)  $AR=1$ , b)  $AR=1.3$ , c)  $AR=1.6$ , d)  $AR=2$

---

---

### 5.2.1.2 Inner wall surface temperature variation

Figure (5.4.-a, b, c, and d) shows the numerical results of inner wall surface temperatures for different rib configurations and aspect ratios. The inner wall surface temperature for the smooth channels is decreased with the increase channel aspect ratio. Due to the increasing of the aspect ratio of the channel, increases the coolant air temperature increases because the increasing aspect ratio will reduce the space between the channel wall, and thus the heat transfer will increase and thus reduce the temperature of the inner wall surface. It is noticeable from this figure that the inner surface of the AR=2 has the lowest temperature as compared to other channels because it is the best channel in which heat transfer and cooling channel walls was achieved. The inner wall surface temperature for a ribbed channel is lower than a smooth one for all cases. The average surface temperature of the inner wall of the channel is less than the surface temperature and the lowest temperature is when channel has AR=2, where the rates of decreasing percentage of temperatures of the inner wall surface of case of ribbed channel fitted with rib1 as compared with smooth channel is (5.8%,5.1%,4.5%, and 3.6 %) and for channel fitted with (rib1, rib 2, rib 3, and rib 4), respectively. This is because ribs make wakes which develop to vortices. This leads to increase the heat transfer from the channel wall to the coolant air, i.e., decreases the inner wall temperature and increase the temperature of coolant air. Therefore, the best condition in cooling the inner wall surface of the channel is the case of rib 1 fitted in the channel with AR=2.

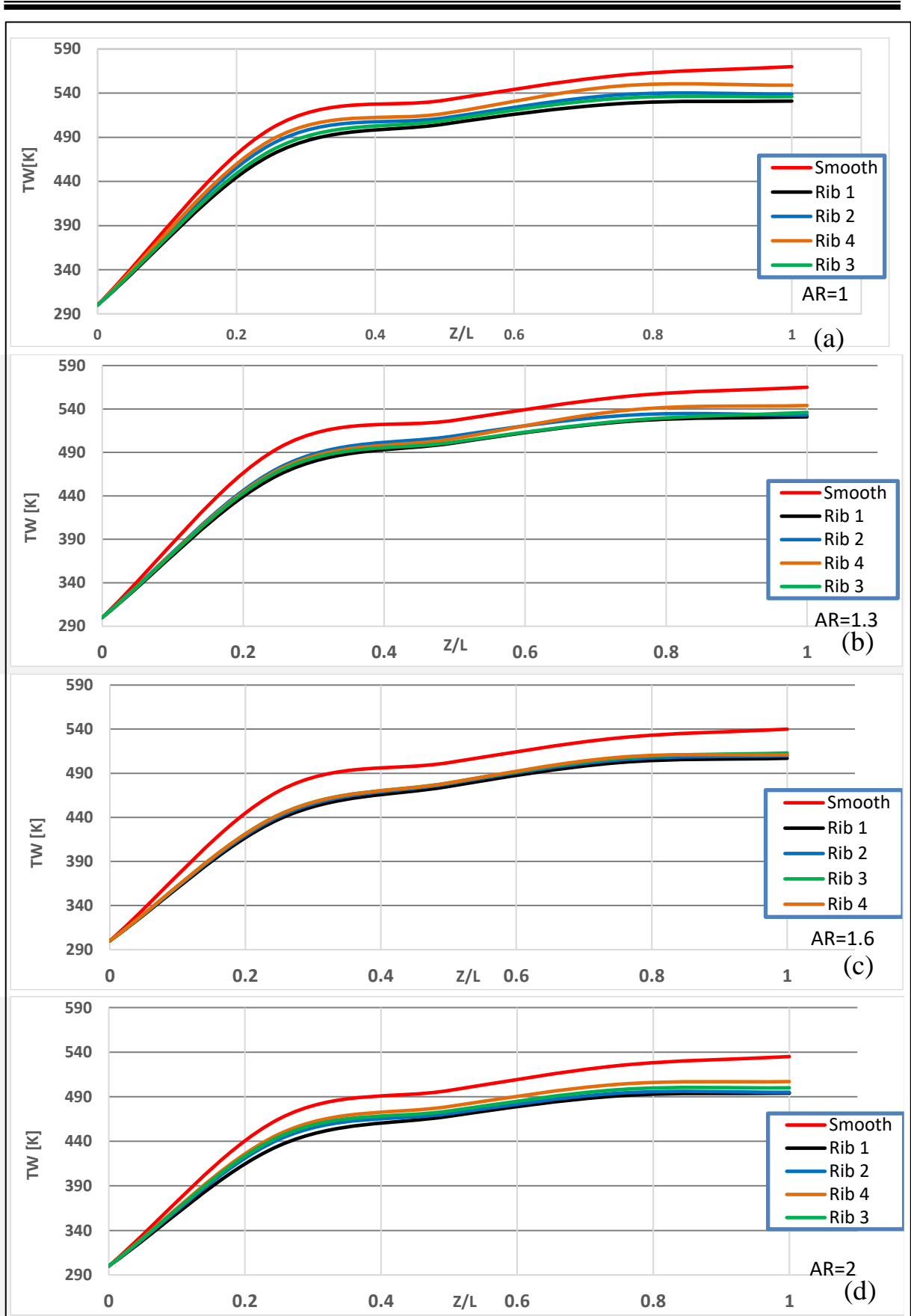


Figure (5.4. (a, b, c, d)): Numerical result of inner wall surface temperature with different channel aspect ratio of  $Re=16000$

---

---

### 5.2.1.3 Effect of rib geometry and channel aspect ratio on coolant air temperature

Figure (5.5 -a, b, c and d) presents the numerical results of coolant air temperatures along the channel centerline for different rib configurations with  $Re=16000$ . The coolant air temperature along the centerline for the smooth channels rises with the increase channel aspect ratio. As it mentioned before, increasing in the aspect ratio reduces the space between the channel wall, and thus the heat transfer increase and this increases the thermal content of the air and thus increases its temperature. It is notable from this figure that the central air temperature is at its highest state at the channel  $AR=2$  as compared to other channels. The air temperature for the ribbed channel was higher than that for a smooth channel. This is because that ribs make wakes which developed vortices. This leads to increase the heat transfer from the channel wall to the coolant air, i.e., increasing the coolant air temperature. For the channel with  $AR (2)$  if it compares the channel with ribs with the smooth channel it can be concluded for case of (rib 1, rib2, rib3, and rib 4) that there is an increase in the temperature percentage of the cooling air outside from the channel from the temperature of the cooling air entering channel by (25%,21.7%,11.3%, and 3.9%), respectively. Case of rib1 have higher coolant air temperatures than the other cases, this indicates that this case has More suitable shape to accelerate the coolant air flow and thus increasing coolant air temperature. Therefore, the case of rib1 fitted in the channel with  $AR=2$  is the most case in which there has been an increase in centerline air temperature, so it is the best case in heat transfer.



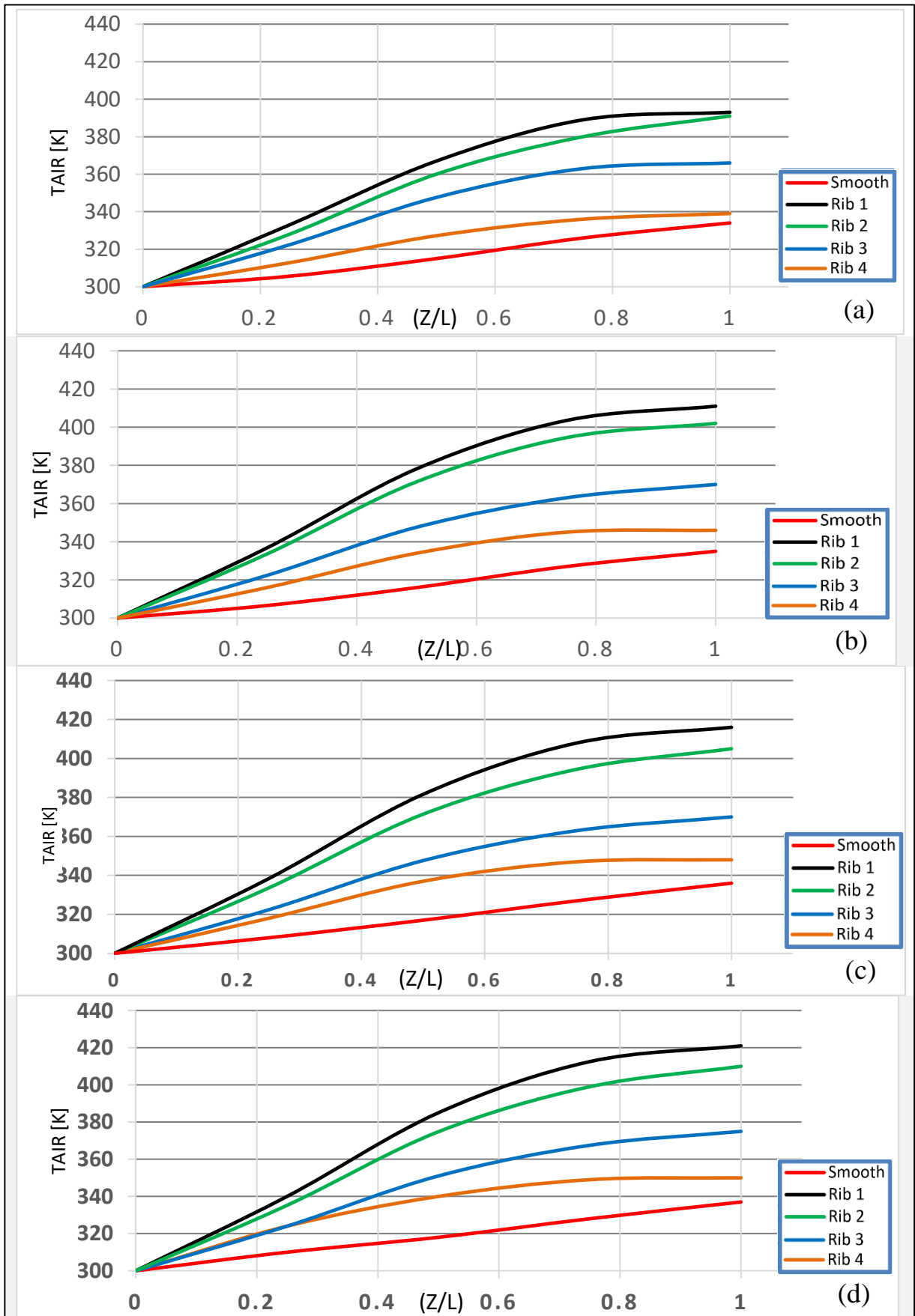


Figure (5.5 (a, b, c, and d)): Numerical air temperature distribution at the channel centerline for (Re=16000) having different aspect ratio with and without ribs

Figure (5.6) shows a right side section of coolant air temperature distribution contour for the case of using rib1 and channel aspect ratio (2) after each rib position along the channel. The figure shows that the temperature after the first rib is low in the center of the channel and increases toward the hot surface due to heat transfer between cooling air and hot surface. Temperature rises as it gets closer to the end of the channel due to the increase in thermal content of the coolant air, which gives a good indicator of the performance of using the elliptical rib in elliptical channel.

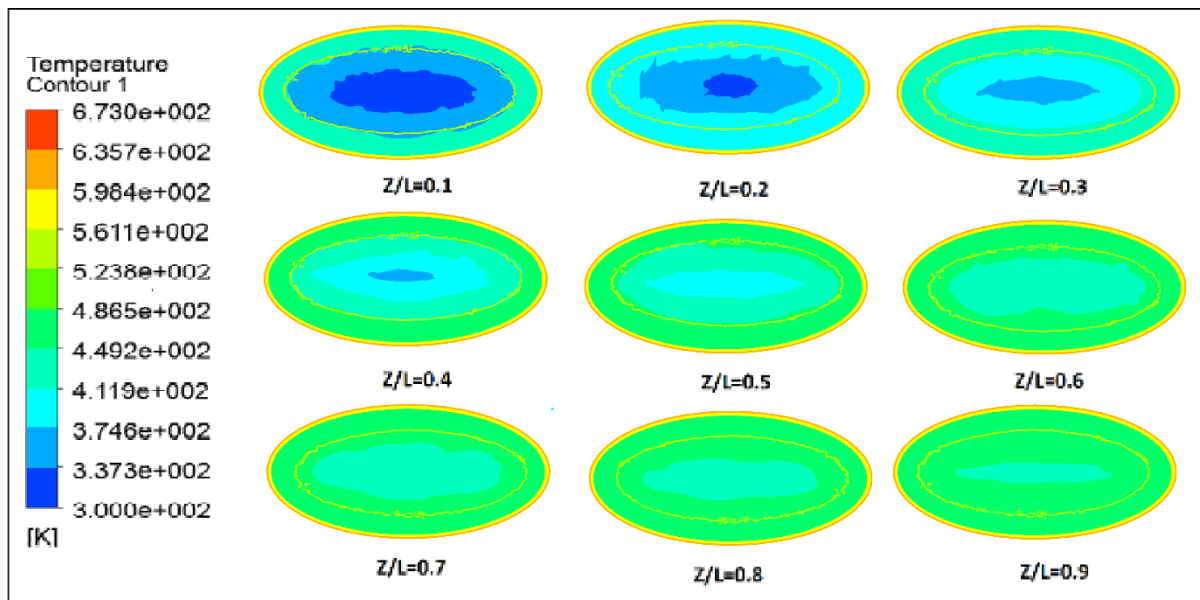


Figure (5.6): Coolant air temperature distribution contour for using rib1 and channel aspect ratio (2) (right side section)

### 5.2.2 Coolant air velocity distribution

Figure (5.7) shows the contour of velocity distribution for a smooth elliptical channel at surrounding hot air temperature of (673 K) and coolant air flow ( $Re=16000$ ). It also reveals that cooling air velocity at channel centerline remains constant throughout the channel.

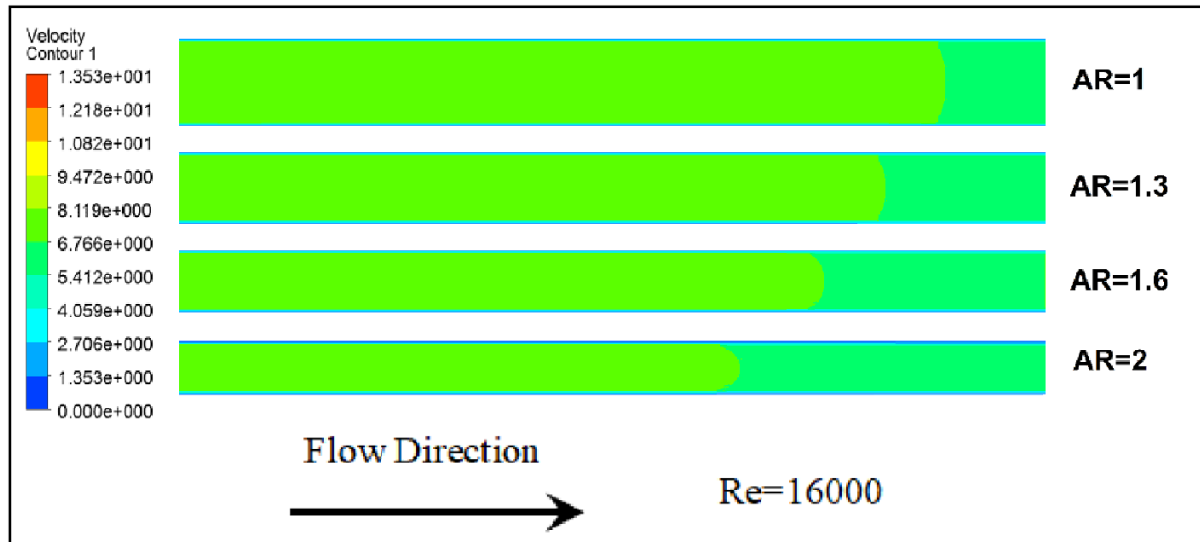


Figure (5.7): Velocity contours of smooth cases with different aspect ratio

Figures (5.8) to (5.11) present the contour of velocity distribution through a channel using different channel aspect ratio fitted with ribs for a coolant air flow of ( $Re=16000$ ), inlet air temperature (300 K) and surrounding hot air temperature (673 K). The coolant air flow was accelerated and decelerated through the channel, due to contraction and expansion for using these ribs. Figure (5.8) shows rib1 fitted in different channel aspect ratio and the effect of increasing the channel aspect ratio where increase AR from 1 to 2 will be accompanied by increased changes in the amount of air velocity and direction inside the channel. The highest disturbance of the speed happens at channel  $AR=2$  and that will cause increase heat transfer from the channel inner wall surface to coolant air and this drives the ribbed channel with  $AR=2$  to be the best in cooling the wall of the channel. The same behavior can be seen in figure (5.9) for rib 2, figure (5.10) for rib 3, and figure (5.11) for rib 4.

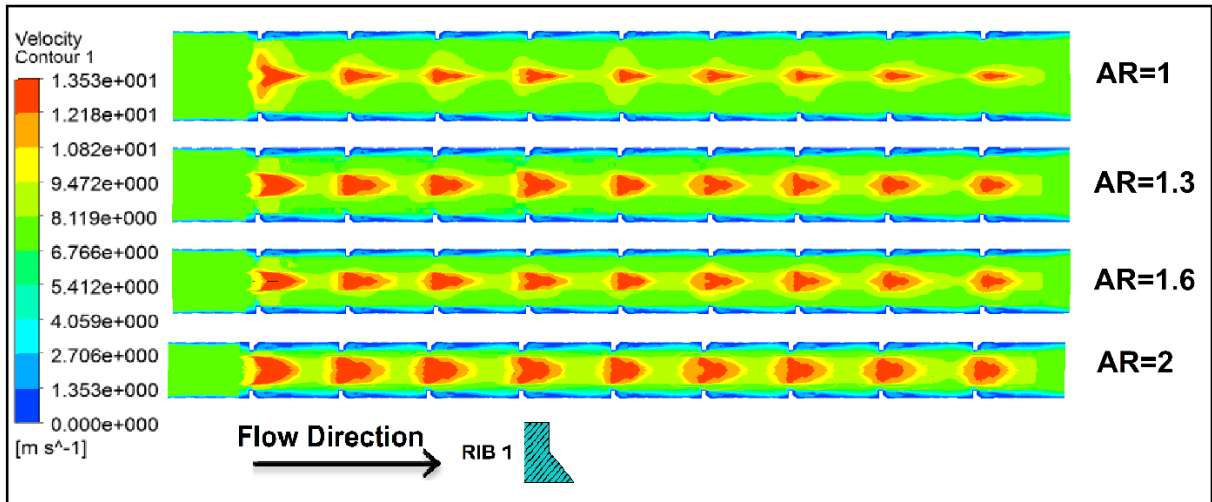


Figure (5.8): Velocity contours for the coolant air at different channel aspect ratio with case of rib (1) at  $Re=16000$

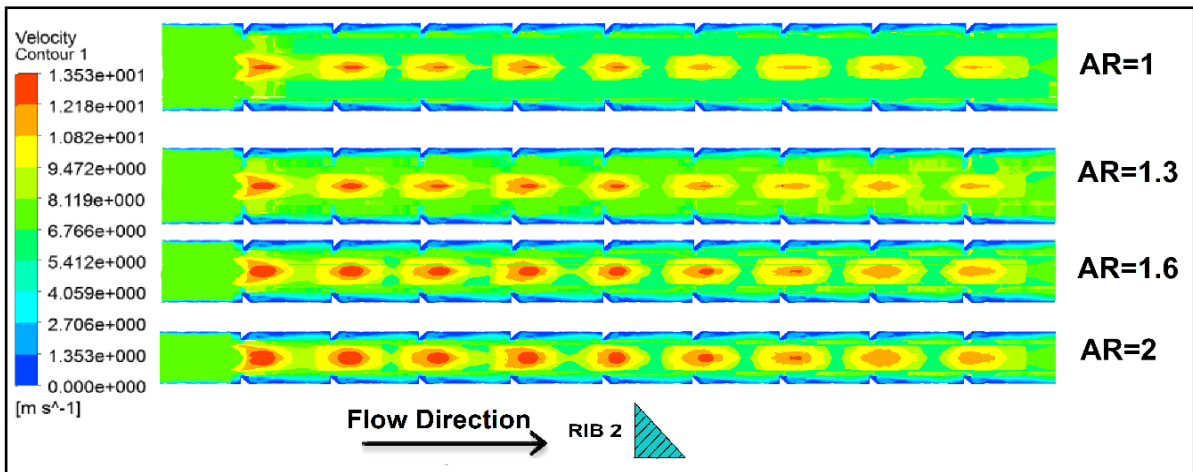


Figure (5.9): Velocity contours for the coolant air at different channel aspect ratio with case of rib (2) at  $Re=16000$

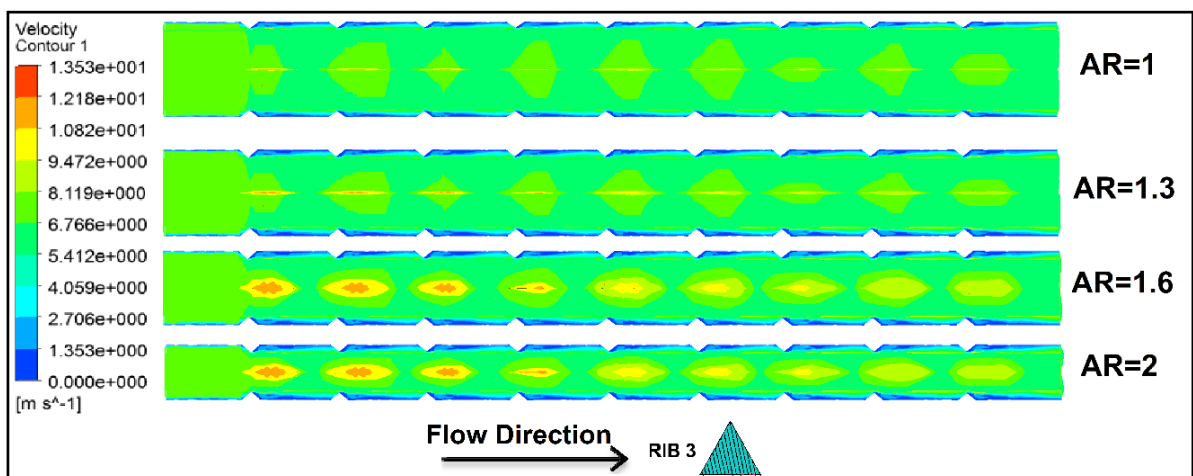


figure (5.10): Velocity contours for the coolant air at different channel aspect ratio with case of rib (3) at  $Re=16000$

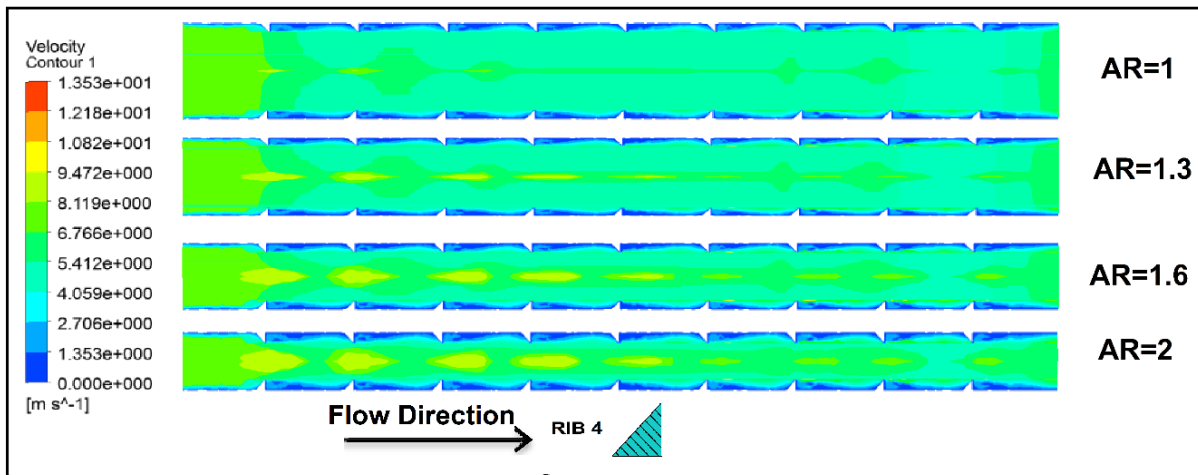


Figure (5.11): Velocity contours for the coolant air at different channel aspect ratio with case of rib (4) at  $Re=16000$

Figures (5.12) to (5.15) present the contour of velocity distribution through a channel using different rib configurations, for a coolant air flow of ( $Re=16000$ ), inlet air temperature (300 K) and surrounding hot air temperature (673 K). The coolant air flow was accelerated and decelerated through the channel due to contraction and expansion for using these ribs (rib1, rib2, rib3, and rib4). In all cases, the velocity distribution depends on the rib shape, and hence different behavior for the velocity distribution for each case was seen. Figure (5.12) shows the channel with  $AR=1$  and fitted with different rib configurations. Figure (5.12) shows the channel with  $AR=1$  which fitted with different rib configurations, it can be concluded that rib1 causes more disturbance and change in the speed of coolant air inside the channel than other ribs, thus it will be the best in the transfer of heat. We observe the same behavior in figure (5.13) for a ribbed channel with  $AR=1.3$ , figure (5.14) for a ribbed channel with  $AR=1.6$ , and figure (5.15) for a ribbed channel with  $AR=2$ .

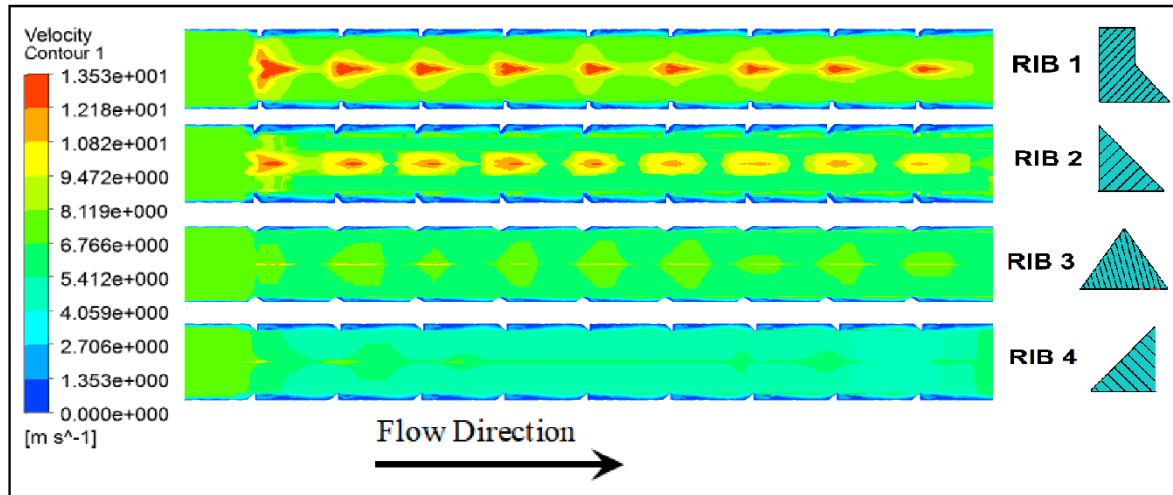


figure (5.12): Velocity contours for coolant air inside the channel of AR=1 with different rib configuration at Re=16000

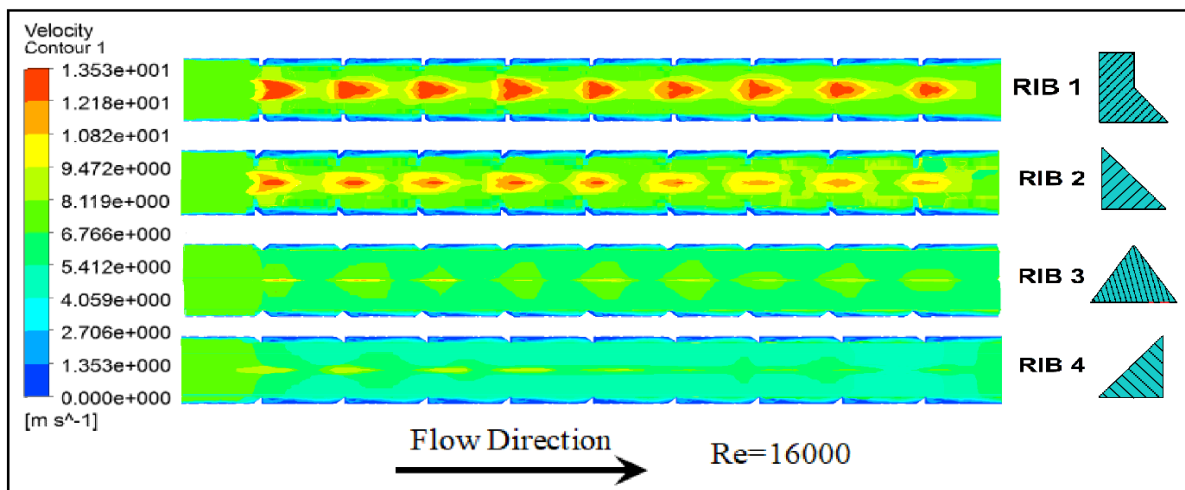


Figure (5.13): Velocity contours for coolant air inside the channel of AR=1.3 with different rib configuration at Re=16000

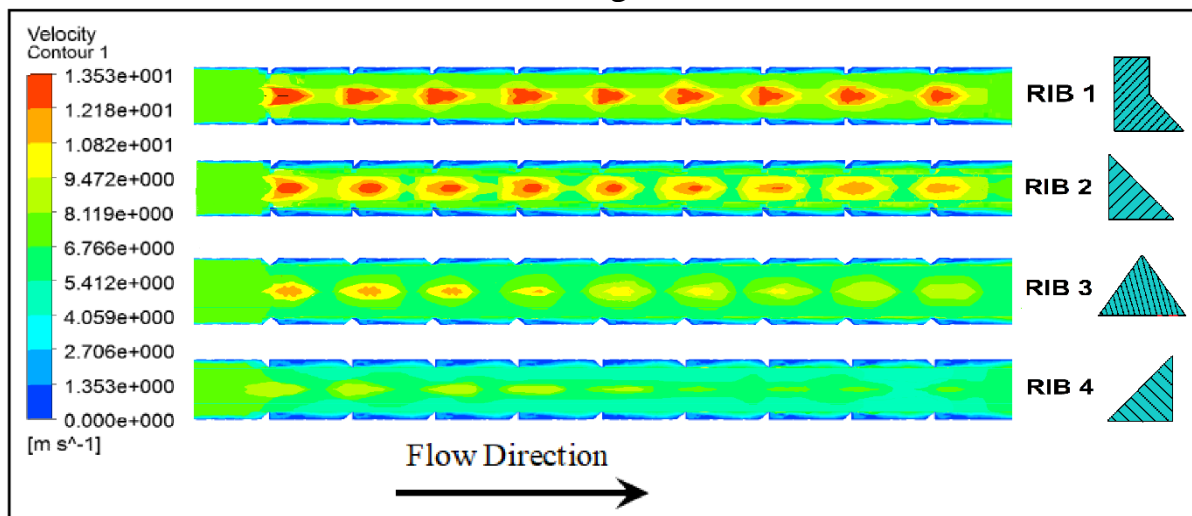


Figure (5.14): Velocity contours for coolant air inside the channel of AR=1.6 with different rib configuration at Re=16000

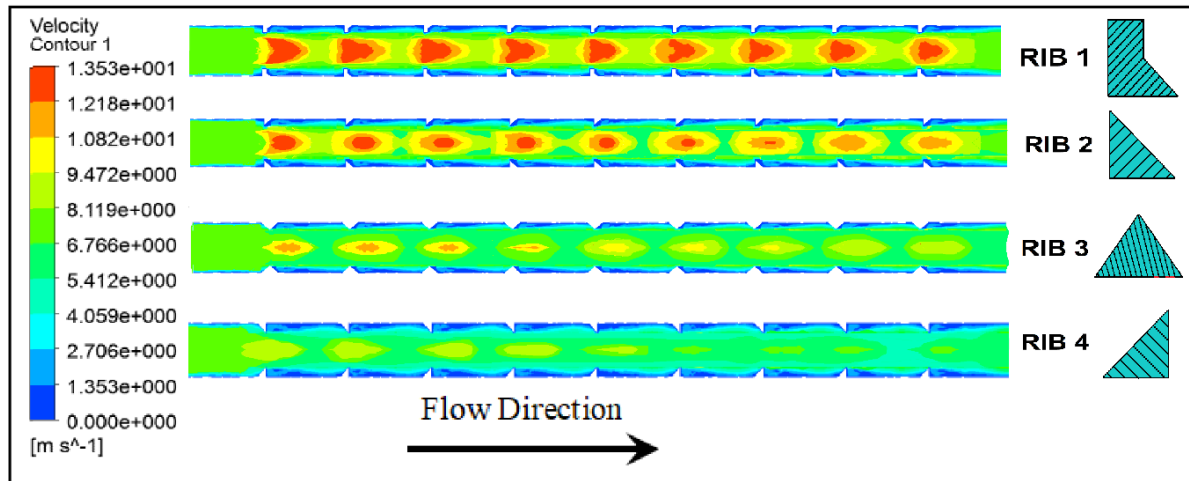


Figure (5.15): Velocity contours for coolant air inside the channel of AR=2 with different rib configuration at Re=16000

In all cases, the velocity distribution depends on the rib shape, and channel aspect ratio and hence different behavior for the velocity distribution for each case was seen. It is clear in figure (5.16) and (5.17) which represent the distribution of velocity along the centerline of the channel.

From the contours and figures of velocity, it can be concluded that channel with AR=2 fitted with rib 1 is more effective in change the velocity magnitude and direction and gives more turbulent inside the ribbed channel. As a result, enhancement in heat transfer was achieved.

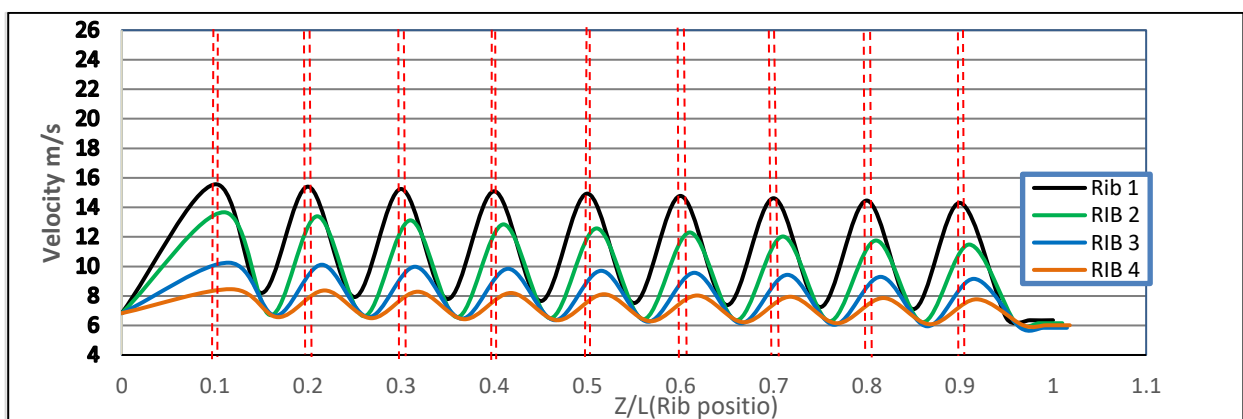


Figure (5.16) Velocity distribution along the channel centerline for Re=16000, and AR=2 and different rib configuration



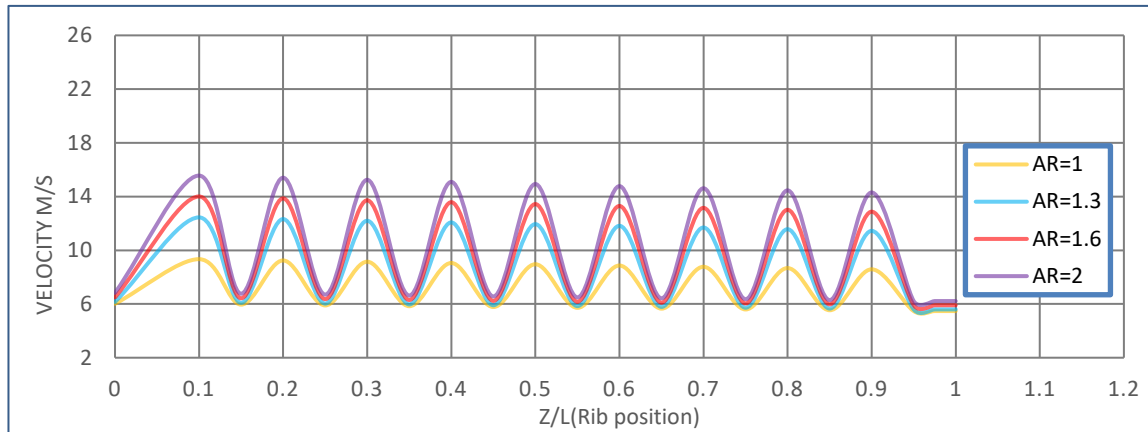


Figure (5.17): Velocity distribution along the channel centerline for  $Re=16000$  and rib 1 with different aspect ratio

Figure (5.18) shows the contour of velocity vector through an elliptical channel with  $AR=2$  fitted with ribs of different configurations for coolant air flow of ( $Re=16000$ ), inlet coolant air temperature (300 K) and surrounding hot air temperature (673 K). The presence of ribs caused flow separation and reattachment. The boundary layer was disturbed and the turbulence of flow increased due to separation and reattachment. This near the wall with the cooler ones in the middle of flow and that caused enhancement in heat transfer.

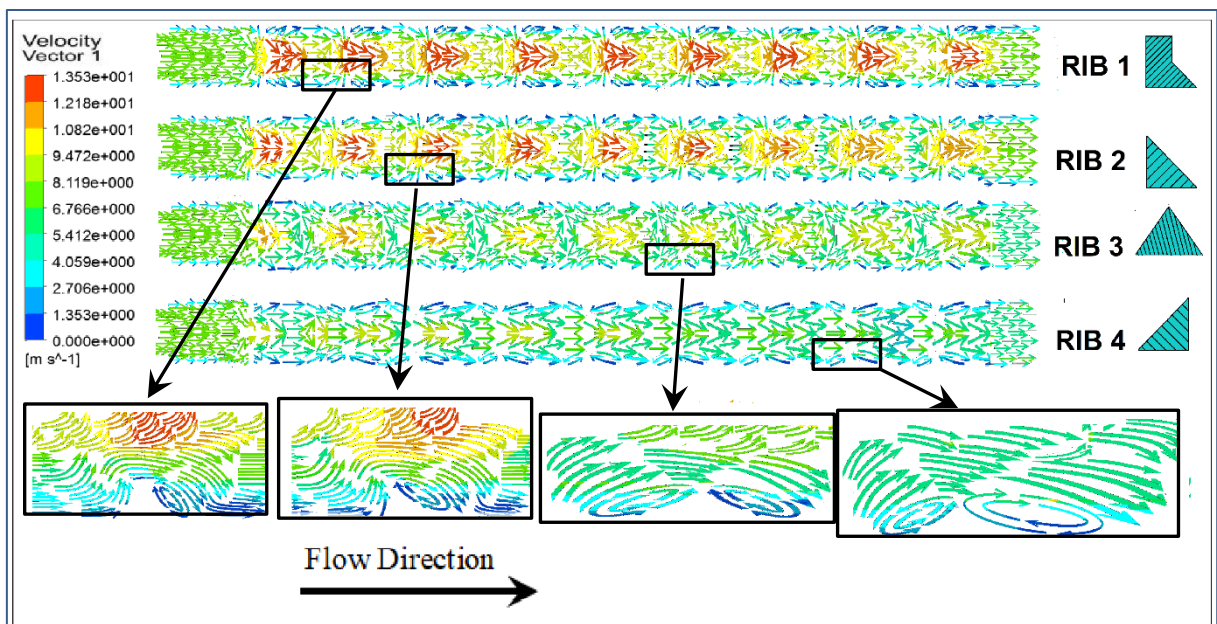


Figure (5.18): Velocity vector through the channel for (rib1, rib2, rib3, and rib4) and  $Re = 16000$  with aspect ratio (2)



Figure (5.19) exposes the pattern of streamline in the zone between the 3rd and 4th rib. It can be seen the eddy formation which represents the dead regions adjoining ribs, together with the upstream and the downstream sides is clearly seen. a downstream side with larger eddies represent the areas with a low rate of heat transfer. The figure exposes the length of flow reattachment of the four ribs shape fitted in the channel with  $AR=2$ . The shorter reattachment length for separated streamline can be seen in the case of using rib1 as compared with the other ribs. It gives a larger area to heat exchange between coolant air and inside wall surface and highly enhanced heat transfer further than other ribs. Rib 3 and rib 4 were seen to be worst cases of the heat transfer because of rib 3, and rib 4 product extremely great separation rejoin just back the rib. The probable reason to this is that upward flow occurring because of the inclining front surface for rib 3, and rib 4. Considering, the rib 1 produced a flow reattachment earlier than other ribs, hence, gives the highest rate of heat transfer.

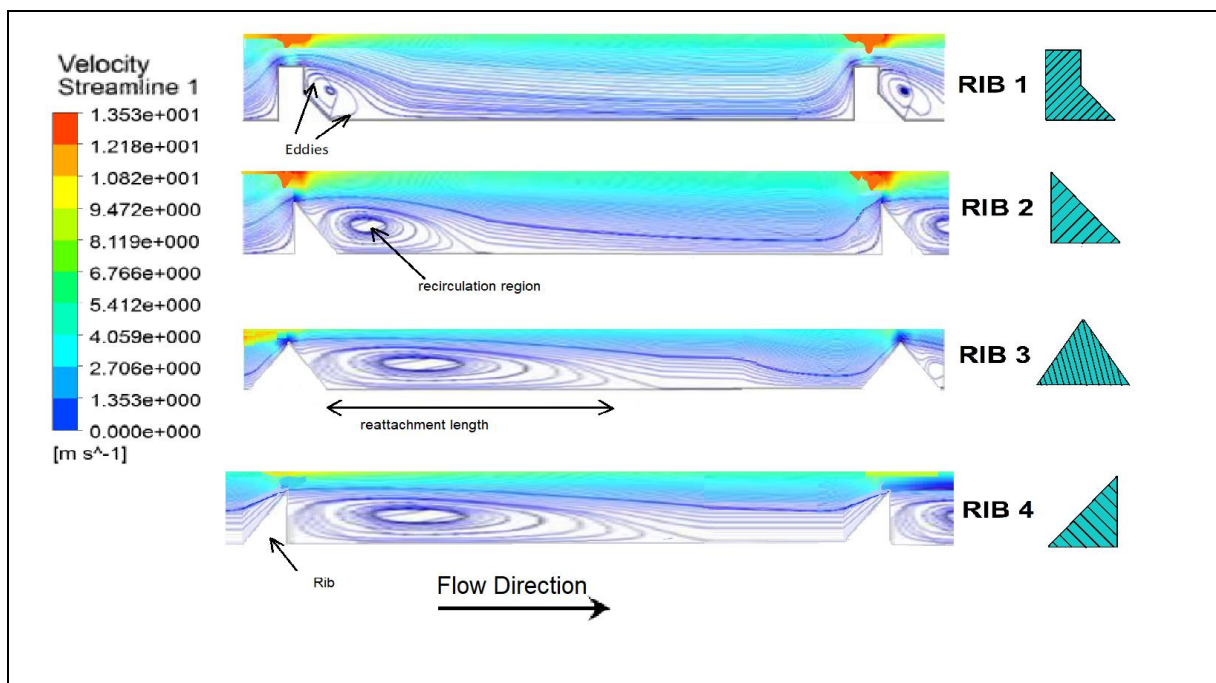


Figure (5.19): Streamlines between the third and fourth ribs on  $y-z$  plane for all ribs with  $AR=2$  and  $Re=16000$

---

---

### 5.2.3 Effect of rib geometry and aspect ratio on the average Nusselt number

Figure (5.20-a, b, c, and d) shows the variation of Nusselt number as a function of Reynolds number for different values of channel aspect ratio ranging from 1 to 2, with and without ribs. It was observed that in all cases the Nusselt number rises with the increase in Reynolds number. The rise in Nusselt number is more prominent at higher Reynolds number as compared to that at lower Reynolds number. This is because the increase in Reynolds number due to the increase in air velocity. That means an increase in the rate of cold air mass flow rate, which will have a greater ability to transfer more heat when passing through the ribbed channel in which Reynold number is increased strength of recirculation, turbulent kinetic energy Thus, heat transfer will be increased by increasing convective heat transfer coefficient ( $h$ ), and the average Nusselt number. It was also observed that the value of Nusselt number increases with an increase in aspect ratio because the increase in aspect ratio will be accompanied by increasing heat transfer and thus increasing the number of Nusselt number. The maximum value of Nusselt number was observed when using rib 1 at all aspect ratio. The boot rib design shows the maximum overall heat transfer rate due to the smallest separation zone downstream the rib, the possible reason for that is the geometry of the rear part of the boot-shaped rib. Thus, rib 1 causes enhancement heat transfer more than the rest ribs. Also, the maximum value of average Nusselt number found at the channel with AR=2, which fitted with rib 1 at Re =16000.

### 5.2.4 Effect of rib geometry on friction factor ratio

Figure (5.21-a, b, c, and d) present the friction factor ratio for all rib configurations and channel aspect ratios with constant surrounding hot air temperature of (673 K) and Reynolds number of (11000,13500, and 16000). It is observed that friction factor ratio increase with raise Reynolds number and that lower pressure drop (lower friction factor ratio) is found for rib 1 at all aspect ratio.

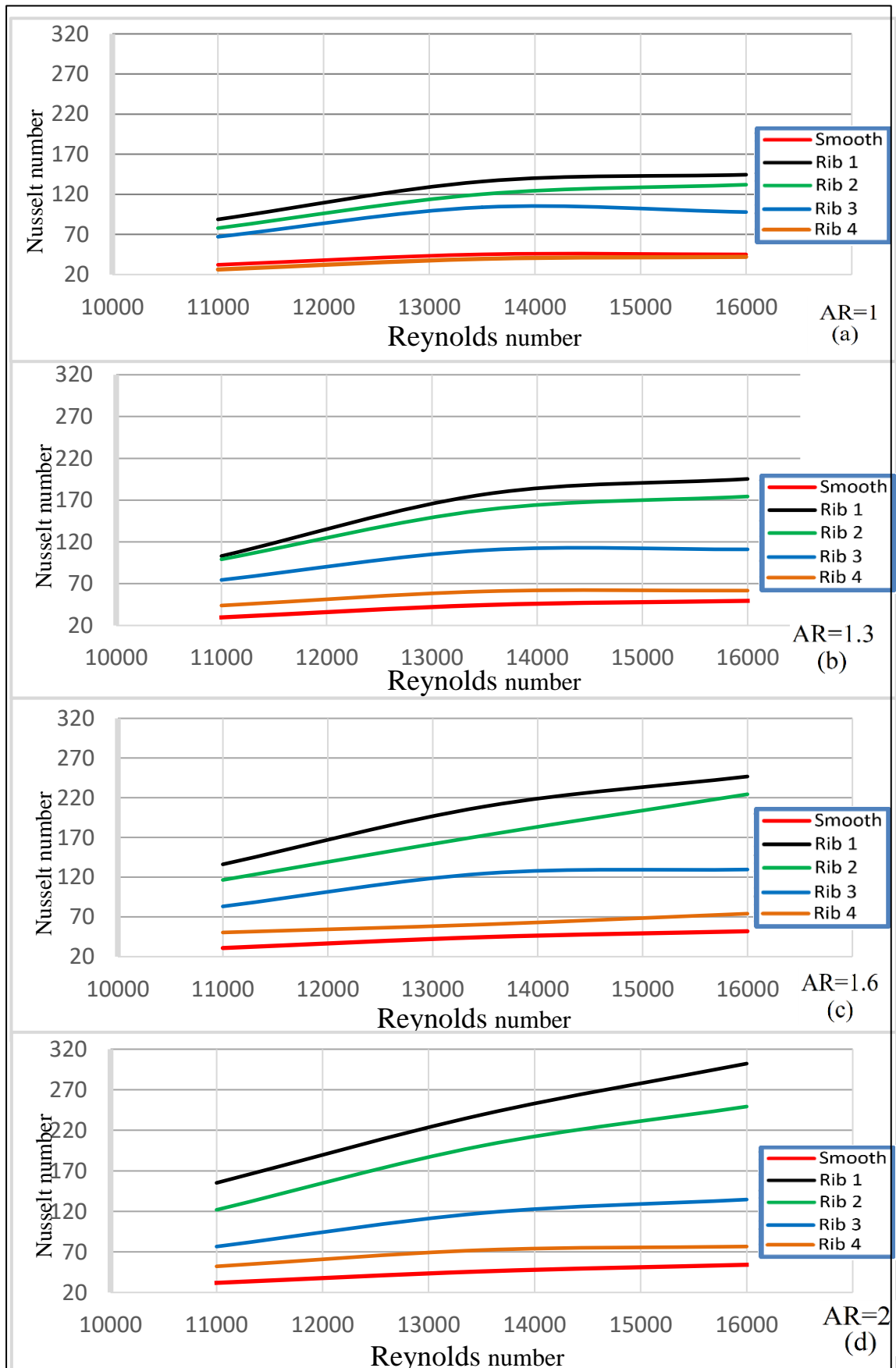


Figure (5.20.a, b, c, and d): The variation of Nusselt number with Reynolds number for different aspect ratio and ribs

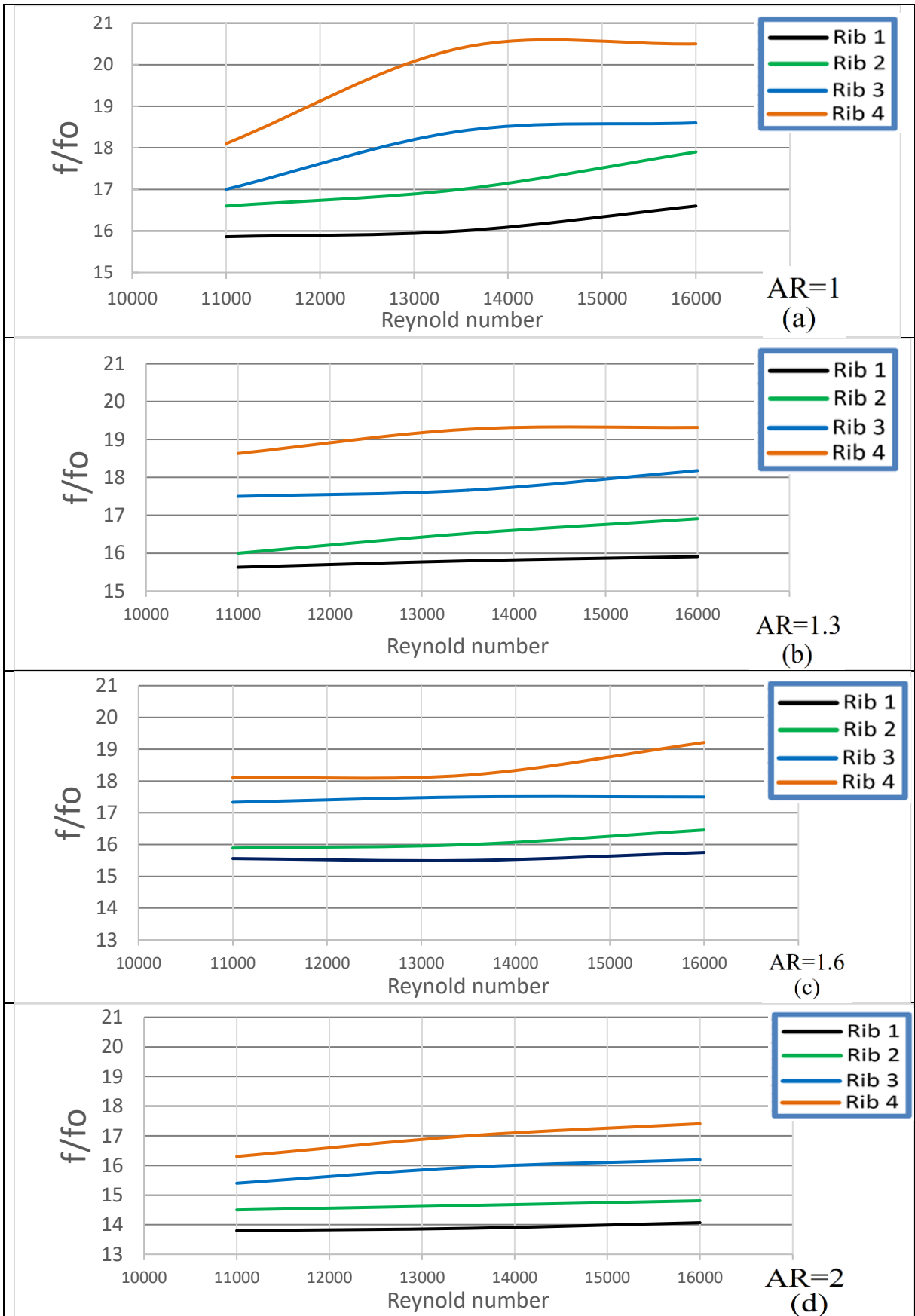


Figure (5.21.a, b, c, and d): Friction factor ratio variation with Reynolds number for all cases

---

---

### 5.2.5 Effect of rib geometry and aspect ratio on thermal performance factor

The average Nusselt number with presence of ribs can be normalized with average Nusselt number of smooth channel ( $Nu_0$ ) and acted as a function of Reynold number and different aspect ratios of channels as shown in the figure (5.22-a, b, c, and d) at constant hot air surrounding temperature of (673 k). The normalize Nusselt number ( $Nu/Nu_0$ ) is greater than (1) for all cases, i.e., using ribs caused a good augmentation in heat transfer than the case of a smooth channel. That resulted due to the use of ribs which lead to enhance the heat transfer rate if it is compared with the smooth channel. The reason for that is the effect of flow and boundary layer distribution which lead to enhancing the heat transfer and momentum change. Rib 1 in all channel aspect ratios has a high normalized Nu when it is compared with other ribs. Also, the channel with AR=2 has high normalize Nu with all ribs as it is compare with other channels so that the channel of AR=2 which fitted with rib 1 has the highest value of normalizing Nusselt number.

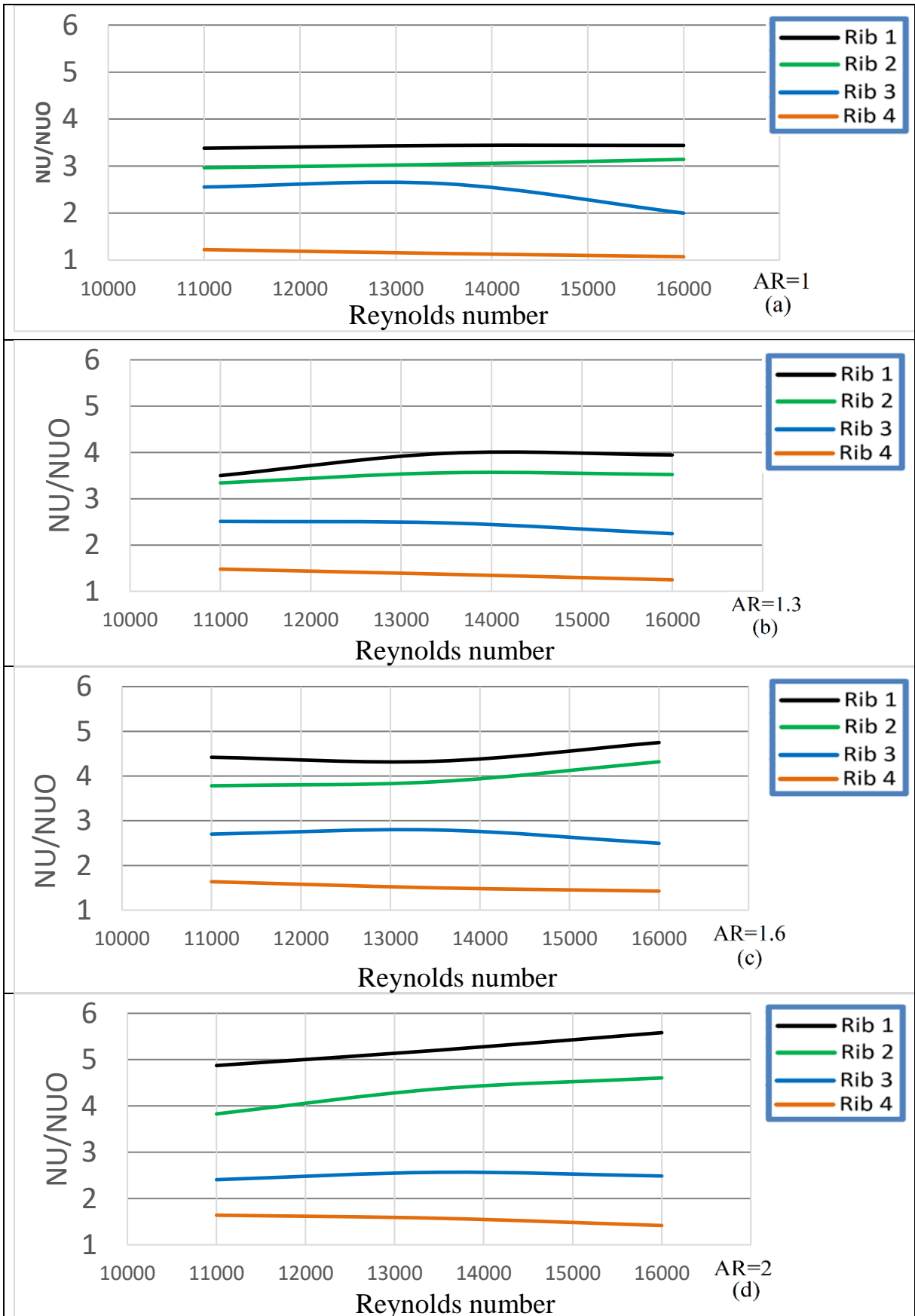


Figure (5.22.a, b, c, and d): Normalize Nusselt number (Nu/Nu0) variation with Reynolds number for different aspect ratio and ribs

---

Figures (5.23) to (5.34) present the compound thermal performance for all cases at constant surrounding hot air temperature of 673 K and the coolant air flow of  $Re=11000$ , 13500 and 16000, respectively. Rib 1 showed the best result in terms of low pressure drop and higher heat transfer enhancement. While rib 4 showed the worst results by providing higher pressure drop and low heat transfer. That means, the ribs cause more obstacle to the flow than enhancing the heat transfer. From the same figures, it is clear that the compound thermal performance is better at the channel with aspect ratio equal 2 due to the increasing of aspect ratio causing an increase in heat transfer and friction factor. However, the rate of increase in the amount of heat transferred is much more than the increase of the friction factor ratio, and that led to a push for the ribbed elliptical channel with aspect ratio of 2. This case was better than the ribbed circular channel with elliptical shape and with AR of 1 under same conditions and the same dimensions and for all cases.

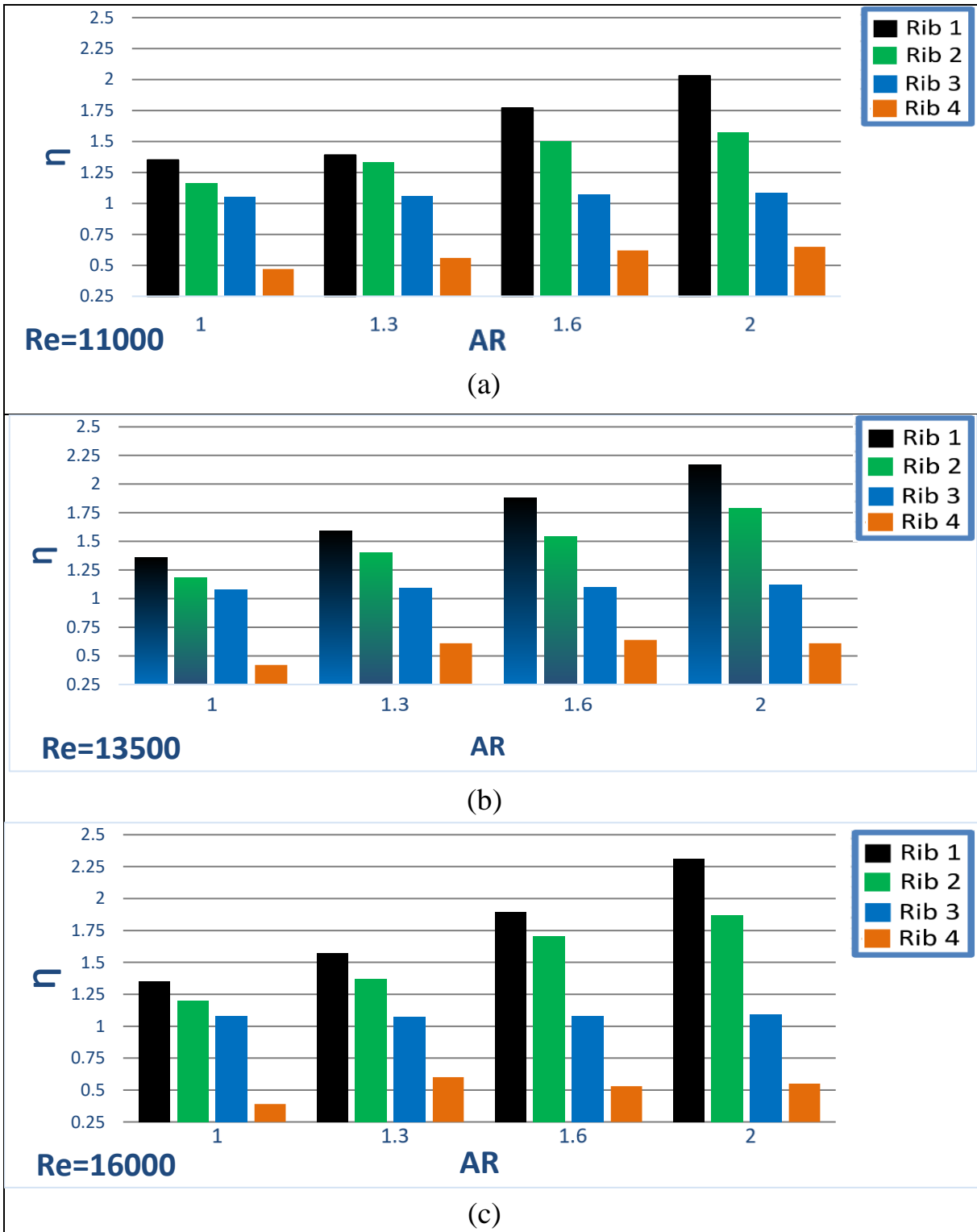


Figure (5.23.a, b, and c): The Numerical Thermal performance factor for ( $Re=11000$ , 13500 and 16000), respectively in all cases.



### 5.3 Experimental Results

Based on the numerical results, the case having aspect ratio of 2 with Reynolds number ranging from 11000 to 16000 showed the best performance. Thus, in this section the experimental results for this case only will be discussed. The error analysis is illustrated in the Appendix D.

#### 5.3.1 Effect of rib geometry on inner wall surface temperature

Figure (5.24) shows the experimental results of inner wall surface temperatures for different rib configurations and channel aspect ratio of 2. The inner wall surface temperature for the ribbed channel is lower than smooth one for all cases. Where the rates of decreasing percentage of temperatures of the inner wall surface of ribbed channel with rib1 as compared with smooth one is (5.7%,5.3%,4.5%, and 3.8 %) for (rib1, rib2, rib3, and rib4), respectively. That was resulted from wakes which were created and developed to vortices. Because of that, an increase the heat transfer from the channel wall to the coolant air occurred. Therefore, the best condition in cooling the inner wall surface of the channel is the case of rib 1 fitted in the channel with AR=2.

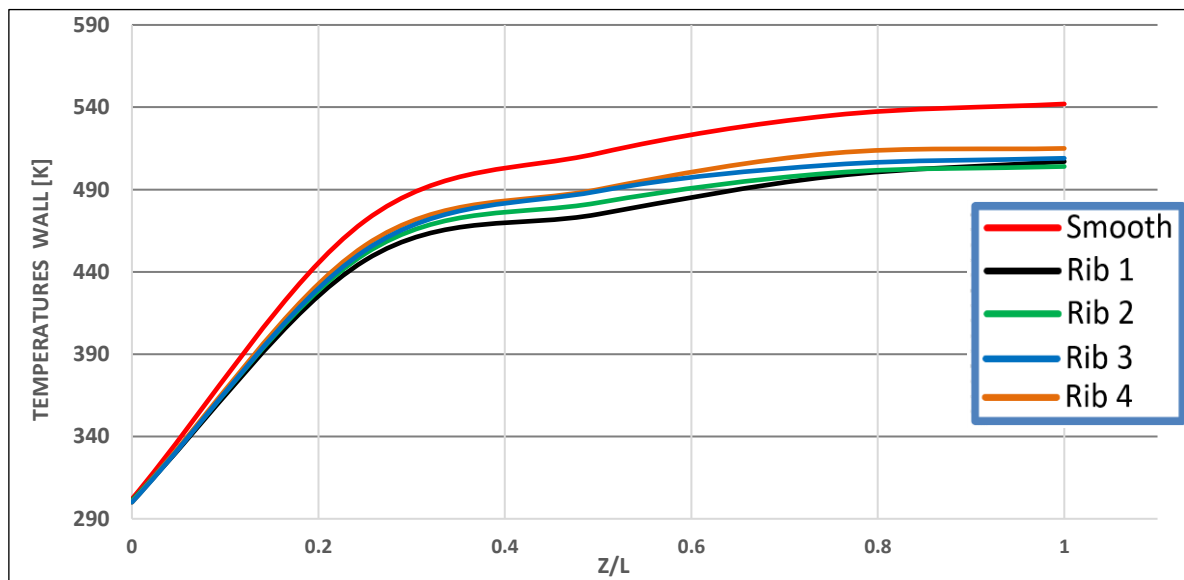


Figure (5.24): Experimental temperature distribution for the inner wall surface channel with AR=2

### 5.3.2 Effect of rib geometry on coolant air temperature

Figure (5.25) presents the experimental results of coolant air temperature along the channel centerline for different rib configurations (rib1, rib2, rib3, and rib 4), and channel aspect ratio (2) compared with smooth channel at surrounding hot air temperature of 673 K and coolant air flow of with  $Re=16000$ . Cooling air temperature for the ribbed channel is higher than smooth channel because ribs make wakes which develop to vortices. This leads to increase the heat transfer from the channel wall to the coolant air such as increasing the coolant air temperature. Comparing the ribbed channel with AR (2) with smooth one shows that there is an increase in the temperature of the cooling air outside from the channel by the temperature of the cooling air inside air by increasing the percentage (17.7%,16.7%,8.3%, and 1.5%) for case of (rib1, rib 2, rib 3, and rib 4), respectively. The case of rib1 has higher coolant air temperatures than the other cases due to the acceleration of the coolant air flow by the effect of this shape. Therefore, the case of rib1 fitted in the channel with  $AR=2$  is the most case in which an increase in centerline air temperature existed, so it is the best case in heat transfer.

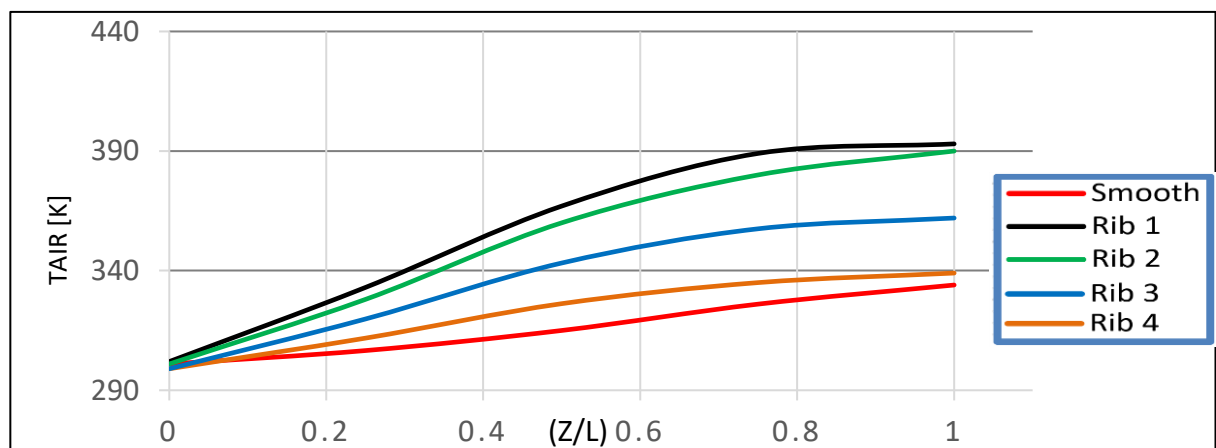


Figure (5.25): Experimental air temperature distribution at the channel centerline for ( $Re=16000$ ) and  $AR=2$

### 5.3.3 Effect of rib geometry on the average Nusselt number

It can be seen from the figure (5.26) that the increase in Reynolds number is accompanied by an increase in the value of the average Nusselt number. The reason behind that is the increased of movement of fluid inside the channel in which turbulent mixing is accrued. Therefore, the value of the seminal nucleus of the three Reynolds values has the same behavior. Figure (5.26) presents the experimental average Nusselt number varying with Reynolds number. It is noted from this figure that the highest value of the Nusselt number provided by the fitted rib 1 in the channel while the lowest value was resulted from the rib 4. Figure (5.27) presents the normalized Nusselt numbers, and it shows that the channel with rib 1 has a higher value than the other ribs.

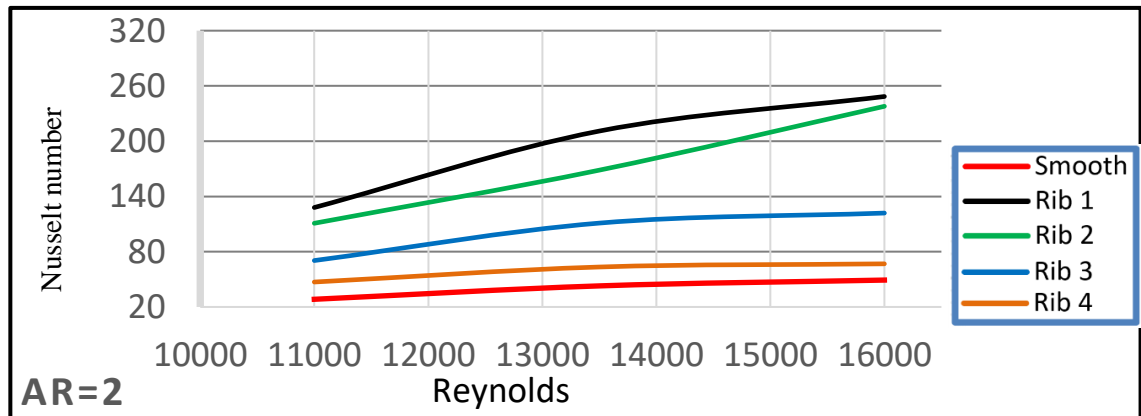


Figure (5.26): Nusselt number with Reynolds number for circular passage with and without ribs

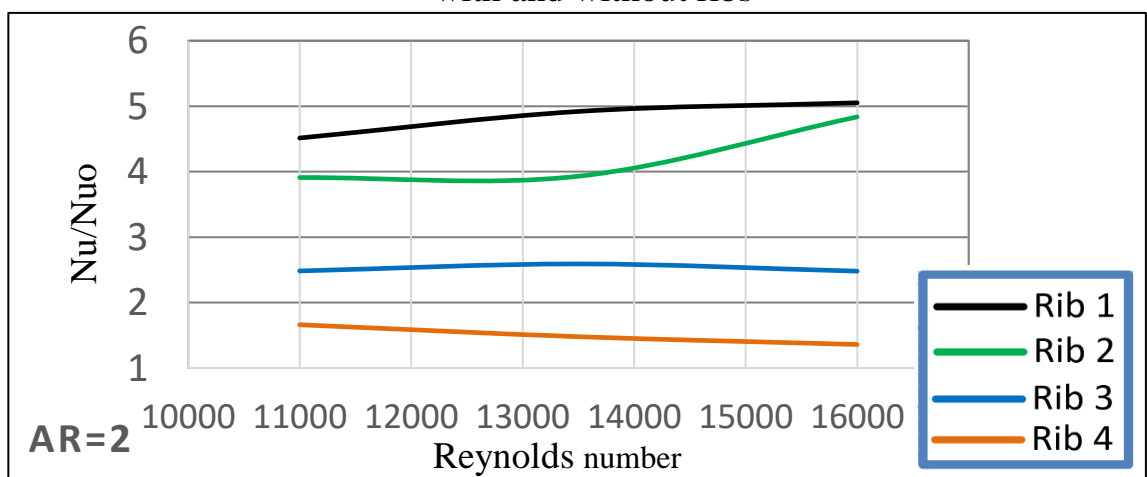


Figure (5.27): Variation of normalized Nusselt number with Reynolds number for AR=2

### 5.3.4 Effect of rib geometry on the friction factor ratio

Figure (5.28) presents the experimental friction factor ratio for all rib configurations and channel aspect ratio (2) with constant surrounding hot air temperature of 673 k and Reynolds number of 11000,13500, and 16000. The friction factor ratio increment with rising Reynolds number and the lowest pressure drop (lower friction factor ratio) is found for the case of rib1.

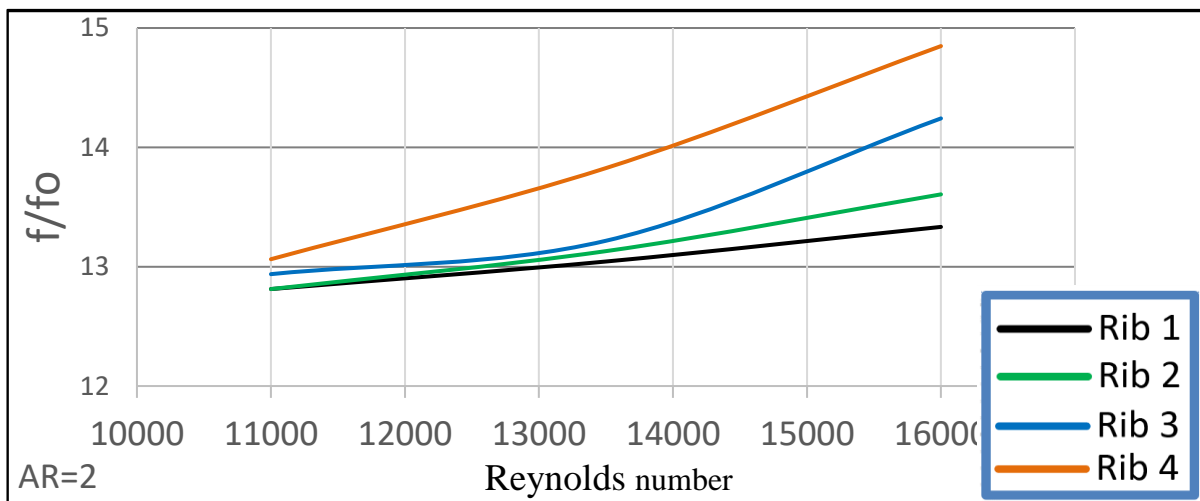


Figure (5.28): Friction factor ratio variation with Reynolds number for different rib configuration and AR=2

### 5.3.5 Effect of rib geometry on the thermal performance factor

By combined averaged Nusselt number ratios and friction factor ratios, the thermal performance factor for each channel can be evaluated. Figure (5.29) shows the variation of the thermal performance factor for the ribbed channel with AR=2. The thermal enhancement factor varies between 0.53 and 2.12 depending on the rib configuration and Reynolds number. The maximum value of thermal enhancement factor was found at the channel with AR=2 fitted with rib 1 at Re=16000.

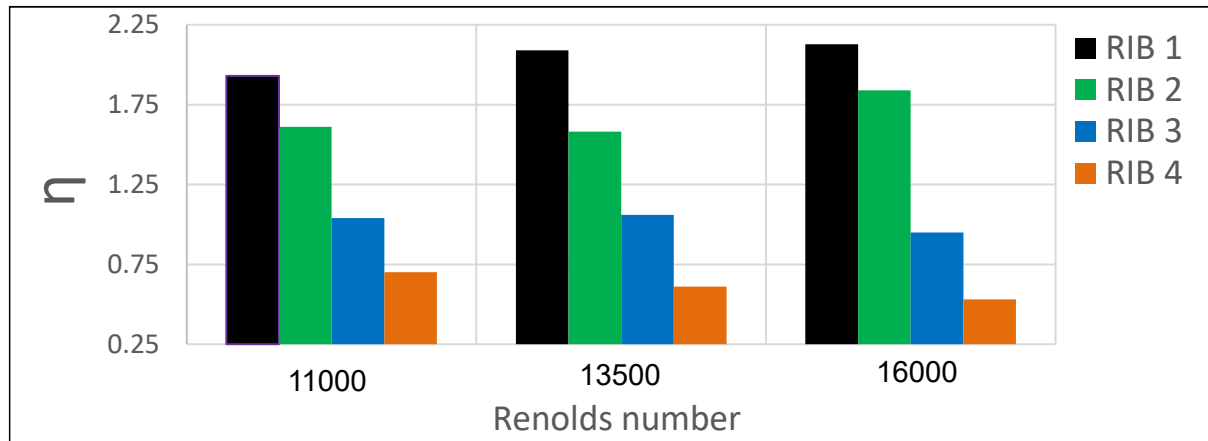


Figure (5.29): experimental thermal performance factor ratio for AR=2 and Re=16000

correlation equation for the present work as in the figure (5.30) was calculated from experimental work as illustrated in the appendix A

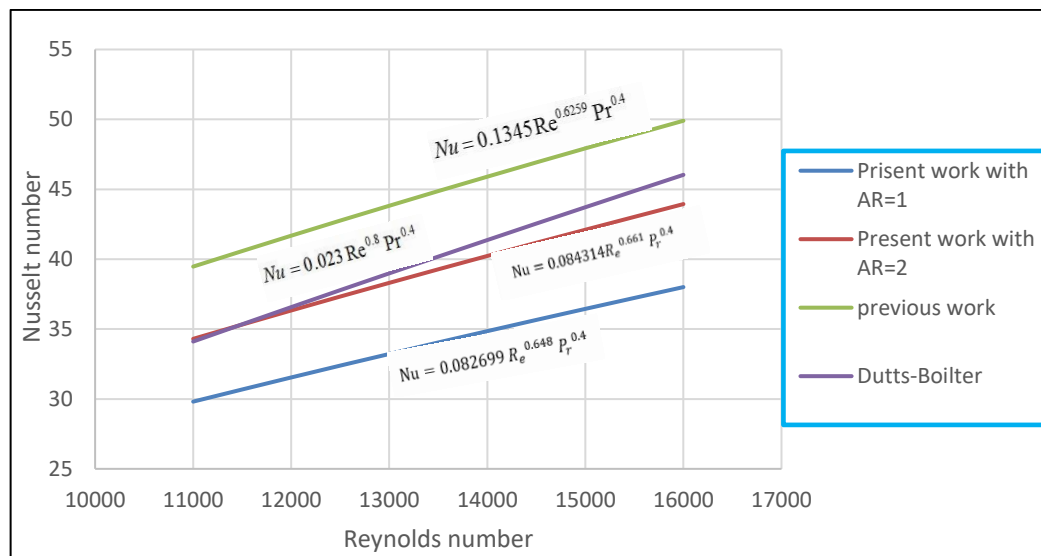


Figure (5.30) The comparison between present experimental average Nusselt number with Reynolds number for smooth channel with previous correlation and Dutts-Boilter correlation.

## 5.4 Results Comparison

### 5.4.1 Comparison of coolant air temperature

Figure (5.31) presents the coolant air temperature along the channel centerline for a smooth elliptical channel with  $AR=2$ . Figure (5.32-a, b, c, and d) presents a comparison between numerical and experimental coolant air temperatures along the channel centerline for ribbed channel cases at constant surrounding hot air temperature of 673 K and coolant air flow with  $Re=16000$ . The experimental results gave good agreement with the numerical simulation for each rib configuration. The result showed that the difference in air temperatures inside and outside the channel coolant air temperature between numerical and experimental temperature were found to be (8%, 5.7%, 4.1%, and 11.9%) for (rib1, rib2, rib3, and rib 4), respectively.

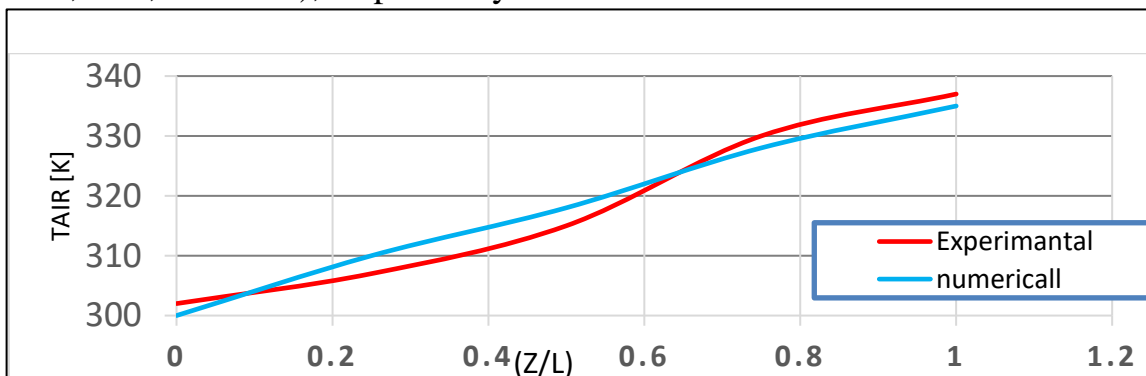


Figure (5.31): Coolant air temperature along the channel centerline for smooth elliptical channel with  $AR=2$

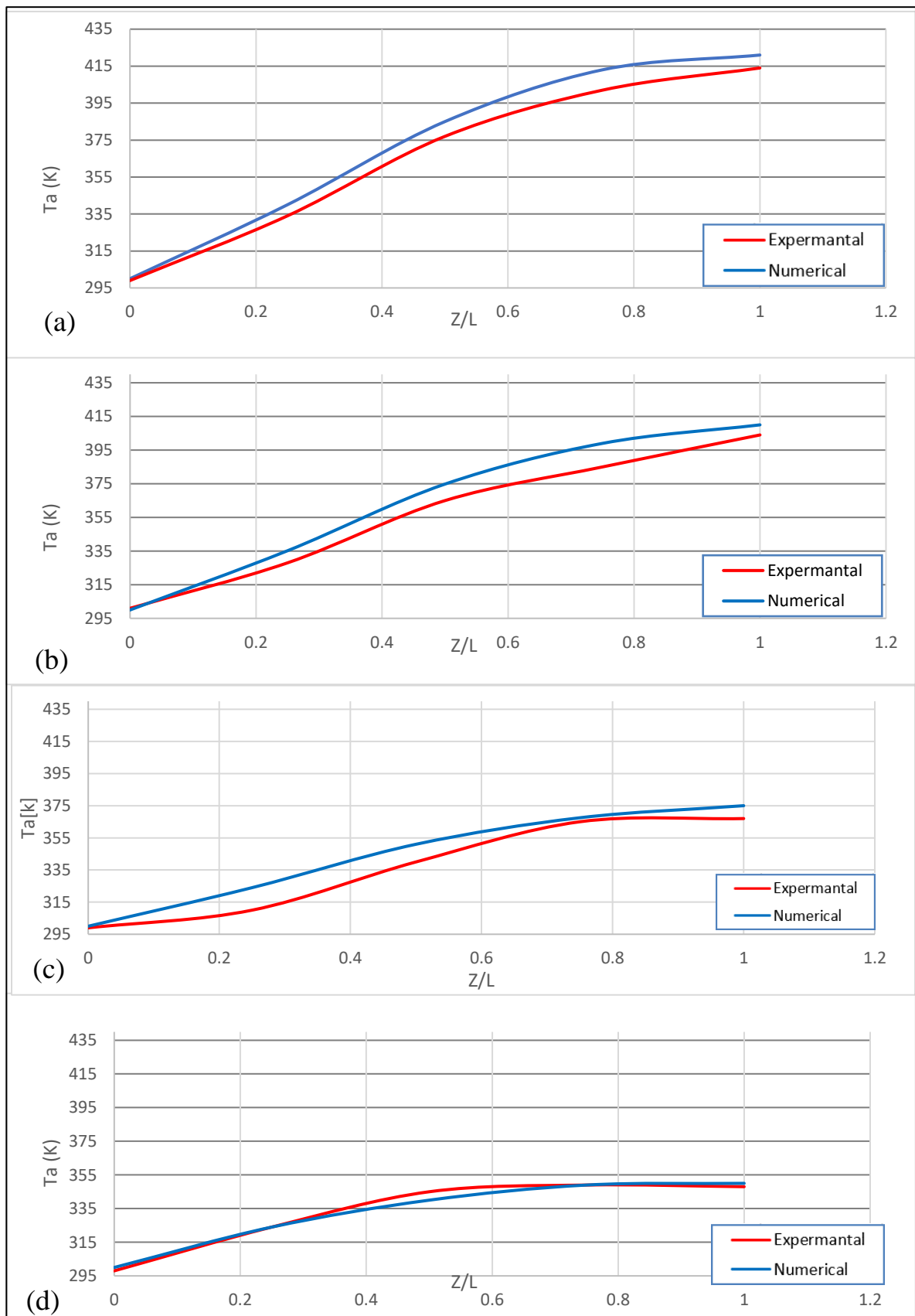


Figure (5.32.a, b, c and d): Coolant air temperature along the channel centerline  $AR=2$ : a) rib 1 b) rib 2 c) rib 3 d) rib 4

### 5.4.2 Comparison of inner wall surface temperatures

Figure (5.33-a, b, c, and d) presents a comparison between numerical and experimental results of the average inner wall surface temperatures of the channel. The experimental results gave a pretty agreement with the numerical simulation for each rib configuration. Result displays that the differences are (7.4%, 5.1%, 4%, and 4 %) for case of (rib1, rib2, rib3, and rib 4), respectively.

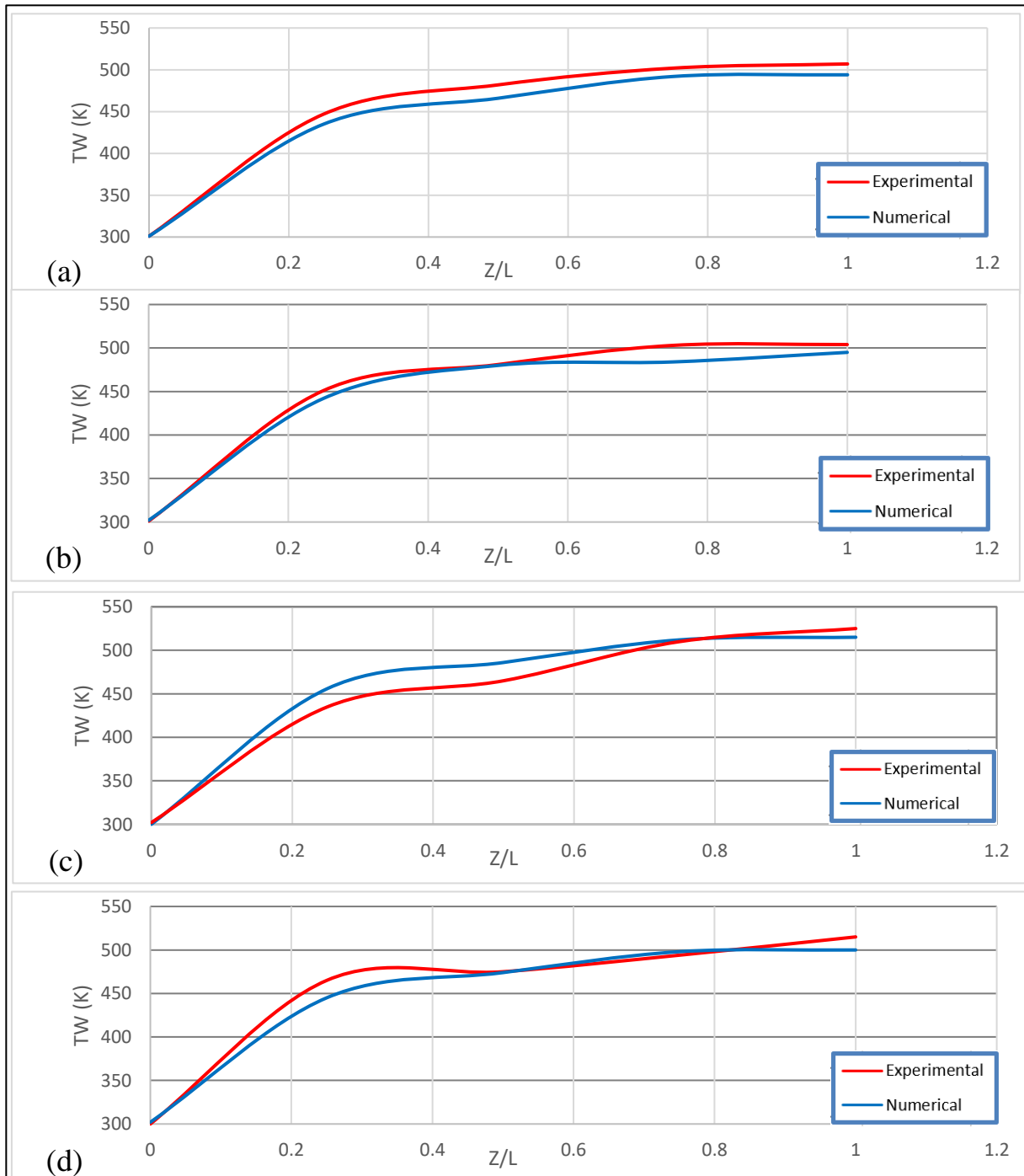


Figure (5.33. a, b, c, and d): Temperature distribution in the inner channel surface for AR=2 and (rib1, rib2, rib3, and rib 4), respectively



### 5.4.3 Comparison of average Nusselt number

Figure (5.34) shows a comparison between numerical and experimental values of the average Nusselt number normalized with the average Nusselt number of smooth channel for constant surrounding temperature of 673 K. The experimental results were in consent with the numerical simulation for each rib configuration. It is found that the difference between numerical and experimental is (7.8%, 5.6%, and 10.3%) for the case of rib 1 with Reynolds number (11000, 13500, and 16000), respectively.

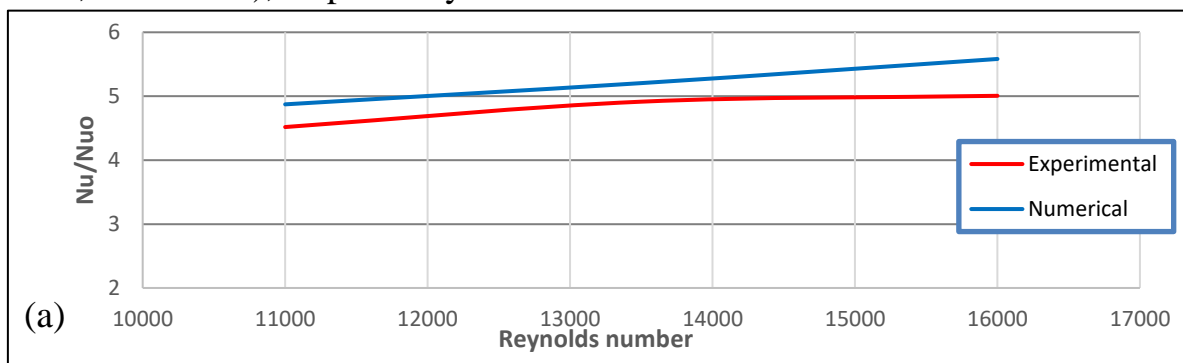


Figure (5.34): Normalized Nusselt number varies with Reynolds number for rib1 with AR=2 and Reynolds number range (11000 to 16000)

### 5.4.4 Comparison of friction factor ratio

Figure (5.35- a, b, c, and d) shows the difference between numerical and experimental results. The friction factor ratio is observed to rise with rising in Reynolds number for the reason that the resistance offered to the flow of fluid. Difference between numerical and experimental are acceptable. The best approximation was at Reynolds numbers (16000) as (5.55%).

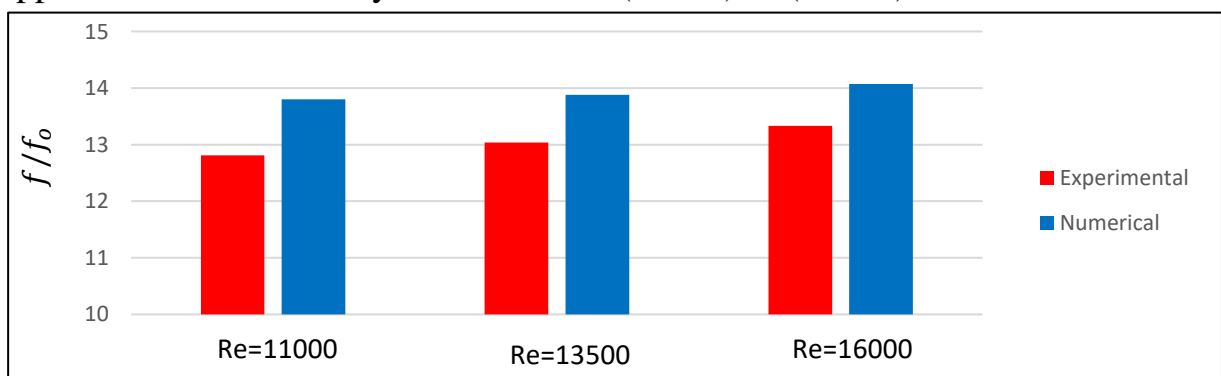


Figure (5.35): Friction factor ratio of rib 1 with AR=2 and Reynolds number range (11000 to 16000)

### 5.4.5 The thermal enhancement factor

With the averaged Nu number ratios and friction factor ratios, the thermal enhancement factor for each channel and each type of rib was evaluated. Figure (5.36) shows the comparison between numerical and experimental value of the thermal enhancement factor for the case of rib1 and channel aspect ratio with Reynolds number of (11000,13500, and 16000). Difference between numerical and experimental are reasonable and the best difference is found for Re=13500 of percentage difference (3.8%).

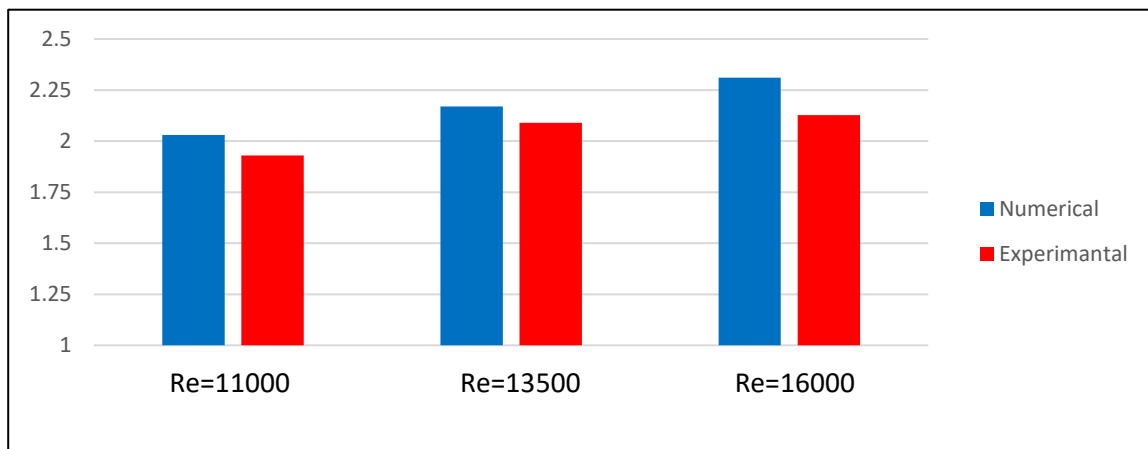


Figure (5.36): Numerical and experimental thermal performance factor for (Re=11000, 13500 and 16000) in all cases

## 5.5 Nanocomposite Material Coating

### 5.5.1 Effect of nanocomposite material coating on coolant air temperature

Figure (5.37-a,b and c) presents the effect of using nanocomposite material ( $Y_2O_3$  and thermal painting) which was applied to the external channel wall surface on the coolant air temperature at the channel centerline for using rib 1 and channel aspect ratio (2) and surrounding hot air temperature of (673 K) for coolant air Reynolds number of (Re=11000,13500, and 16000). Coated channel walls decreased coolant air temperature by (1.86%, 1.61%, and 1.56%) at the channel exit for rib 1 and (Re=11000,13500, and16000), respectively. That happened due to the low thermal conductivity of the prepared nanocomposite material which enables reducing the heat transfer from the channel wall to the coolant air. Also,

it reduced the amount of heat transfers from the outer wall surface to the inner wall surface which reduces the inner wall surface and then decrease the amount of heat transferred by convection to the coolant air.

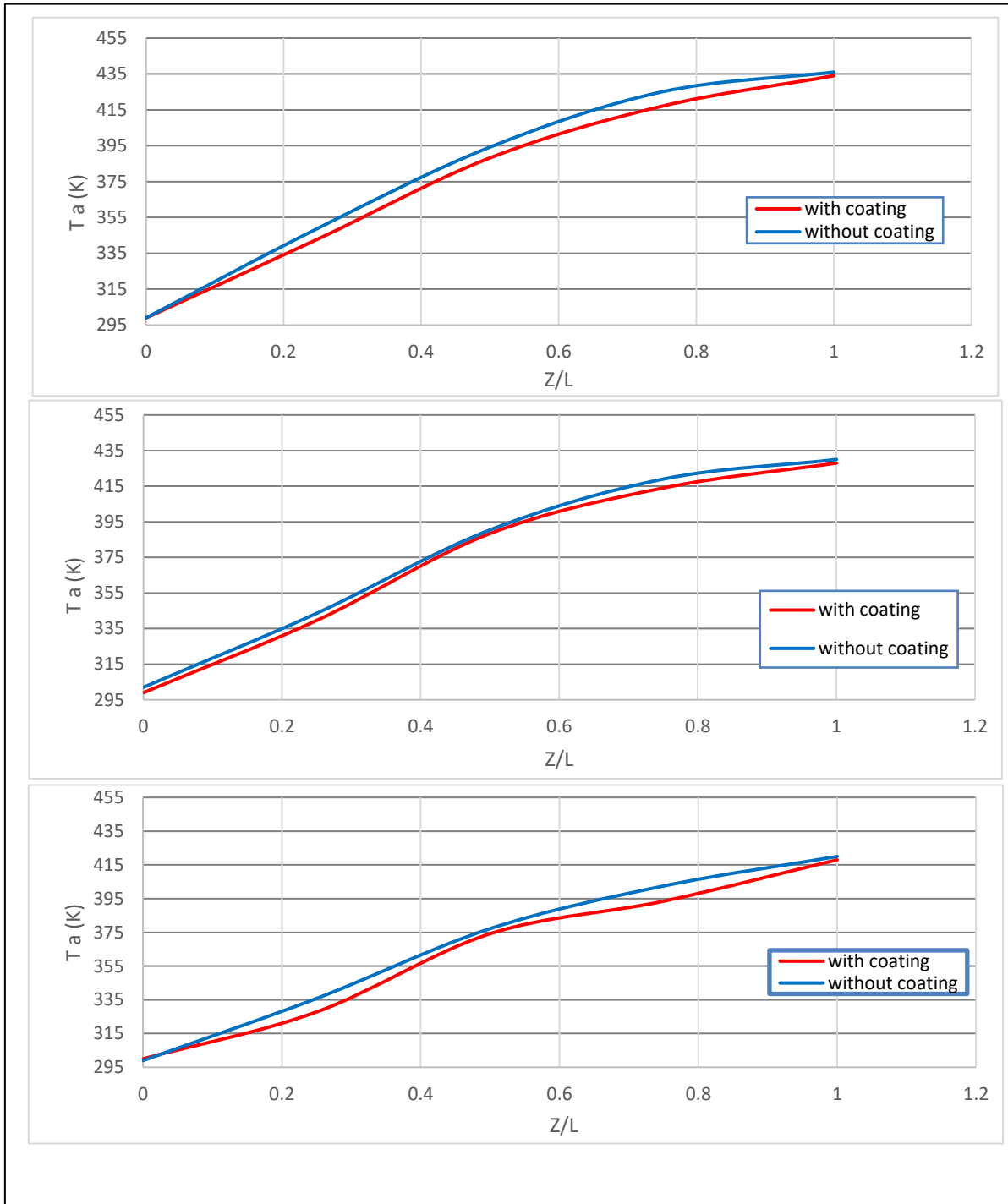
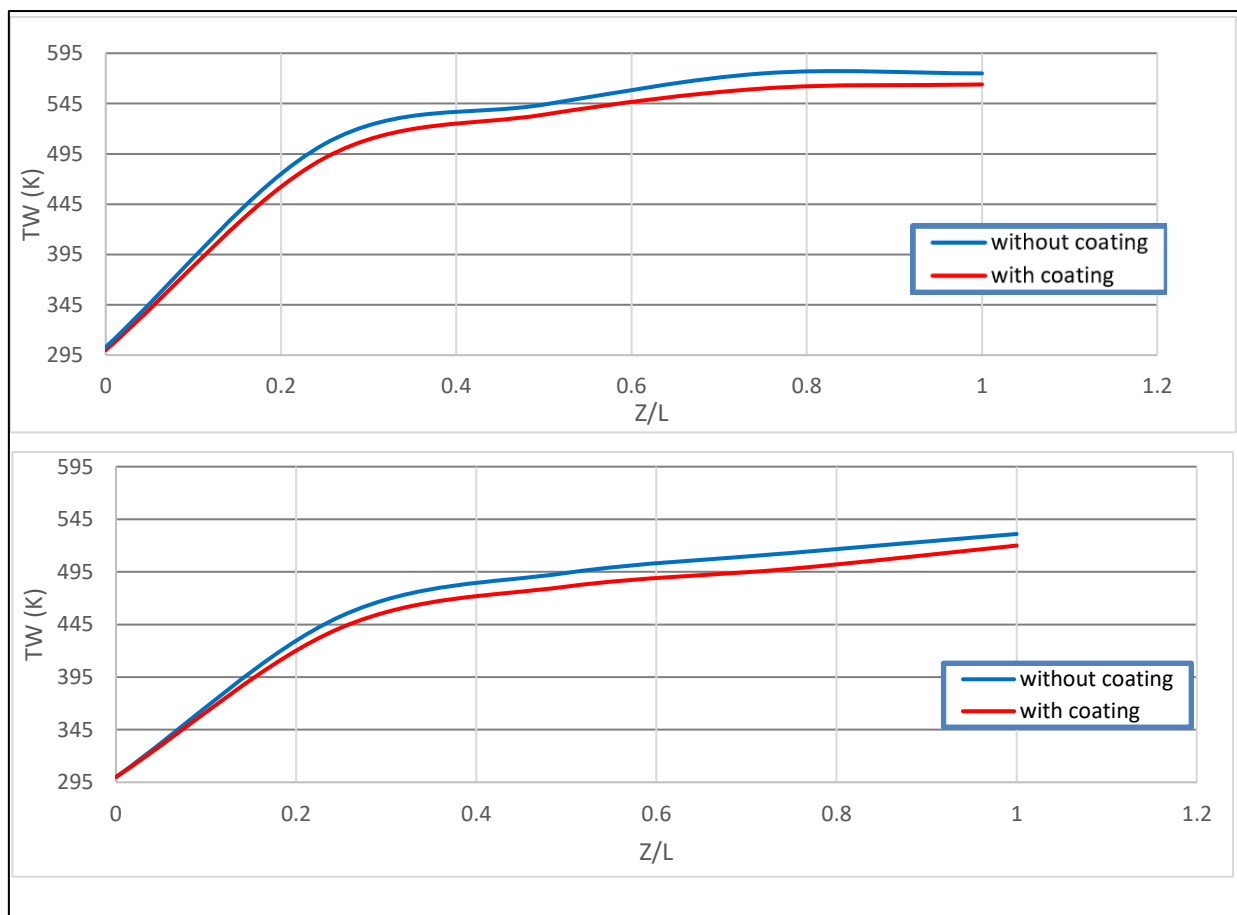


Figure (5. 37.a, b and c): Air temperature distribution at the channel centerline with ( $Re=16000$ ) for using rib 1 and channel aspect ratio (2) with and without coating

### 5.5.2 Effect of nanocomposite material coating on inner wall surface temperatures

Figure (5.38) presents the effect of coating outer channel wall surface with the prepared nanocomposite material on the inner wall channel surface temperature for using rib 1 and channel aspect ratio (2), for Reynolds number ( $Re=11000, 13500$ , and  $16000$ ) at surrounding hot air temperature of (673 K). Channel with nanocomposite material had a lower percentage of inner wall temperatures than the channel without nanocomposite material by (2.61%, 2.23%, and 2.04%), for using rib 1 and channel aspect ratio (2) and flow Reynolds number (11000, 13500, and 16000) respectively. This is because of using low thermal barrier coating, the low thermal conductivity enables reducing the heat transfer from the channel wall to the coolant air. And thus reduce the amount of heat transfers from the outer wall surface to the inner wall surface that will reduce the inner wall surface temperature as compared with the non-coating channel.



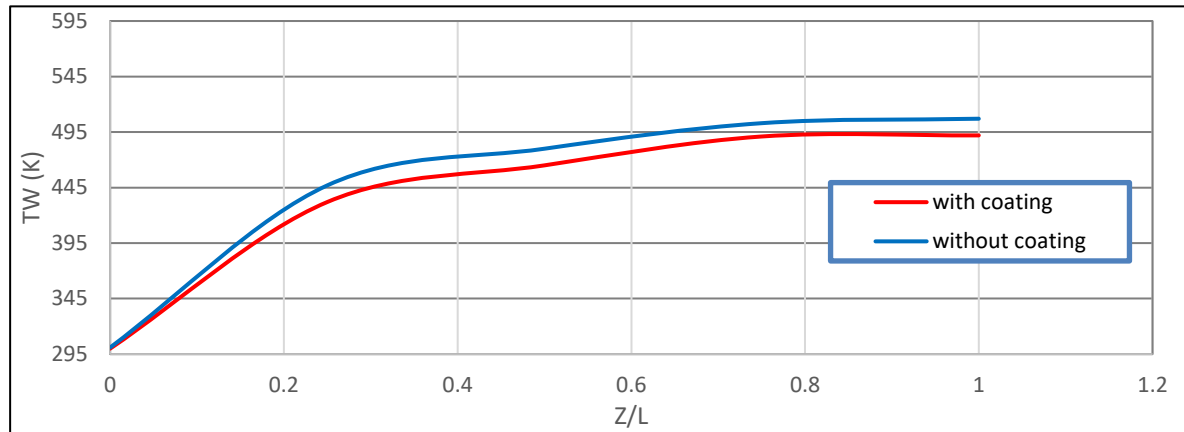


Figure (5.38 a, b and c) Temperature distribution of the channel inner wall for using rib 1 and channel aspect ratio (2) with and without coating: a)  $Re=11000$ , b)  $Re=13500$ , c)  $Re=16000$

### 5.5.3 Effect of the thermal barrier coating on the enhancement factor

Channel with barrier coating has a higher enhancement factor than uncoated channel by (9.97%) for rib1 and aspect ratio (2) at  $Re$  (16000) as shown in figure (5.39) and in figure (5.40). By coating the outer surface of the channel with low thermal conductivity, the amount of heat transfer from the outer surface to the inner surface of the channel wall is reduced. thus the temperature of the inner surface is reduced more than the case without coating. Consequently, this increased the difference between the internal surface temperature and air temperature and this difference in temperature is greater than temperature difference in the absence of coating. The absence of coating has the effect of increasing the heat transfer driving force due to the increase in the difference between wall surface temperature and coolant air temperature. This leads to raising the amount of heat transfer by convection ( $Q$ ) that cause an increment in the convection heat transfer coefficient ( $h$ ). Therefore, to increase the Normalized Nusselt number as compared with Normalized Nusselt number of non-coating channel and that led to increase the thermal performance factor of ribbed coating channel.

The aim of present work was achieved by reducing the temperature of the inner parts of the turbine blade through the coating process and the use of internal cooling.

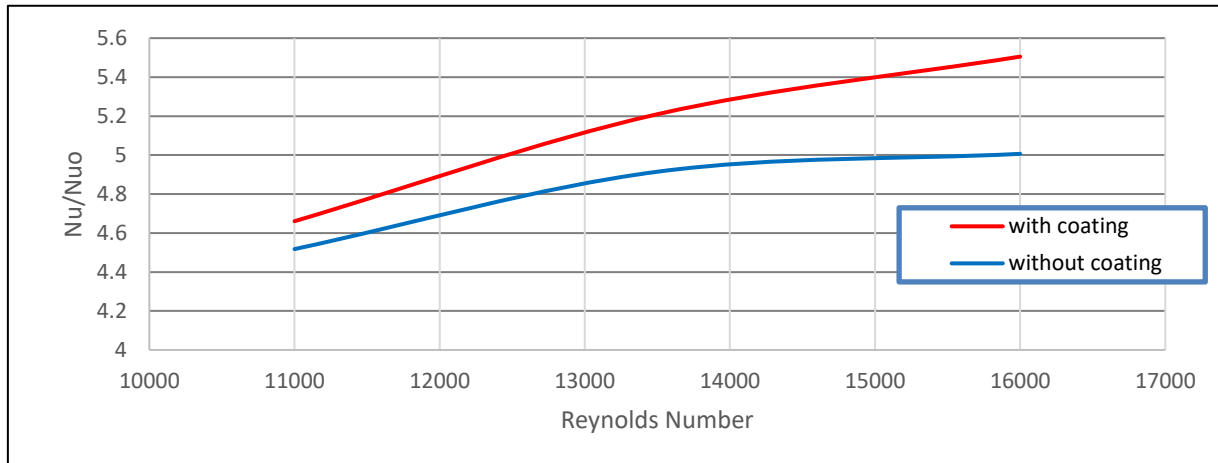


Figure (5. 39): Normalize Nusselt number variation with (Re=11000, 13500 and 16000) for using rib 1 and channel aspect ratio(2) with and without coating

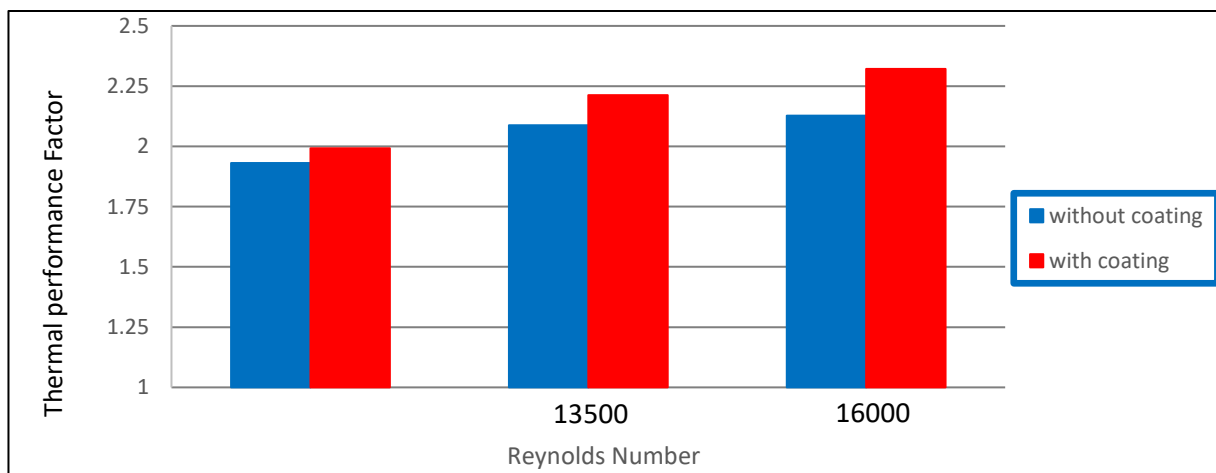


Figure (5. 4): Thermal performance variation with (Re=11000, 13500 and 16000), respectively for using rib 1 and channel aspect ratio(2) with and without coating

# **CHAPTER SIX**

## **CONCLUSIONS AND RECOMMENDATIONS**

## CHAPTER SIX

### CONCLUSIONS AND RECOMMENDATIONS

#### 6.1 Introduction

In this work, numerical and experimental analyses of air cooled heated elliptical channel were conducted. The present work was done to simulate the heat transfer and fluid flow in air cooled turbine blade. Different rib's geometries with four channels aspect ratios as well as using nanocomposite material as thermal barrier were investigated.

#### 6.2 Conclusions

In this work, the following conclusions were obtained:

1. Cooling was enhanced by using different rib geometries at constant surrounding hot air temperature of 673K, and coolant air flow of ( $Re = 16000$ ). The best case was case of rib1 with AR (2) in which the average Nusselt number was enhanced by 5.0 times the smooth channel and 5.5 when it is coated by composite Nanomaterials. Also, enhancement thermal performance factor( $\eta$ ) was achieved by 211.1 % and 232.1 % without/with coating by composite Nanomaterials.
2. Average Nusselt number increased with increasing Reynolds number, and the highest value was found for using rib 1 and channel aspect (2).
3. Increasing coolant air flow velocity lead to decreases the coolant air temperature at channel centerline, so the temperature of the inner wall channel decreases.



4. Using ribs decreases the inner wall channel temperature and increases the coolant air temperature at channel centerline.
5. Increase the aspect ratio of elliptical channel decreases the inner wall channel temperature and increases the coolant air temperature at channel centerline.
6. Average Nusselt number increased with increasing channel aspect ratio, the highest value was found for aspect ratio 2.
7. Using nanocomposite material reduced the inner wall channel temperature. Improving the enhancement factor by (9.97%)
8. The experimental results gave good agreement with the numerical simulation.

### **6.3 Recommendations**

For future work, the followings are recommended:

1. Using an external hot air flow instead of a stationary hot air.
2. Using groove and rib together in elliptical channel to have more heat transfer.
3. Using an elliptical cross section channel with two pass instead of one pass.
4. Using other ribs configuration in the same test section, half elliptical rib to be fitted in an elliptical channel.

# REFERENCES

## References

- [1] Yang, W. J., "Reduction of Specific Fuel Consumption in Gas Turbine Power Plants", *Energy Convers. Mgmts.*, 38, pp. 1219 – 1224 (1997).
- [2] Tran, L., Valentino, M., Ricklick, M., & Kapat, J. (2011). Effect of rib aspect ratio on heat transfer and friction in rectangular channels. In 47th AIAA/ASME/SAE/ASEE Joint Propulsion Conference & Exhibit (p. 6020).
- [3] Rallabandi, Akhilesh P. Parametric Study of Turbine Blade Internal Cooling and Film Cooling. Diss. Texas A & M University, 2010
- [4] Belle W., Marijnissen G. and Lieshout A.," Surface Coating Technology", pp. 120-121, 61 (1999).
- [5] Görgülü, Đlhan." Numerical Simulation of Turbine Internal Cooling and Conjugate Heat Transfer Problems with Rans Based Turbulence Models". Diss. Middle East Technical University, 2012.
- [6] Han J.C.; Dutta S.; Ekkad S.V "Gas Turbine Heat Transfer and Cooling Technology," Taylor & Francis, Inc, New York.(2000)
- [7] Chandra P. R.; Han, J. C.; and Lau, S. C. "Effect of Rib Angle on Local Heat/Mass Transfer Distribution in a Two-Pass Rib-Roughened Channel". *Journal of Turbomachinery*, Vol. 110, pp. 233–241(1988)
- [8] Han J. C.; Park J. S. "Developing Heat Transfer in Rectangular Channels with Rib Turbulators", *International Journal of Heat and Mass Transfer*, Vol. 31, pp.183-195(1988)
- [9] Han J. C.; Zhang Y. M.; and Lee C. P "Influence of Surface Heat Flux Ratio on Heat Transfer Augmentation in Square Channels With Parallel, Crossed, and V-Shaped Angled Ribs". *Journal of Turbomachinery*, Vol. 114, pp. 872 (1992)
- [10] Aravind R.Sampath, " Effect of Rib Turbulators on Heat Transfer Performance in Stationary Ribbed Channels" M.Sc. Thesis,

Department Of Mechanical Engineering , Cleveland State University,(2009).

- [11] F. J. Edwards and N. Sheriff.” The heat transfer and friction characteristics for forced convection air flow over a particular type of rough surface”. In International Developments in Heat Transfer, pages 415–425. ASME, 1961.
- [12] W. H. Emmerson. Heat transfer in a duct in regions of separated flow. In Proc. Third Int. Heat Transfer Conf., volume 1, pages 267–275, 1966.
- [13] R. L. Webb, E. R. G. Eckert, and R. J. Goldstein. Heat transfer and friction in tubes with repeated-rib roughness. International Journal of Heat and Mass Transfer, 14:601–617,1971.
- [14] Han J.C. , Dutta S., and Ekkad S., "Gas turbine heat transfer and cooling technology", Taylor & Francis (2012).
- [15] Goward G., "Progress in coatings for gas turbine airfoils," Surface and Coatings Technology, Vol. 108, pp. 73-79 (1998).
- [16] Tse and McGrath, “A Combined Experimental/Computational Study of Flow in Turbine Blade Cooling Passage”, Part I: Experimental Study,” ASME pp. 95-GT-355 (1995).
- [17] Morrell P., Rickerby D., and Derby D., "Advantages/disadvantages of various TBC systems as perceived by the engine manufacturer.", ROLLS ROYCE PLC-PEPORT-PNR (1998).
- [18] Schulz U., Saruhan B., Fritscher K., and Leyens C., "Review on Advanced EB-PVD Ceramic Topcoats for TBC Applications," International Journal of Applied Ceramic Technology, Vol. 1, pp. 302-315 (2004).
- [19] Padture N. P., Gell M., and Jordan E. H., "Thermal barrier coatings for gas-turbine engine applications," Science, vol. 296, pp. 280-284 (2002).

- [20] Patnaik P. C., Huang X., and Singh J., "State of the Art and Future Trends in the Development of Thermal Barrier Coating Systems," DTIC Document (2006).
- [21] Clarke D. R. and Levi C. G., "Materials design for the next generation thermal barrier coatings," *Annual Review of Materials Research*, vol. 33, pp. 383-417 (2003).
- [22] Eldridge J., Spuckler C., and Nesbitt J., "TBC Integrity," *American Ceramic Society Bulletin*, Vol. 83, pp. 9701-9704 (2004).
- [23] Ozceyhan, Veysel, and Sibel Gunes. "Heat transfer enhancement in a tube using triangular ribs." *ASME 2008 Heat Transfer Summer Conference collocated with the Fluids Engineering, Energy Sustainability, and 3rd Energy Nanotechnology Conferences*. American Society of Mechanical Engineers, 2008.
- [24] Yongsiri, K., Eiamsa-Ard, P., Wongcharee, K., & Eiamsa-ard, S. "Augmented heat transfer in a turbulent channel flow with inclined detached-ribs." *Case Studies in Thermal Engineering* 3 (2014): 1-10.
- [25] Altaie, Arkan, Moayed R. Hasan, and Farhan Lafta Rashid. "Numerical Investigation of Heat Transfer Enhancement in a Circular Tube with Rectangular Opened Rings." *Bulletin of Electrical Engineering and Informatics* 4.1 (2015): 18-25.
- [26] Aditi Neekhara, Pooja Tiwari and Shailesh Gupta. "Effect of rib height on heat transfer and friction factor in a square channel roughened by inclined ribs with a gap." (2017).
- [27] Kumar, Sourabh, and Ryoichi S. Amano. "Gas Turbine Blade Cooling Passage with V and Broken V Shaped Ribs." *ASME Turbo Expo 2016: Turbomachinery Technical Conference and Exposition*. American Society of Mechanical Engineers, (2016).
- [28] Patel, D. K., Jain, K. K., Dave, R. K., & Singh, A. P. P. "Heat Transfer Enhancement of Gas Turbine Blade's Cooling Rectangular Channel with Internal Ribs of Different Rib Cross Sections Using Cfd." (2016).

- [29] AlTaie, Arkan K., and Mohammad J. Kadham. "Enhancement In A Square Duct Fitted With Circular Inserts."(2016)
- [30] Han, J. C., and J. S\_ Park. "Developing heat transfer in rectangular channels with rib turbulators." *International journal of heat and mass transfer* 31.1 (1988): 183-195.
- [31] Amro, M., Weigand, B., Poser, R., & Schnieder, M."An experimental investigation of the heat transfer in a ribbed triangular cooling channel." *International Journal of Thermal Sciences* 46.5 (2007): 491-500.
- [32] Baraskar, Sachin, K. R. Aharwal, and A. Lanjewar. "Experimental Investigation of Heat Transfer and Friction Factor of V-shaped Rib Roughed Duct with and without Gap." *International Journal of Engineering Research and Applications* 2.6 (2012): 1024-1031.
- [33] Potdar, Umesh, Nilesh Shinde, and Manoj Hambarde. "Study of heat transfer coefficient & friction factor of stationary square channel with V shaped & 45° angled arc of circle ribs with different blokage ratio." *International Journal of Applied Science and Engineering Research* 1.1 (2012): 47-56.
- [34] Shailesh Gupta , Alok Chaubeb and Prakash Vermac, "Augmented Heat Transfer in Square ducts with Transverse and Inclined Ribs with and without a gap", *International Journal of Current Engineering and Technology*, Vol.3, No.2, pp. 688-694 ( 2013).
- [35] Chung, H., Park, J. S., Park, S., Choi, S. M., Rhee, D. H., & Cho H. H. "Augmented heat transfer with intersecting rib in rectangular channels having different aspect ratios." *International Journal of Heat and Mass Transfer* 88 (2015): 357-367.
- [36] Srivastava, Om Prakash, K. K. Jain, and Shailesh Gupta. "International journal of engineering sciences & research technology effect of rib attack angle on heat transfer and friction factor in a square channel roughened by v shaped ribs with a gap."(2018)

- [37] Ruck, S., Köhler, S., Schlindwein, G., & Arbeiter, F. "Heat transfer and pressure drop measurements in channels roughened by variously shaped ribs on one wall." *Experimental Heat Transfer* 31.4 (2018): 334-354.
- [38] Al-Qahtani, M., Jang, Y. J., Chen, H. C., & Han, J. C. "Prediction of flow and heat transfer in rotating two-pass rectangular channels with 45 rib turbulators." *ASME Turbo Expo 2001: Power for Land, Sea, and Air*. American Society of Mechanical Engineers, 2001.
- [39] Moon, Mi-Ae, Min-Jung Park, and Kwang-Yong Kim. "Evaluation of heat transfer performances of various rib shapes." *International Journal of Heat and Mass Transfer* 71 (2014): 275-284.
- [40] Hasan A. Jurmut, " Enhanced Turbine Blade Cooling System ", PhD Thesis, University of Technology, Mechanical Engineering Dept., Baghdad (2014).
- [41] Farhan L. Rashid," Heat Transfer Enhancement for Different Ribs Geometry in Circular Tube ", PhD Thesis, University of Technology, Mechanical Engineering Dept., Baghdad (2015).
- [42] Forsyth, Peter, Matthew McGilvray, and David RH Gillespie. "Secondary flow and heat transfer coefficient distributions in the developing flow region of ribbed turbine blade cooling passages." *Experiments in Fluids* 58.1 (2017)
- [43] Al-Jibory, Mohammed W., Farhan Lafta Rashid, and Hasan Qahtan +Hussein. "Heat Transfer Augmentation in Gas Turbine Blade Rectangular Passages Using Circular Ribs with Fins." *Journal of University of Babylon* 26.1 (2018): 247-258.
- [44] Arkan Al Taie, " Experimental Study of Radiation from coated turbine blades", PhD. Thesis, Cranfield University, Cranfield, UK (1990).

- [45] Arai M. and Suidzu T. " Porous Ceramic Coating for Transpiration Cooling of Gas Turbine Blade", Journal of Thermal Spray Technology, Vol. 22(5), pp. 690-698 (2012).
- [46] Aydin, O., Iwata, M., Arai, N., & Yang, W. J."Theoretical analysis of heat transfer through an idealized gas turbine blade model with thermal barrier coating." International Journal of Rotating Machinery 8.2 (2002): 81-86.
- [47] Anderson, John David, "Computational Fluid Dynamics : The Basics with Applications", New York: McGraw-Hill (1995).
- [48] Theodore L. Bergman, Adrienne S. Lavine, Frank P. Incropera and David P. Dewitt, "Introduction To Heat Transfer", Sixth Edition ,By John Wiley & Sons, Inc (2011).
- [49] Bruce R. Munson ,Donald F. Young, Theodore H. Okiishi and Wade W. Huebsch, " Fundamentals Of Fluid Mechanics", Sixth Edition ,By John Wiley & Sons, Inc(2009).
- [50] Panton R. L., "Incompressible flow", John Wiley and Sons, Inc. (1995).
- [51] Frank M. White, " Fluid Mechanics", Fourth Edition , McGraw-Hill Series in Mechanical Engineering.
- [52] Tu, Jiyan, Guan Heng Yeoh, and Chaoqun Liu, "Computational Fluid Dynamics", A Practical Approach, Elsevier (2008).
- [53] Robert W. Fox, Alan T. McDonald And Philip J. Pritchard, " Introduction To Fluid Mechanics", Sixth Edition, John Wiley & Sons, Inc.(2004).
- [54] Arkan K. Al-Taie And Mohammad J. Kadham, "Numerical Heat Transfer Enhancement In Square Duct With Internal Rib" , Eastern Academic Journal , Issue 3, pp.87-100( 2015).
- [55] Teerapat C, Chinaruk T., Sutapat K and Pongjet P, "Heat transfer augmentation in wedge-ribbed channel using winglet vortex generators", International Communications in Heat and Mass Transfer, pp.163-169 (2010).



- [56] T. Ravi Teja AND S. Krishna Chaitanya, " Case study on Turbine Blade Internal Cooling", International Journal of Engineering Research & Technology (IJERT), Vol.2,Issue 3, pp. 1-5 (2013).
- [58] Lu, Ben, and Pei-Xue Jiang. "Experimental and numerical investigation of convection heat transfer in a rectangular channel with angled ribs." *Experimental Thermal and Fluid Science* 30.6 (2006): 513-521
- [59] Nikuradse, Johann. "Gesetzmäßigkeiten der turbulenten Strömung in glatten Rohren (Nachtrag)." *Forschung im Ingenieurwesen* 4.1 (1933): 44-44.
- [60] Bergman, Theodore L., et al. *Fundamentals of heat and mass transfer*. John Wiley & Sons, (2011).
- [61] Lee, S. W., H. S. Ahn, and S. C. Lau. "Heat (Mass) Transfer Distribution in a Two-Pass Trapezoidal Channel With a 180deg Turn." *Journal of Heat Transfer* 129.11 (2007): 1529-1537.
- [62] Ahmed M. Bagabir, Jabril A. Khamaj, Ahmed S. Hassan, "Numerical Study of Turbulent Periodic Flow and Heat Transfer in a Square Channel with Different Ribs", *Journal of Applied Mathematics and Physics*, Vol. 1, pp. 65-73 (2013).
- [63] Li, Nan, and Kazumichi Yanagisawa. "Yttrium Oxide Nanowires. *Nanowires Science and technology*, InTech, 2010." 151-164.
- [64] Holman J. P., " *Experimental methods for engineers*", fourth edition, p.46 (1984).
- [65] Sundberg, "Heat Transfer Correlations for Gas Turbine Cooling", M.Sc. Thesis, Department of Mechanical Engineering Linköping University, Linköping, Sweden (2006).
- [66] Olsson, C-O., and B. Sunden. "Thermal and hydraulic performance of a rectangular duct with multiple V-shaped ribs." *Journal of heat transfer* 120.4 (1998): 1072-1077.

# APPENDICES

# Published Papers

## Research published in Scopus magazines

### Paper 1

2nd International Conference on Engineering Sciences

IOP Publishing

IOP Conf. Series: Materials Science and Engineering **433** (2018) 012057 doi:10.1088/1757-899X/433/1/012057

## An Experimental and Numerical Investigation of Heat Transfer Enhancement Using Annular Ribs in a Tube

Mohammed Wahhab Aljibory<sup>1</sup>, Farhan L. Rashid<sup>2</sup>, Shahid M. Abu Alais<sup>3</sup>

<sup>1</sup> Department of Mechanical.Engineering University of Kerbala,Kerbala,Iraq.

<sup>2</sup> Department of Petroleum and Petrochemical Engineering.University of Kerbala,Kerbala,Iraq.

<sup>3</sup> Department of Mechanical.Engineering University of Kerbala,Kerbala,Iraq.

<sup>1</sup>E-Mail: [Dr.Mohammad.wahab@uokerbala.edu.iq](mailto:Dr.Mohammad.wahab@uokerbala.edu.iq)

<sup>2</sup>E-Mail: [engfarhan71@gmail.com](mailto:engfarhan71@gmail.com)

<sup>3</sup>E-Mail: [shaheedt2017@gmail.com](mailto:shaheedt2017@gmail.com)

### Abstract

In this study, heat transfer and fluid flow features were numerically and experimentally studied in a circular steel passage of length 50 cm with an outer diameter of 40 mm and inner diameter of 37 mm under a constant surrounding temperature of 673 K for Reynolds numbers  $Re=10,800$ ,  $12,900$ , and  $15,700$ , in order to simulate a gas turbine blade cooling passage. Turbulence was simulated using ANSYS - FLUENT (version 16.1), and the ( $k-\epsilon$ ) turbulence model was utilised. The rib constructions (of 5 x 10 mm equilateral triangular cross-section) were fixed inside the circular passage and diverged by 5 cm. The results of temperature and velocity distribution along the circular passage's centreline for the smooth passage were compared with those of a circular passage fitted with these enclosed ribs. An improvement in the rate of heat transfer, especially at  $Re=12,900$ , was observed in the tube with ribs, with a rate of heat transfer increase of 84.3% compared to the smooth case; the ribbed tube was also observed to have a greater performance factor for turbulent flow.

**Keywords:** Gas turbine; heat transfer enhancement; rib turbulator; turbulent flow, internal cooling.



Content from this work may be used under the terms of the [Creative Commons Attribution 3.0 licence](https://creativecommons.org/licenses/by/3.0/). Any further distribution of this work must maintain attribution to the author(s) and the title of the work, journal citation and DOI.

Published under licence by IOP Publishing Ltd

## Numerical Investigation of Heat Transfer Enhancement in Ribbed Elliptical Passage

<sup>1</sup>Mohammed W. Al-Jibory, <sup>2</sup>Farhan Lafta Rashid and <sup>3</sup>Shahid Mahdy Talib

<sup>1</sup>University of Kerbala, Kerbala, Iraq

<sup>2</sup>Department of Mechanical Engineering, College of Engineering, Iraq

<sup>3</sup>Department of Petroleum Engineering, College of Engineering, Iraq

**Abstract:** This study presents a numerical investigation for heat transfer enhancement and fluid flow in elliptical and circular passages equipped with circular ribs having triangular cross section. Boundary conditions are inlet coolant air temperature is 300 K with Reynolds numbers ( $Re = 7901$ ). The surrounding constant hot air temperatures was (673 K). The numerical simulations were done by using Software FLUENT Version 15 in this part, it was presented the effect of using circular ribs in circular and elliptical passage channel on the fluid flow and heat transfer characteristics. Ribs used with pitch-rib height of 10, circular passage of 36 mm internal diameter and elliptical passage of 46×26 mm, 1.5 mm passage thickness and 0.5 m long. The temperature, velocity distribution contours, cooling air temperature distribution at the passage centerline, the inner wall surface temperature of the duct and thermal performance factor, the turbulent Eddy dissipation and turbulent kinetic energy are presented in this study. Passage with ribs was the better case which leads to increase the coolant air temperature by 9.1% for circular passage and 5% for elliptical passage, the temperature at the exit of centerline passage is greater than the elliptical passage by 3.96%. The turbulent Eddy dissipation for ribbed circular passage be higher than for ribbed elliptical passage by 100%. The values of turbulent kinetic energy for ribbed circular passage be larger than that for elliptical passage by 300% at the exist. The enhancement performance factor for ribbed circular passage be higher than that for elliptical one 120%. The higher friction factor ratio was found for elliptical cross section passage with ribs. Circular cross section with ribs is the best result (lower pressure drop and higher heat transfer enhancement).

**Key words:** Heat transfer, enhancement, internal cooling, gas turbine, rib, turbulator cooling

### INTRODUCTION

Heat transfer augmentation is a substantial field of engineering, since because it enhances the heat exchangers effectiveness. Suitable techniques of heat transfer enhancement do benefit technical advantages and cost savings. There are different available techniques like heat exchangers, industrial processes and solar heater, Bergles (1998) specified many different techniques which can be divided into two groupings: 'Passive' and 'Active'. Passive appoints special surface geometries such as coated surfaces and rough surfaces. While the active techniques need external power sources such as mechanical aids as indicated by Webb *et al.*

Metzger and Sham (1986) studied heat transfer effects around smooth rectangular channels with sharp, 180° turns. Carlomagno (1996) reported heat transfer measurements performed by means of infrared thermography in an internal flow through a 180° turn in a square channel which is relevant to the internal cooling of

gas turbine blades. He showed that the Nusselt number increased ahead of the bend while some very high heat transfer coefficient regions were present at the wall towards the partition wall axis.

Liu *et al.* (2017) discovered that rounded cylindrical ribs have a big advantage over the classical ribs in both heat transfer enhancement and minimizing pressure loss. So, cylindrical ribs can increase the flow impingement at the upstream of the ribs which will increase the heat transfer areas. The design of groove and rounded cylindrical ribs will be an important way to enhance heat transfer and then overall thermal performance of internal channels.

Parkpoom and Paranee (2017) studied the heat transfer enhancement in a case of heat exchanger by supplying inclined baffles to generate vortex of co-rotating flow using the CFD method with the k-ε model. The circulating fluid is air which is flowing in a rectangular passage with height of 30 mm and the range of Reynolds number of 12000-35000. The CFD experiment presented a smooth channel and baffles channel (ratios of

**Corresponding Author:** Mohammed W. Al-Jibory, University of Kerbala, Kerbala, Iraq



## NUMERICAL INVESTIGATION OF HEAT TRANSFER AUGMENTATION IN ELLIPTICAL PASSAGE WITH DIFFERENT RIB GEOMETRIES AND ASPECT RATIOS

**Dr. Farhan Lafta Rashid**

College of Engineering, Petroleum Engineering Department,  
University of Kerbala

**Dr. Mohammed W. Al-Jibory, Shaheed Mahdi Talib**

College of Engineering, Mechanical Engineering  
Department, University of Kerbala

### ABSTRACT

*This paper presents a numerical investigation for heat transfer enhancement and fluid flow in elliptical passages fitted with different rib configurations. Boundary conditions for the present work include: temperature of inlet coolant air is 300 K and range of flow Reynolds number (11000, 13500 and 16000). The temperature of surrounding hot air is (673 K). Numerical simulations were done using Ansys Fluent version (16.1), in this part, it was presented the effect of using different rib configurations in different elliptical passage aspect ratio on the fluid flow and heat transfer characteristics. The contours of temperature, velocity distribution, cooling air temperature at the passage centerline, the inner wall channel surface temperature, and thermal performance factor are presented in this paper. Average Nusselt number increased with increasing Reynolds number, and the highest value was found for using rib 1 and channel aspect (2). Increasing coolant air flow velocity decreases the coolant air temperature at channel centerline, so decreases the inner wall channel temperature. Using ribs decreases the inner wall channel temperature and increases the coolant air temperature at channel centerline. Increase the aspect ratio of elliptical channel decreases the inner wall channel temperature and increases the coolant air temperature at channel centerline. Average Nusselt number increased with increasing channel aspect ratio, the highest value was found for aspect ratio 2. Friction factor ratio increase with increase Reynolds number and the lower pressure drop (lower friction factor ratio) is found for rib 1 at all aspect ratio.*

**Keywords:** Elliptical Passage, Heat Transfer Enhancement, Internal Cooling, Gas Turbine.

International Journal of Mechanical Engineering and Technology (IJMET)  
Volume 9, Issue 13, December 2018, pp. 1033–1048, Article ID: IJMET\_09\_13\_109  
Available online at <http://www.iaeme.com/ijmet/issues.asp?JType=IJMET&VType=9&IType=13>  
ISSN Print: 0976-6340 and ISSN Online: 0976-6359

© IAEME Publication



Scopus Indexed

## AN EXPERIMENTAL INVESTIGATION OF HEAT TRANSFER ENHANCEMENT IN ELLIPTICAL PASSAGE FITTED WITH DIFFERENT RIB GEOMETRIES

**Dr. Mohammed W. Al-Jibory, ShaheedMahdi Talib**

College of Engineering, Mechanical Engineering Department,  
University of Kerbala

**Dr. Farhan Lafta Rashid**

College of Engineering, Petroleum Engineering Department,  
University of Kerbala

### ABSTRACT

*This paper presents an experimental investigation for heat transfer enhancement and fluid flow in elliptical passages fitted with different rib geometries. Boundary conditions are: inlet coolant air temperature is 300 K and flow Reynolds number range (11000, 13500 and 16000). The surrounding constant hot air temperatures was (673 K). Results present the effect of using different rib geometries in different elliptical passage aspect ratio on the fluid flow and heat transfer characteristics. The cooling air temperature distribution at the passage centerline, inner wall surface temperature of the channel, average Nusselt number, friction factor ratio, and thermal performance factor are presented in this paper. It was shown that average Nusselt number increased with increasing Reynolds number, and the highest value was found for using rib 1 and channel aspect (2). Increasing coolant air flow velocity decreases the coolant air temperature at channel centerline, so decreases the inner wall channel temperature. Using ribs decreases the inner wall channel temperature and increases the coolant air temperature at channel centerline. Friction factor ratio increase with increase Reynolds number and the lower pressure drop (lower friction factor ratio) is found for rib 1 at all aspect ratio.*

**Keywords:** Gas Turbine, Heat Transfer Enhancement, Internal Cooling, Rib Turbulator.



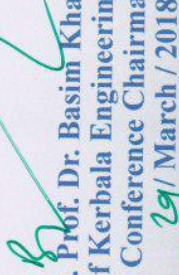


**2<sup>nd</sup> International Conference On Engineering Sciences**

*Certificate of Participation*

I, hereby, certify that **Shahid M. Abu Alais**  
submitted the paper entitled  
**Experimental and Numerical Investigation of Heat Transfer  
Enhancement in a Tube by Using Annular Ribs.**  
to the “Second International Conference On Engineering Sciences - ICES”  
The paper was accepted for presentation and publication in the conference proceeding.



  
Asst. Prof. Dr. Basim Khalil Nile  
Dean of Kerbala Engineering College  
Conference Chairman  
29/ March / 2018




**2<sup>nd</sup> International Conference on Engineering Sciences**  
**University of Kerbala, Engineering College**

**Dear Authors : Mohammed W. Al-Jibory , Farhan L. Rashid and  
Shahid M. Abu Alais**

Your paper, number ICES.M0028 entitled “**Experimental and Numerical Investigation of Heat Transfer Enhancement Using Annular Ribs within Gas Turbine Blade Cooling Passage**” has been thoroughly reviewed by expert reviewers in the field of your research. Based on the peer review results, I am pleased to inform you that your paper has been accepted for publication in the 2<sup>nd</sup> International Conference of Engineering Science. The 2<sup>nd</sup> ICES will be held March 26<sup>th</sup> - 27<sup>th</sup> in the University of Kerbala, Iraq.

Thank you for submitting your article to the 2<sup>nd</sup> ICES, and congratulations on your fine contribution. We look forward to welcoming you soon in Kerbala.

**Best Regards**

  
Assist. Prof. Dr. Basim K. Nile

Chair of Organizing Committee

2<sup>nd</sup> International Conference on Engineering Science

<http://eng.uokerbala.edu.iq/wp/2nd-international-conference-on-engineering-sciences/>







Republic of Iraq /Ministry of planning  
Central Organization for Standardization &  
Quality Control / COSQC  
Industrial Property Division  
Iraqi Patent Office

جمهورية العراق / وزارة التخطيط  
الجهاز المركزي للتقييس والسيطرة النوعية  
قسم الملكية الصناعية  
مكتب براءات الاختراع العراقي

شهادة الاولوية (الاسبقية)  
Priority certificate

المرفقة هي نسخ طبق الأصل من نص طلب البراءة العراقية كما وصفت في هذه الصفحة .  
The attached documents are exact copies of the text in which Iraqi patent application described on this page.

رقم الطلب : 575/2018  
Application Number

تاريخ الطعن : 16/10/2018  
Filing Date

طبيعة : ١- براءة اختراع  
Nature of application

٢- عنوان الاختراع : استخدام مواد متراكبة نانوية جديدة لتحسين تبريد ريشة التوربينات مقاومة للتآكل وموهنة لموجات الرادار  
Title of the invention

٣- اسم وعنوان مقدم الطلب او مالك البراءة : المهندس شهيد مهدي ص  
The name and address of the applicant or patent owner submitted.  
عنوانه: وزارة التربية / قسم التعليم المهني - تربية كربلاء

٤- اسم المخترع

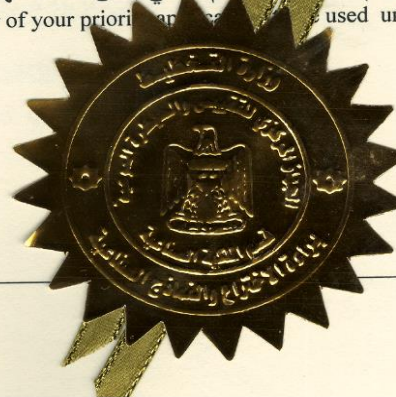
١- م. د. فرحان لفته رشيد عنوانه: جامعة كربلاء / كلية الهندسة / قسم هندسة النفط الجنسية : عراقي

٢- م. د. محمد وهاب كاظم عنوانه: جامعة كربلاء / كلية الهندسة / قسم الهندسة الميكانيكية الجنسية : عراقي

٣- المهندس شهيد مهدي طالب الجنسية : عراقي

رقم طلب الأولوية (الاسبقية) : IQ.575/2018  
The number of your priority application used under the Paris convention .

سعد عبدالوهاب عبدالقادر  
توقيع المسجل  
رئيس الجهاز



## الخلاصة

تناول البحث الحالي دراسة عددية وعملية لوضع اضلاع بأشكال هندسية مختلفة ولتغير نسبة الطول الى العرض لمقطع القناة بوجود و بعدم وجود طلاء الجدار الحراري على الجدار الخارجي وأثرها على خصائص الجريان والانتقال الحراري بحالة الجريان المتطور والمضطرب كلياً في أربعة قنوات بمقطع عرضي بيضوي مسخن بدرجة حرارية ثابتة لمدى من اعداد الرينولد (11000,13500,and16000) .

تمت الدراسة العددية بحل المعادلات الحاكمة (الاستمرارية، الزخم، الطاقة) باستخدام الانموذج المناسب للحل والمتعلق بالجريان المضطرب ولنموذج (k-ε) بثلاثة ابعاد وباستخدام FLUENT version (16.1). تضمن الحل العددي دراسة تأثير اضلاع بأشكال هندسية مختلفة وبنفس الابعاد من حيث نسبة ارتفاع الضلع الى القطر المكافئ ( $e/D_h=0.135$ ) ونسبة تباعد الاضلاع الى ارتفاعها ( $p/e=10$ ) في أربعة قنوات بمقطع عرضي بيضوي من الفولاذ المقاوم للصدأ وبطول (0.5 m) ومقطع عرضي داخلي (57x29, 50x31,43x33,37x37mm) وسمك جدار (1.5 mm).

استخدمت اضلاع داخلية بيضوية ذات مقاطع مختلفة سميت الاضلاع ب 1, 2, 3, 4. في ظروف تحاكي وتشابه الظروف التي تتعرض لها الممرات في ريشة التوربين الغازي تم التحقق من الأداء الحراري من حيث انتقال الحرارة والجريان في أربعة قنوات بيضوية (لها نفس القطر الهيدروليكي وتختلف في نسبة القطر الكبير الى القطر الصغير) .

في الجانب العملي تم انشاء منظومة عملية لهذا الغرض تحاكي ظروف تبريد ريشة التوربين الغازي. تمثلت الظروف التشغيلية: بالهواء الذي يدخل قناة الاختبار عند درجة حرارة (300K) ودرجة حرارة ثابتة خارج الانبوب (673K). وتم مقارنة جميع الحالات للقناة بوجود الاضلاع مع حالة القناة بدون اضلاع حيث بينت النتائج العملية ان الانبوب بوجود الاضلاع له اداء حراري عالي .

و قد بينت النتائج ان القناة البيضوية المصنوعة من مادة الفولاذ ذات (2) AR كانت افضل في الأداء الحراري من بقية القنوات البيضوية الأخرى و كانت الزيادة في معدل رقم نسلت لحالة القنوات المحتوية على الاضلاع اكثر بمقدار (1.4, 2.4, 4.5, 5.0) مرة بمقدار رقم نسلت لحالة القناة الملساء وللحالات (rib1,rib2,rib3,rib4) على التوالي وكانت قيمة معامل الأداء (rib1,rib2,rib3,rib4) للحالات (2.31,1.87,1.09,0.55) على التوالي.

أظهرت حالة الضلع 1 المثبتة في القناة ذات (2) AR أفضل نتيجة (اقل انحدار في الضغط وأكثر تحسن بانتقال الحرارة). في حين أظهرت حالة الضلع 4 اقل أداء. وتمت مقارنة النتائج التجريبية مع النتائج العددية وأظهرت اتفاق جيد بحوالي (3.8%).

يتضمن العمل الإضافي طلاء القناة لأفضل حالة بالمواد النانوية المركبة (الطلاء الحراري الممزوج مع جسيمات أكسيد اليتريوم النانوية ( $Y_2O_3$ ) بمقدار (5 wt. %) كطلاء للحاجز الحراري. حيث حصل تحسن في مقدار الأداء الحراري بعد الطلاء بمقدار (9.97%).

تمت مقارنة الحالات المدروسة بقناة بيضوية ناعمة (بدون أضلاع) في نفس ظروف التشغيل القناة ذات (2) AR والتي بينت النتائج العددية انها هي أفضل قناة في نقل الحرارة، وتبين أن القناة ذات الأضلاع لها أداء حراري أعلى من تلك التي تكون بدون أضلاع.



جمهورية العراق  
وزارة التعليم العالي والبحث العلمي  
جامعة كربلاء - كلية الهندسة  
قسم الهندسة الميكانيكية

## تحسين التبريد لممرات ريش التوربين باستخدام الاضلاع والطلاء الحاجز الحراري

رسالة مقدمة الى كلية الهندسة - جامعة كربلاء كجزء من متطلبات نيل درجة ماجستير علوم  
في الهندسة الميكانيكية

من قبل

المهندس شهيد مهدي طالب أبو العيس الموسوي  
(بكالوريوس هندسة ميكانيكية 2003)

بإشراف

ا.م.د. محمد وهاب كاظم الجبوري د. فرحان لفته رشيد الطائي